Design and Performance Analysis of Functional Split in Virtualized Access Networks

by

Ziyad Alharbi

A Dissertation Presented in Partial Fulfillment
of the Requirements for the Degree
Doctor of Philosophy

Approved February 2019 by the
Graduate Supervisory Committee:

Martin Reisslein, Chair
Akhilesh Thyagaturu
Yanchao Zhang
Michael McGarry

ARIZONA STATE UNIVERSITY

May 2019

ABSTRACT

Emerging modular cable network architectures distribute some cable headend functions to remote nodes that are located close to the broadcast cable links reaching the cable modems (CMs) in the subscriber homes and businesses. In the Remote-PHY (R-PHY) architecture, a Remote PHY Device (RPD) conducts the physical layer processing for the analog cable transmissions, while the headend runs the DOCSIS medium access control (MAC) for the upstream transmissions of the distributed CMs over the shared cable link. In contrast, in the Remote MACPHY (R-MACPHY) architecture, a Remote MACPHY Device (RMD) conducts both the physical and MAC layer processing. The dissertation objective is to conduct a comprehensive performance comparison of the R-PHY and R-MACPHY architectures. Also, development of analytical delay models for the polling-based MAC with Gated bandwidth allocation of Poisson traffic in the R-PHY and R-MACPHY architectures and conducting extensive simulations to assess the accuracy of the analytical model and to evaluate the delay-throughput performance of the R-PHY and R-MACPHY architectures for a wide range of deployment and operating scenarios. Performance evaluations extend to the use of Ethernet Passive Optical Network (EPON) as transport network between remote nodes and headend. The results show that for long CIN distances above 100 miles, the R-MACPHY architecture achieves significantly shorter mean upstream packet delays than the R-PHY architecture, especially for bursty traffic. The extensive comparative R-PHY and R-MACPHY comparative evaluation can serve as a basis for the planning of modular broadcast cable based access networks.

I dedicate this dissertation to my father and mother.

ACKNOWLEDGMENTS

My deepest regards and thanks to my advisor Prof. Martin Reisslein, without whom this would have not been possible.

I am immensely grateful to Dr. Akhilesh Thyagaturu for his generous support, advice and trust. Also, I am immensely thankful to the committee members, Prof. Yanchao Zhang, and Prof. Michael McGarry for their advice and support.

My heartfelt thanks to my friends, lab-mates and colleagues, Yousef Dashti, Anu Mercian, Po-Yen Chen, Xing Wei, Prateek Shantharama, Ahmed Nasrallah, Dr. Xing Shao and Dr.Yu Liu for their sincere friendship and support.

In addition, I am also very grateful to Hesham ElBakoury, Chief Architect, Huawei for his insightful discussion as a part of our collaboration project with Huawei..

TABLE OF CONTENTS

CHAPTER Page

CHAPTER Page

LIST OF TABLES

LIST OF FIGURES

CHAPTER 1

INTRODUCTION

Internet connectivity dominates our everyday activities, which are driven by the creation and exchange of information. Facilitated by the advances in communications, the Internet has seen significant growth and the demand for data communication continues to soar. Cable networks were traditionally designed to carry broadcast video, such as tv channels, to a large number of households. However, as the demand for unicast Internet services increased, Cable Modems (CMs) were introduced to transmit unicast data over the shared broadcast channel in a cable network. Cable links that were originally deployed for video broadcast transmissions are an attractive platform for delivering Internet services to distributed user locations.

Driven by this motivation, advances in cable technologies have enabled the CMs to deliver Internet speeds up to 1 Gbps in both the uplink and downlink direction to each CM. As a result, Multi-System Operators (MSOs) see unprecedented opportunities for the development of innovative techniques that utilize the already deployed cable infrastructures so as to meet present and future Internet connectivity demands. However, the traditional cable network elements were not developed to be flexible, resulting in increased capital and operational expenditures (CAPEX/OPEX) for installing new infrastructures and upgrading existing infrastructures as technologies advance. Recently, numerous techniques have been proposed to reduce the cost for MSOs, such as the Distributed Converged Cable Access Platform (DCCAP) Remote-PHY (R-PHY), and Remote MACPHY (R-MACPHY) [2–5].

The distributed converged cable access platform architecture (DCCAP), a shifting paradigm is a key step towards revolutionizing the Internet connectivity

through the hybrid fiber cable (HFC) network. However, the benefits of DCCAP, such as flexibility and high scalability, come with the price of associated challenges, which include the operator investment, the design of new remote PHY/MAC devices, and the deployment of new fiber nodes for the digital transmissions. One way to address the growing operator concerns towards the increased operational cost is by virtualizing the DCCAP functions which can be deployed in the Headend of the operator core. However, a careful study needs to be conducted to examine the impact of virtualization of DCCAP functions at the headend to ensure the user satisfaction while achieving cost reduction and maximizing the resource utilization.

Cable Television Laboratories has recently released the technical report (TR) on distributed CCAP Architecture (DCA) [3] for a functional split. The TR specification defines two flavors of the DCA, namely remote PHY (R-PHY) and remote MAC&PHY (R-MACPHY). In the R-PHY, the control plane and the DOCSIS-MAC (the core) are implemented at the head end. However, DOCSIS-PHY is implemented at the remote node in the field. For the R-MACPHY, the head end has the implementation of L2/L3 aggregation, which is connected to the remote nodes. DOCSIS-MAC and -PHY are implemented in the remote node in the field. The remote nodes in the field are connected via digital fiber to the head end.

In this dissertation, a careful investigation will be conducted across multiple functions. In addition to virtualization of the DOCSIS functions, a functional split based on PHY, MAC, or higher protocol layers can be made to achieve the desired levels of flexibility and scalability at the virtualized DCCAP. However, each split at the higher layers, i.e., higher than PHY, will increase the complexity at the remote nodes. Therefore, we propose a research study focusing on the trade-offs across multiple splits, whereby our studies will be focused within the framework of the functional

split in a *virtualized DCCAP*. In particular, we will conduct a performance comparison of the R-PHY and R-MACPHY approaches in the context of a CCAP. We will examine the impact of the propagation distance between CM and the location of the upstream scheduler in both approaches and compare the resulting throughput-delay performance as well as packet loss and delay jitter performance. We will consider a wide range of realistic traffic patterns, including bursty self-similar data and multimedia traffic as well as time-constrained gaming traffic.

1.1 Dissertation Outline

The remainder of this thesis is organized as follows. Chapter 2 gives general background on cable access networks and reviews the related work. Also, it provides overviews of the architectural and protocol concepts of R-PHY and R-MACPHY. In Chapter 3, we develop mathematical models of polling based medium access control to analyze the mean upstream data packet delay in R-PHY and R-MAC cable access networks. Furthermore,we investigates the performance comparison of the R-PHY and R-MACPHY approaches in the context of a Distributed CCAP Architecture considering a WAN digital Ethernet link. In Chapter 4, We investigate the open research challenges in the context of EPON based R-PHY and R-MACPHY distributed cable access architectures and performe extensive simulations to evaluate the performance of EPON basedarchitectures.

CHAPTER 2

FUNCTIONAL SPLIT IN CABLE ACCESS NETWORKS

Presently in the access networks, the Centralized Access Architecture (CAA) and the Distributed Access Architecture (DAA) are the two common deployed types of Hybrid Fiber Coaxial (HFC) cable networking architectures [1]. The CAA architecture implements all cable networking functions at a centralized network location, typically at the headend. That is, as show in Fig. 2.1, the CCA architecture implements the CCAP functions and CMTS functions, including DOCSIS MAC, PHY, and Edge QAM for video in the headend, hub, or the cloud. The analog optical transceivers generate the amplitude modulated analog optical signals to carry the information over a fiber to a remote analog fiber node which converts the optical signals to RF signals for transmissions over coaxial link to CMs.

2.1 Converged Cable Access Platform (CCAP)

The dramatic demand growth for both video and high-speed data services combined with the inability of conventional cable systems to meet capacity demands without high OPEX /CAPEX motivated MSOs to push for a new system called the Converged Cable Access Platform (CCAP). The CCAP combines and integrates the headend functions of a physical EQAM and the cable modem termination system (CMTS) devices into a single system [2]. That is, an integrated CCAP (I-CCAP) has the CMTS and EQAM in single physical chassis, similar to the illustration in Fig. 2.1 (however, the I-CCAP location is not restricted to a specific location).

Analog fiber deployments are complex, require regular maintenance, and are highly sensitive to environmental factors. Additionally, deep fiber penetrations would result in poor optical signal quality at the remote node optical receivers, limiting the range of passive fiber deployments. As the bandwidth demands continue to increase

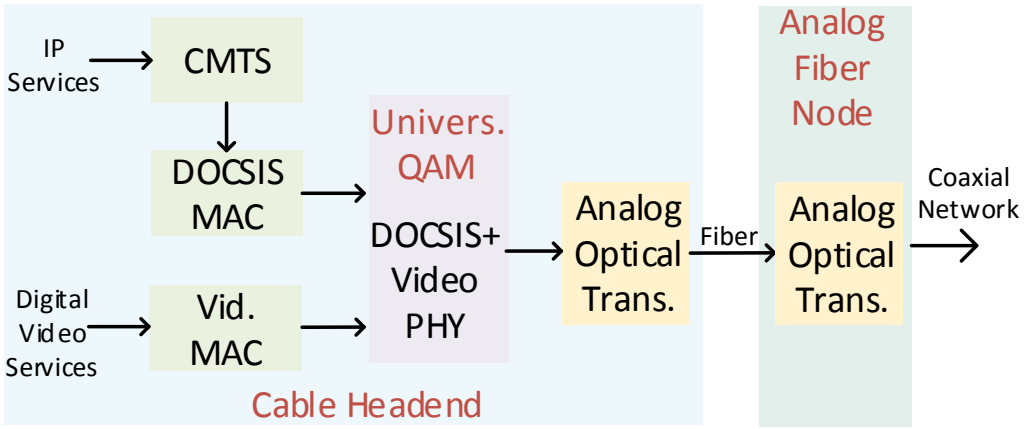

Figure 2.1: Modular Headend Architecture and Converged Cable Access Platform (MHA-CCAP) in an Analog HFC Cable Network. The CCAP Architecture Integrates the PHY QAM Modulators for Video and Data Into an Universal QAM ([1, Fig. 3]).

rapidly, current infrastructures experience an unprecedented challenge to operate in cost effective ways while addressing the bandwidth demands. Distributed access architectures (DAAs), as outlined in the next section, can offer potential solutions to overcome the limitation of the analog fiber deployments [3].

2.2 Distributed CCAP

The Modular Headend Architecture (MHA) defines CCA network functions in modular fashion such that the network functions can distributed among (split between) remote nodes and core entities, whereby the remote nodes and core entities are connected by a digital fiber. In the MHAv1 architecture, the downstream PHY is implemented externally at the remote node, while the upstream PHY is implemented internally at the core. In contrast, the MHAv2 [5] architecture implements both upstream and downstream PHY at the remote node. Although both MHAv1 and MHAv2 are technically similar in terms of their implementation, they provide MSO-specific deployment flexibilities. Typically, a remote node is located outside as a

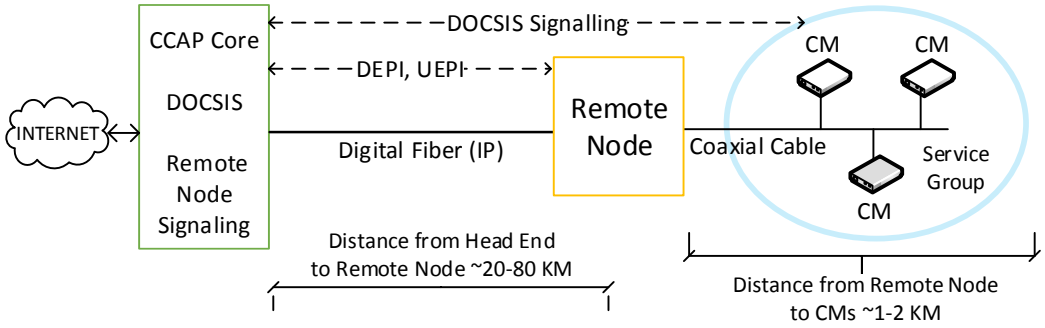

Figure 2.2: The MHAv2 Architecture Separates the CCAP Core Functions between Headend and Remote Node. The Remote Node is Typically Connected to the CCAP Core via a Digital Fiber Network.The Remote Node May Operate as a Remote-PHY (R-PHY) Node or a Remote-MACPHY (R-MACPHY) Node.

pole-mounted fiber node or remote cabinet and transfers DOCSIS frames between an IP network interface and an RF interface.

The CCAP network functions, such as DOCSIS MAC and PHY, can be implemented at the remote nodes based on the requirements to achieve the desired levels of deployment and operational flexibility. For example, Remote PHY (R-PHY) [4] implements the DOCSIS PHY layer at the remote node, whereas DOCSIS upper layers and MAC are centrally implemented at the headend or cloud. More specifically, the centralized functions can be physically implemented in the headend; however, they can also be implemented at the remote site beyond the headend, e.g., in a regional datacenter or cloud. A CCAP core typically consists of all the traditional CMTS function, except for functions implemented at the remote nodes in a MHA architecture. The network between the CCAP core and the remote node contains both Layer 2 switches and Layer 3 routers and can encompasses either the hub access network or the optical access network, or both types of access networks. The network between the CCAP core and the remote node is commonly referred to as the Converged Interconnect Network (CIN) [6].

Figure 2.2 illustrates the implementation of distributed CCAP functions at the remote nodes near the CMs. The implementation of the CCAP functions near the CMs reduces the analog RF transmission distances, thus improving the Signal to Noise Ratio (SNR) at the CMs [7]. Digital fiber supports long distance transmissions, unlike analog fiber where the transmission distances are limited by the maximum power levels supported by the optical signals. Additionally, digital fiber readily supports variants of 802.1x Ethernet protocols, such as EPON. A secure Layer 2 Ethernet or PON link over a digital fiber connects the remote node to the headend through multiple logical or physical channels, thus forming a Digital Fiber Coax (DFC) network to the attached CMs [8].

CCAP cores are always located in the trusted area of the MSO network. However, remote nodes can be located in an untrusted network domain and deployed in variety of configurations over an Ethernet link. A remote node located in an untrusted network is first authenticated with the CCAP core and then a secure IP Security (IPsec) tunnel is established for the control sessions. Authentication can be performed based on the IEEE 802.1x and 802.1ae (MACsec) standards [9]. A single remote node can be simultaneously connected to multiple CCAP cores, e.g., for DOCSIS and video, or for load balancing and fault tolerance (i.e., principle and auxiliary). Upon boot-up, the remote node in an untrusted network authenticates itself with the CCAP core and then requests an IP address through DHCP procedures. The DHCP server, managed by an MSO, provides the IP addresses of single or multiple CCAP cores to the requesting remote node. Subsequently, the remote node sends a connection request to the CCAP core. The CCAP core then accepts, denies, or forwards the request to another CCAP core. The CCAP uses the Generic Control Plane (GCP) protocol for all control plane signalling [10]. The DHCP server also provides the initial timing to the remote nodes.

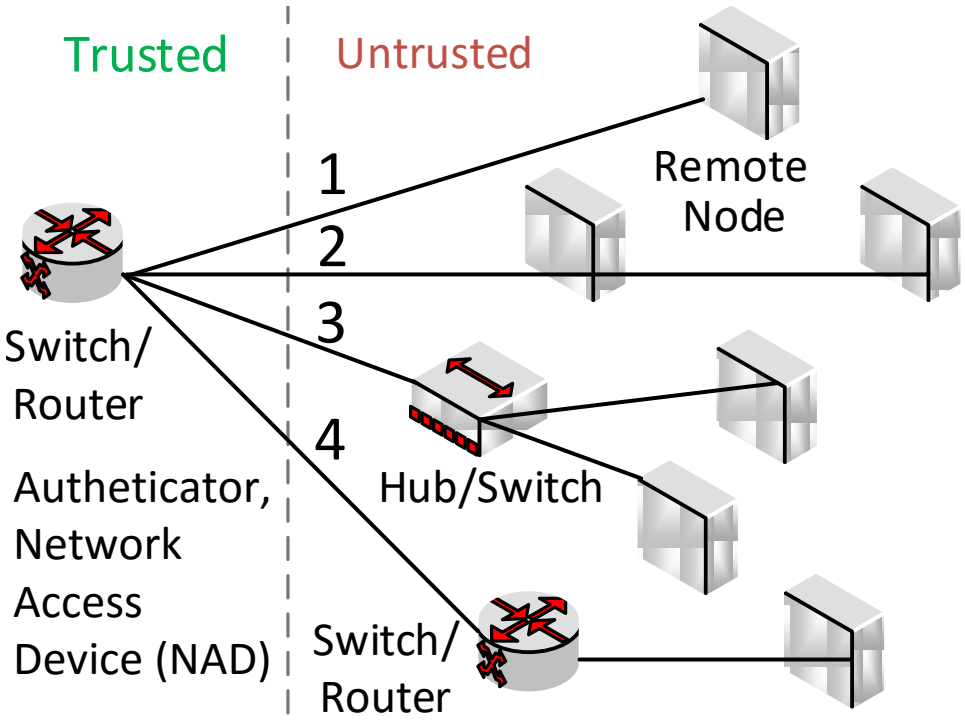

Figure 2.3: Remote Node Topologies Supported by 802.1x Technologies in The CIN.

2.3 Remote Node Topologies

Figure 2.3 shows the types of topologies for connecting a remote node via the CIN to the CCAP core, as described in the R-PHY specifications [4]. The switch/router that provides the remote node with access to the trusted MSO CIN is also known as Authenticator, or Network Access Device (NAD). Type 1 is the simplest and most widely used topology; whereby a single remote node is connected per port of the switch or the router in the CIN. Type 2 is a daisy chained remote node connection, whereby a single NAD port in the CIN connects multiple remote nodes. In the Type 3 topology, a single hub or switch with connections to multiple remote nodes is connected to a NAD port in the CIN. Additionally, multiple remote nodes are connected to the NAD by an intermediate switch or router in the Type 4 topology.

2.4 Request-Grant Delay

The time duration from the time instant when the CM issues a bandwidth request (REQ) to the time instant when the corresponding grant MAP message is received by the CM is defined as the request-grant delay. An important aspect of the MHAv2 architecture is the impact of the scheduler implementation in the CCAP core on the request-grant delay. The CIN is typically shared by multiple remote nodes through over-subscription so as to achieve multiplexing gains. As a result, the MAP messages could be affected by other traffic types in the CIN. Therefore, the DOCSIS control signalling traffic is prioritized by sending it independently through independent logical interfaces (tunnels). The routers and switches in the CIN support Differentiated Services Code Points (DSCPs) and can be configured with Per Hop Behaviors (PHBs) [11] such that control signalling traffic is prioritized. That is, the DOCSIS control packet traffic is forwarded with priority to achieve low latency while traversing the CIN [12]. The overall performance experienced by the remote node depends on the scheduling of the various signalling messages as well as the data (payload) messages. This scheduling can become especially critical when the scheduler is physically separated (by a large propagation distance) from the remote node across the CIN [13]. Ideally, the operation and performance of the centralized upstream scheduler should match the operation and performance of the integrated CMTS (I-CMTS) system (where all the network functions, including the DOCSIS scheduler, are co-located at the headend or hub). The main purpose of this project is to formulate, evaluate, and discuss the throughput-delay (as well as loss and jitter) performance implications of the remote nodes in the MHAv2 architecture for a range of scheduling mechanisms, traffic types, and CIN designs.

2.5 Related Work

Cable Laboratories (CableLabs) is a non-profit innovation and R&D lab that publishes, maintains, and updates the specifications and technical reports related to DOCSIS, video, security and cable technologies. DCA architectures can reduce space and power requirements at the headend, increase spectral efficiency at the CMs, and support increased numbers of wavelengths in WDM. There are several DCA variants, including R-PHY and R-MACPHY with or without EQAM [1].

2.5.1 DOCSIS

DOCSIS provides MAC [14] and PHY layer specifications for the CMs to communicate with the CMTS. Basic principles of DOCSIS, including scheduling procedures, have been reviewed in [15]. While earlier DOCSIS versions had limited capabilities, the recent DOCSIS 3.1 version supports downstream data peak throughputs on the order of Gbps [16]. DOCSIS 3.1 uses OFDM based transceivers to utilize narrowband subcarrier modulations over the broadband spectrum to achieve high spectral efficiency. High levels of QAM modulation, up to 16K, Low Density Parity Check (LDPC) Forward Error Correction (FEC), and a wide spectrum of 1.2 GHz in downstream and 204 MHz in upstream are some of the distinguishing features of DOCSIS 3.1 from earlier versions [17]. DOCSIS 3.1 also supports different QoS levels for business and residential application. The service operations, administration, and management capabilities of L2VPN can be applied to the DOCSIS 3.1 framework to reduce the cost of operations [18].

2.5.2 Bandwidth Allocation

The DOCSIS scheduler allocates the upstream bandwidth with bandwidth allocation map (MAP) messages to the CMs. A dynamic bandwidth allocation (DBA) algorithm

sizes (dimensions) the grants (upstream transmission windows) based on the reports received by the CMs and sends the grants via MAP messages to the respective CMs. Initial DBA designs for QoS based grant allocations have been discussed in [19]. A CM can content with other CMs for the upstream transmissions of request messages to the CMTS. The DOCSIS contention behavior in CATV networks has been examined in [20]. In order to resolve the contention, Kuo et al. [21] have presented a priority access based collision resolution scheme for different traffic priorities, such as delay sensitive and best effort streams. Similarly, Heyaime-Duvergé et al. [22] have proposed a application traffic based DBA to reduce the control signaling and increase bandwidth utilization. As an improvement to the earlier DOCSIS versions, Liao et al. [23, 24] proposed to adaptively allocate the TCP flow transmission slots by using fast request transmission and long packet deferment techniques. The impacts of the DOCSIS MAC protocols on TCP have been investigated in [25]. DOCSIS simulation models have been presented in [26–28].

DOCSIS 3.1 allows the OFDM subcarriers to be modulated with different QAM modulation levels. That is, the same modulation constellation is not necessarily used across all OFDM subcarriers. This technique is also referred to as the mixed modulation codeword scheme. Jung et al. [29] have compared the performance of mixed modulation codewords and shortened codewords. Their evaluation show that mixed modulation achieves better performance for low SNRs as compared to shortened codewords. The performance monitoring of practical HFC network deployments is very important to deliver services with high reliability to the customers. Benhavan et al. [30] have presented a cost-effective and time-efficient network state analyzer that uses 3 dimensional data, upstream power, upstream SNR, and downstream power parameters to represent the state of the HFC network. The proposed technique separates the regions in the state representation to evaluate the HFC network

performance. Ra et al. [31] in an effort to extend the current DOCSIS capabilities, have recently implemented high performance UHD video transmission systems based on OFDM over an HFC network using FPGAs to facilitate next generation designs.

2.5.3 Functional Split: Remote PHY (R-PHY)

In an attempt to evolve DOCSIS 3.1, the cable industry has been exploring to utilize deep fiber technologies, such as HFC, to improve customer experience and operational cost. The R-PHY architecture separates the DOCSIS PHY functions from the traditional CCAP chassis. Pseudowire technology is extended over an IP network to connect an RPD with rest of the CCAP. The motivation for the R-PHY architecture has been presented in [32] by Breznick. Similarly, Sowinski [33] has discussed the impact of R-PHY on cable service convergence. Separating functions in the CCAP platform can achieve several benefits, such as independent scaling of MPEG video delivery, and flexible management of DOCSIS and OOB. For example, the software and physical hardware upgrades in the R-PHY architecture are modular and independent, resulting in improved availability and manageability. However, the CM performance in functional split architectures can be significantly impacted by several network characteristics, such as remote node and CM distances from the CCAP core, traffic types, numbers of users and CIN network characteristics. Chapman et al. [13, 34] have presented a preliminary performance analysis of the impact of CM distance from the CCAP core in an R-PHY architecture. Their simulations indicated, that when CM to CCAP core distance was 0 to 100 miles, the observed downstream delay was between 0 to 1 MAP duration, which corresponds to 0 to 2 ms. The corresponding upstream delay was on the order of 10 ms, mainly due to REQ retries, CM and CMTS buffering and processing as well as reassembly of packets at the CCAP and R-PHY systems.

2.5.4 QoS

Introduced in DOCSIS 3.0, channel boding combines two or more physical channels to form a single logical channel of aggregated bandwidth capable of delivering higher throughputs to a single CM. However, the system complexity increase with the number of channels, particularly at the receivers. Therefore, in an effort to design low-complexity receivers, Lee et al. [35] demonstrated a novel CM receiver design supporting up to four upstream channels using digital down-converters and FPGAs. Larger bandwidths may be required to support 10 Mbps data rate capabilities in coaxial network transmission systems. A phase mismatch between carrier frequency and center frequency of the operational bandwidth can occur in systems operating over large bandwidths. Common phase rotation compensation techniques applied at the receivers can mitigate the phase mismatch effects. Bae et al. [36] have presented implementation results of such a phase rotation compensation technique on an OFDM transmission system capable of 10 Gbps data rate using only digital signal processors and FPGAs.

Large buffers at the CM help the network to operate with high utilization. However, TCP automatically adjusts the transmissions rate to reach the maximum capacity of the link resulting in the filling up of buffers for a large traffic flow. A packet belonging to an application requiring low bandwidth may arrive to an almost full buffer causing the packet to unnecessarily wait in the buffer. In certain situations, a deployed CM can experience buffer delays on the order of 2 to 3 seconds [37]. This phenomenon of large buffers resulting in performance degradations of latency sensitive applications is referred to as Bufferbloat [38]. Active Queue Management (AQM) is a technique employed at the buffers to ensure that applications do not suffer due to the high buffer utilizations of TCP. A common AQM approach when a TCP standing

queue is detected is to drop packets and to send a signal to the source to reduce the rate before the buffer is full. DOCSIS 3.0/3.1 employs an AQM based on the Proportional Integral Controller Enhanced (PIE) algorithm, referred to as DOCSIS-PIE [39]. Advanced buffer management techniques for DOCSIS networks are discussed in [40]. More specifically, an optimal queue capacity maximizing throughput and minimizing the delay is achieved by identifying the relationship between cable modem upstream buffer management and best effort application performance. White et al. [41] have evaluated the performance of the DOCSIS-PIE mechanism through simulations under various traffic scenarios, such as gaming, VoIP, and HTTP. Their simulations showed the reduction in upstream latency from several thousands of milliseconds to tens of milliseconds under loaded condition. Similarly, Hong et al. [42] have presented an evaluation of AQM performance based on fairness in broadband cable networks.

DOCSIS 3.1 also utilizes the benefits of narrowband multi-carrier OFDM modulation to achieve high data rates. OFDM enables its subcarriers to be modulated at different modulation orders, independent of each other. This flexibility allows CMTS to assign the modulation order based on the CM to CMTS channel characteristics, such as channel quality and link utilization. The bit loading profile is a map of modulation orders to the subcarriers in an OFDM symbol. The trade-offs associated a specific bit loading profile can vary from choosing uniform single bit loading to independent bit loading for each subcarrier. When a single bit loading profile is used, all the CMs are assigned to the same modulation order to meet a minimum SNR level across all the CMs. This can lower the overall throughput due to inefficient use of the high SNR levels. Conversely, a large number of bit loading profiles can significantly increase the system complexity, processing delay, overhead, and memory requirements. Therefore, DOCSIS 3.1 allows up to 16 and 4 bit loading profiles in downstream and upstream, respectively. CMs are categorized into multiple groups

and each group is assigned a bit loading profile from all the possible profiles such that the minimum SNR is met across all CMs within the group. Performance of the DOCSIS can largely vary with the number bit loading profiles and grouping techniques. Mehmood et al. [43] have discussed the performance trade-off under various grouping techniques, such as BiSort and K-Means (vector quantization).

Theoretical performance analysis of cable networks conducted by Gao et al. [44] has shown that when the network components, such as the CMs, operate independently with localized decisions, their actions, such as contentions, may lead to poor performance of the overall system. That is, a prescribed quality of service is hard to achieve under existing control mechanisms. Therefore, an alternative method of regulated operation through centralized control of the CMs was recommended to precisely meet QoS requirements for the MSOs. In addition, Gao et al. [45] have also theoretically investigated the performance of cable networks when the users and network entities function strategically in a coordinated fashion to show that overall performance of the network may degrade when the network entities function independently.

2.5.5 Optical Networks

The traditional PON network connects an OLT with multiple distributed ONUs. In addition to layer 2 functions, the OLT can support higher layer networking functions, such as layer 3 routing, and Multiprotocol Label Switching (MPLS). Moreover, the OLT in a PON network can be extended to support DOCSIS networking and management functions. DOCSIS Provisioning of EPON (DPoE) [46] is an evolutionary mechanism for existing EPON whereby DOCSIS functions are provisioned through the PON. Rapid changes in both access and aggregation networks, equipment requirements, and provisioning techniques are driven by new MSO business services in the

DOCSIS area, including point-to-point, point-to-multipoint, and multipoint Ethernet services over the HFC network [47]. The traditional way of upgrading the network components would involve skilled staff physically inspecting devices for errors, copying the configuration files via an RS-232 cable, and installing the configurations; this is a labor intensive process and prone to human errors. Therefore, Mallette et al. [48] presented a DOCSIS provisioning automation, a software based configuration solution for a DPoE network based on a demarcation Device Auto Configuration (DAC).

Emmendorfer et al. [49] have extensively discussed PON deployments for DOCSIS management in both CAA and DAA architectures. CAA employs a PON extender node for improved fiber utilization. In contrast, DAA implements the OLT functions at the remote node to save space at the headend. In either case, the PON deployments increase the fiber distance between headend and customers. The IEEE has defined a new project, EPON Protocol over Coax (EPoC) 802.3bn, to enable 1G/10G EPON services over HFC networks. As the optical and coaxial transport mechanisms are functionally different, the integration of the two technologies is challenging. Bhumika et al. [50, 51] have discussed the design issues and challenges of the EPoC networks. The MSOs offer several EPoC deployments addressing the challenges in different ways: i) through passive coax, where a fiber coax unit is installed to bridge the optical and coaxial medium, ii) overlay through amplifiers and coax, and iii) overlay through complete HFC network.

Complementary to DOCSIS networks, PON technology also plays a significant role in Digital Subscriber Line (DSL) networks. Mercian et al. [52–54] have presented an approach to control the upstream buffer occupancies at the drop-point devices (DPDs) or the ONUs. In their approach, the DPD, which is similar to a remote node in the MHAv2 architecture is connected to OLT in the headend and schedules up-

stream transmissions for DSL modems which are connected to DPDs. The algorithms discussed in the article can be adapted for DOCSIS 3.1 networks involving OFDM and can be a key step in promoting protocol convergence of DSL with cable access technologies.

2.5.6 Virtualization

Network virtualization allows multiple isolated virtual networks to operate based on one installed physical network [55–58]. Virtualization of network functions can benefit MSOs in many different ways, including reduction in the CAPEX/OPEX, as well as increased flexibility and scalability. Network Function Virtualization (NFV) implements network functions, which were traditionally implemented on proprietary and dedicated hardware devices, such as firewalls and NAT devices, as software entities. NFV can therefore leverage virtualization (i.e., softwarization) of complex functions, such as CCAP, provided there is sufficient processing capacity at the hosting machines in the data centers. Kurtz et al. [59] have discussed important aspects of network virtualization at the headend. More specifically, Kurtz et al. have discussed the importance of virtualizing Cloud DVR, CCAP, OLT and the user interface for set bop boxes for the MSOs. Virtualization of such complex functions would require large memories and high computing processing which can be the limiting factors for NFV implementation. Therefore, hardware acceleration techniques based on NIC, PCI-E, and on-Chip/multi-Chip module accelerators were recommended as potential solutions to efficiently utilize hardware resources for the virtualization.

In the case of R-PHY, the DOCSIS MAC entity can be implemented at the headend or cloud. One of the possibilities to implement the DOCSIS MAC is through virtualization, in contrast to implementation through dedicated hardware. The DOCSIS MAC protocol involves relative complex operations as compared to other MAC

operations, such as Ethernet and PON. A complete DOCSIS MAC module would include data and control plane functions for upstream and downstream, such as encryption/decryption and fragmentation, as well as management functions, such as load balancing, CM control, dynamic flow changes, QoS and subscriber management. Zhang et al. [60] have evaluated the performance of virtualizing DOCSIS MAC in a data center to understand the implications of virtualization. The DOCSIS MAC was virtualized on a generic CPU, and FPGA. Their evaluation showed that the power consumption of an X86 CPU MAC was 24 times higher than a FPGA MAC to achieve the same bandwidth. In addition, the hardware cost of the CPU was about 77 times higher than the cost of the FPGAs. As the hardware supporting the virtualization technologies evolves, the implementation of DOCSIS vMAC in the R-PHY architecture still needs to be thoroughly investigated and improved.

Availability of NFV in the framework of cable infrastructures has been discussed by Bernstein [61]. A VM which implements the NFVs for CMTS can be broadly categorized into non-critical functions, such as hardware or software dependent functions that can be replaced, and critical functions which require minimum packet loss and stateful recovery. Critical functions need to be protected with high availability of the VMs by sharing run-time states and information among the redundant resources. Therefore, NFV needs to be carefully evaluated in terms of both hardware capabilities as well as implementation cost for the high availability network function with redundant hardware components.

2.5.7 SDN

Software Defined Networking (SDN) is a networking paradigm that separates the control and data planes across the network elements. SDN allows for for a wide range of flexibilities and adaptations, while supporting scalable network operation [62–70].

As the number of users increase over the access networks, MSOs face numerous challenges to accommodate their growing demands. The demand for new and interactive services requires regular upgrades of existing infrastructures. In general, there can be thousands of CMTSs and millions of CMs, Set top boxes, and embedded Multimedia Terminal Adapters (eMTAs) connected across access networks to the headend. Provisioning of these devices is certainly a challenging task, especially for the devices that require experienced technical staff at a remote site. Sundaresan [71] has presented benefits and challenges of SDN for MSOs to address the growing number of users and service demands. SDN can leverage the centralized control mechanisms, where all devices are controlled and provisioned through a network operating system hosting the SDN applications at the headend. In the present MSO deployments, CMs are configured with static configuration of services, using the CM configuration file. When a new service needs to be enabled to a CM, the CM configuration file is updated followed by a restart of the CM. Therefore, the CM reconfiguration is currently not scalable, causes outages, and can often lead to human errors. When SDN principles are adapted to the cable network, reconfigurations of the CMs can be conducted on-the-fly, when required.

Dai et al. [72] have discussed the benefits SDN applications for optical access networks which are employed in cable technologies. Other use cases of the SDN in cable networks include management of L2VPN services, DOCSIS 3.1 profile management, such as variable bit loading, and CCAP management abstractions. Patel et al. [73] have presented an implementation of SDN based programmable DOCSIS networks using the Open DayLight Controller (ODL). The DOCSIS network has been functionally divided into application, SDN control, and resource layers for defining the boundaries between application, control, and data planes for SDN. Patel et al. have developed the ODL based PacketCable Multimedia (PCMM) plug-in, i.e., an SDN

application, to demonstrate the control of multimedia QoS management in DOCSIS networks.

OpenFlow based DOCSIS architectures have been investigated in [74, 75]. These architectures are based on an ALien Hardware INtegration Proxy (ALHINP), whereby the DOCSIS access network is abstracted as a wide-area OpenFlow virtual switch. This enables an OpenFlow controller to operate independently with the DOCSIS functions. The proposed mechanisms enable L2 based QoS services for DOCSIS by creating logical flow pipes in OpenFlow enabled network devices. In contrast, an architecture based on SDN and NFV to integrate the heterogeneous access networks has been presented by Nandiraju et al. [76].

2.5.8 Wireless

Mobile broadband has seen unprecedented technology developments to grapple with data and services demands due to the exponential user growth. Advancing wireless technologies are grealty improving the wireless resource utilization [77–81]. At the same time, novel coding mechanisms make wireless communication highly robust [82–91]. Although deployments of small cells can achieve capacity increases and satisfy data demand requirements, backhaul network complexity increases when trying to accommodate small cells. However, access networks that have already been deployed by MSOs, such as the HFC networks for cable access, provide an opportunistic platform to support both small cells and the backhaul. Driven by this motivation, Gambini et al. [92] have presented a Femto-Wireless over Cable (FemtoWoC) architecture. In FemtoWoC, the cable links are terminated at the common Multi-cell Base Station (McBS) processing unit which then jointly processes the signals from small cells connected to the cable networks. The centralized McBS has distinct advantages to address some of the critical challenges of small cell deployments, such as interference

coordination. Additionally, the compounded MIMO channel resulting from the cascade of air-MIMO and cable-MIMO links can be exploited by centralized processing at McBS.

Mehmood et al. [93] have presented a user clustering mechanism based on user channel characteristics for variable bit assignments to maximize the data rates supporting small cell backhaul over coaxial cable. Users are grouped based on similarities in channel characteristics, then bit-loading profiles are independently assigned to each group. The proposed joint grouping and profile assignment algorithm achieves near to optimum performance with low implementation complexity. The resulting high data rates enable coaxial cable to provide high backhaul capacity for small cells.

2.5.9 Energy

Large numbers of network nodes, such as CMTSs and CMs, can be connected to an HFC network. As a result, there can be significant power consumption within the HFC network. A CMTS configuration that maps the physical CMTS ports to downstream/upstream channels for a CM are referred to as Receiver Channel Set (RCS) and Transmitter Channel Set (TCS). Traditionally, the DOCSIS channel bonding connects a CM to the CMTS with multiple upstream and downstream channels based on RCS/TCS configuration such that the peak traffic load at a CM is accommodated by the network. However, when a CM has lower traffic requirements, the aggregated upstream and downstream channels would remain connected and active, leading to energy loss. Zhu [94] has proposed energy-saving algorithms for CMTS and CM such that energy consumption is minimized, independent of large packet delays and number of operational changes. A channel bonding technique groups multiple physical channels into a single logical channel to increase channel capacity for a single CM and to deliver higher data rates. The proposed Dynamic Bonding Change (DBC)

algorithm is targeted to dynamically adapt TCS and RCS configurations based on traffic requirements. More specifically, the DBC algorithm at the CMTS and CM is able to add, delete, and replace upstream and downstream channels assigned to a specific CM such that the network-wide energy consumption is minimized. In another proposed CMTS-side algorithm, a sleep mode is enabled and a shut down performed on the idle or underutilized CMTS ports to conserve energy.

A similar approach for channel bonding with a QoS aware scheduling algorithm has been proposed by Lu et al. [95]. Analytical expressions for the packet delay and power consumption based on M/M/n queuing models and a three dimensional Markov chain were developed. Performance results for the proposed scheduling algorithm showed significant power savings of up to 75% compared to transmitters and receivers being always active at the CMTS and CM.

CHAPTER 3

PERFORMANCE COMPARISON OF VIRTUALIZED R-PHY AND R-MACPHY CABLE ACCESS NETWORK ARCHITECTURES

3.1 Introduction

Cable networks were traditionally designed to carry broadcast television (TV) to a large number of households. However, as the demand for unicast Internet services increased, Cable Modems (CMs) and the Data Over Cable Service Interface Specification (DOCSIS) were introduced to transmit unicast data over the shared broadcast channel in a cable network. Advances in cable technologies have enabled Internet speeds up to 1 Gbps in both the uplink and downlink direction to each CM.

As a result, multi-system operators that operate multiple cable TV systems see unprecedented opportunities for the development of innovative techniques that utilize the already deployed cable infrastructures so as to meet present and future Internet connectivity demands. However, the traditional cable network elements were not developed to be flexible, resulting in increased capital and operational expenditures (CAPEX/OPEX) for installing new infrastructures and upgrading existing infrastructures as technologies advance. Recently, numerous techniques have been proposed to reduce the costs, such as the converged cable access platform (CCAP) and the modular Cable Modem Termination System (CMTS), see Section 4.2.1 and [1–3, 96].

In order to reduce the propagation distances of analog signals in these broadcast cable based Internet access systems there has been a trend to modularize the cable headend processing. Digital signals are then transmitted to the headend processing modules that are distributed to remote nodes placed in close proximity to the CMs; thus analog signals travel only short distances from the headend processing modules to the CMs. Two main competing strategies have recently been proposed: Remote-PHY

(R-PHY), where the physical layer processing for the cable transmission is conducted in distributed remote nodes while the medium access control (MAC) is conducted in a centralized headend location, and Remote MACPHY (R-MACPHY) [2–5], where both physical and MAC processing are conducted in remote nodes.

3.1.1 Related Work

Access networks based on broadcast cable have been extensively studied during the development of the IEEE 801.14 protocol mechanisms, see e.g. [97–108], which subsequently influenced the DOCSIS specification [109–111]. Several studies have evaluated and refined the basic DOCSIS mechanisms. Simulation models for DOCSIS have been developed in [15, 26, 27], while the upstream throughput of DOCSIS 1.1 has been examined in [112–115], and the transmission of MPEG and IPTV video [116–122] on DOCSIS has been considered in [123–125]. Initial dynamic bandwidth allocation designs for Quality of Service (QoS) based grant allocations have been discussed in [19]. A CM can content with other CMs for the upstream transmissions of request messages to the CMTS at the headend. The DOCSIS contention behavior has been examined in [20, 45, 126–129]. In order to resolve the contention, Kuo et al. [21] have presented a priority access based collision resolution scheme for different traffic priorities. Similarly, Heyaime-Duvergé et al. [22] have proposed an application traffic based dynamic bandwidth allocation (DBA) to reduce the control signaling and increase bandwidth utilization. As an improvement to the earlier DOCSIS versions, Liao et al. [23, 24] proposed to adaptively allocate the TCP flow transmission slots by using fast request transmission and long packet deferment techniques. The impact of the DOCSIS MAC protocols on TCP have been further investigated in [25]. DOCSIS simulation models have been presented in [26–28]. All of these prior studies have considered conventional cable access architectures where all headend functions are co-located in the headend.

In contrast, we examine modular cable access architectures in this study, where some headend functions are distributed to remote nodes. Prior studies on modular cable access network architectures have mostly been qualitative in nature, exploring the various features and possibilities opened up by modularizing the cable headend [1, 32–34, 130] We are only aware of one prior quantitative study on modular cable network architectures, namely the study by Chapman et al. [13]. Chapman et al. [13] have presented a preliminary performance analysis of the impact of the CIN distance from the remote node to the headend (CCAP core) in the R-PHY architecture for Poisson traffic. In contrast, we provide a comprehensive performance evaluation of both the R-PHY and R-MACPHY modular cable architectures for both Poisson and bursty self-similar traffic.

The cable DOCSIS MAC protocol is based on the general polling strategy [131–133], which has been mathematically analyzed in various other network contexts, such as passive optical access networks, see e.g., [134–142]. Most mathematical analysis work for cable access networks has focused on the contention of bandwidth requests, see for instance [20, 21, 45, 126–129]. Complementary to these existing mathematical analyses of the bandwidth request contention in cable access networks, we consider the piggybacking of bandwidth requests on upstream data transmissions [143] and focus on the polling MAC dynamics. Specifically, we adapt existing delay analysis strategies for polling to the cable DOCSIS MAC protocol.

3.1.2 Contributions

This article makes two main original contributions to the research on access networks based on broadcast cable networks. First, we adapt mathematical models of polling based medium access control to mathematically analyze the mean upstream data packet delay in cable access networks. In particular, we develop delay models for

the R-PHY and R-MACPHY modular cable architectures. That is, we develop delay models for the R-PHY architecture, which makes upstream MAC decisions in the headend, as well as the R-MACPHY architecture, which makes MAC decisions in the remote nodes.

Second, we conduct an extensive numerical comparison of the throughput-delay performance of the R-PHY and R-MACPHY architectures for a wide range of scenarios. We examine traffic burstiness levels ranging from Poisson traffic to highly bursty self-similar traffic. We consider CIN network distances ranging from tens of miles to 2000 miles, which may arise when conducting the DOCSIS MAC processing in a headend that is virtualized in the cloud. We consider dynamic bandwidth allocation based on Gated grant sizing and Excess sharing grant sizing in combination with offline and double-phase polling (DPP) scheduling, which closely approximates pipelined scheduling.

3.1.3 Organization

Throughout this article, we compare the R-PHY and R-MACPHY modular architectures of access networks based on the broadcast cable medium. Towards this end, this article is organized as follows:

1. Overviews of the architectural and protocol concepts of R-PHY and R-MACPHY are given in Sections 3.2 and 3.3.

2. The end-to-end upstream mean packet delays in the R-PHY and R-MACPHY architectures are analytically modeled in Section 3.4.

3. Numerical performance comparisons based on analytical and simulation results for a wide range of cable network parameters are presented in Section 4.4.

Table 3.1: Summary of Main Acronyms

CCAP	Converged Cable Access Platform (CCAP core implements CMTS headend functions)
CIN	Converged Interconnect Network (between RN and CMTS)
CM	Cable Modem
CMTS	Cable Modem Termination System (DOCSIS cable headend)
DEPI	Downstream External PHY Interface (downstream CCAP core to RPD PWs)
DOCSIS	Data Over Cable Service Interface Specification
MAP	Bandwidth Allocation MAP
PW	Pseudowire (logical link between RN and CCAP core)
RMD	Remote MACPHY Device
RN	Remote Node (either RMD or RPD)
RPD	Remote PHY Device
SG	Service Group (group of CMs)
UEPI	Upstream External PHY Interface (upstream RPD to CCAP core PWs)
vMAC	virtual MAC (implemented in cloud)

The main acronyms used in this article are summarized in Table 4.1.

3.2 Background on Distributed Cable Access Architectures

3.2.1 General Background on Cable Access Networks

3.2.1.1 Converged Cable Access Platform (CCAP)

The Converged Cable Access Platform (CCAP) integrates the physical layer QAM modulators [144] for video and data into an universal QAM for DOCSIS connectivity to the CMs. DOCSIS specifies the MAC [26] and PHY layers for communication between the distributed CMs and the central cable modem termination system (CMTS) at the headend. Traditionally, hybrid fiber coax access networks [145, 146] used analog optical transceivers at the headend to generate amplitude modulated analog optical signals to carry the information over a fiber to a remote analog fiber node which converted the optical signals to radio frequency (RF) signals for transmission over the coaxial cable to the CMs. Limitations of analog transmissions have motivated the development of modular headend architectures with digital transmission over the

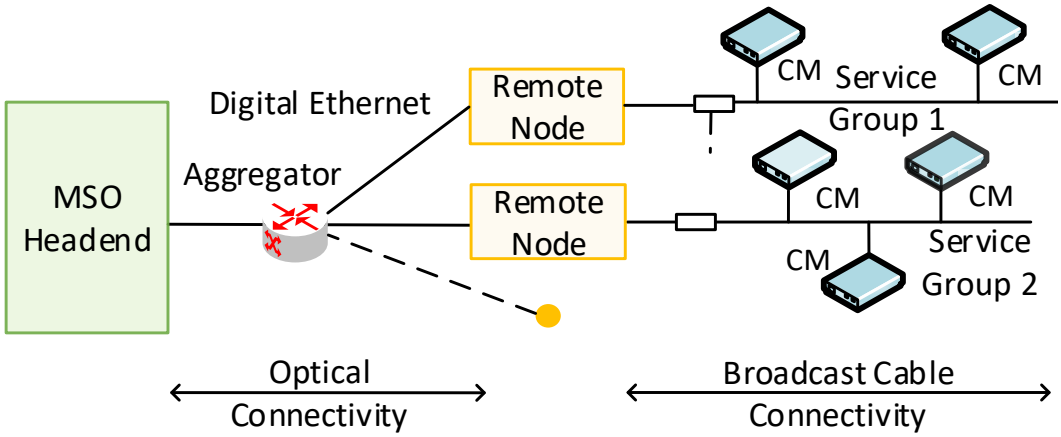

Figure 3.1: The Modular Headend Version 2 (Mhav2) Architecture Moves Some Ccap Functions from the Headend to the Remote Nodes. The Remote Nodes Are Typically Connected to the Headend/CCAP Core via a Digital Ethernet Fiber Network. In the Remote-PHY (R-PHY) Architecture, The Remote Node Implements the Docsis Phy. In the Remote-MACPHY (R-MACPHY) Architecture, the Remote Node Implements Both Docsis Phy And Mac. The R-PHY and R-MACPHY Nodes Serve the Attached Cable Access Networks in Broadcast Mode.

fiber segment from headend to remote node.

3.2.1.2 Modular Headend Architecture (MHA)

The Modular Headend Architecture (MHA) modularizes the CCAP network functions so that the network functions can be distributed among (split between) headend and remote nodes, whereby the headend and remote nodes are connected by a digital fiber, as illustrated in Fig. 4.1. Digital fiber supports long distance transmissions and variants of the 802.3 family of Ethernet protocols, such as Ethernet Passive Optical Networks (EPONs, IEEE 802.3ah, IEEE 802.3av). A secure Layer 2 Ethernet or PON link over a digital fiber connects the remote node to the headend through multiple logical or physical channels, thus forming a digital fiber coax network to the attached CMs [8]. Implementing some CCAP functions in remote nodes near the CMs reduces the analog transmission distances, thus improving the signal to noise ratio at the CMs [7].

Typically, a remote node is located outdoors as a pole-mounted fiber node or remote cabinet and transfers DOCSIS frames between an IP network interface and an RF interface. The centralized functions can be physically implemented in the headend; however, they can also be implemented at a remote site beyond the headend, e.g., in a regional datacenter or in the cloud. The CCAP core at the headend typically consists of all the traditional CMTS function, except for functions implemented at the remote nodes. The network between the CCAP core and the remote node can contain both Layer 2 switches and Layer 3 routers and is commonly referred to as the Converged Interconnect Network (CIN) [6].

3.2.2 Remote PHY (R-PHY) Architecture

The Remote-PHY (R-PHY) [4] architecture implements the DOCSIS PHY layer at the remote node, whereas the DOCSIS upper layers and MAC are centrally implemented at the headend or cloud. More specifically, the R-PHY architecture separates the DOCSIS PHY functions from the traditional CCAP chassis. Separating functions in the CCAP platform can achieve several benefits, such as independent scaling of MPEG video delivery, and flexible management of DOCSIS and out-of-band (OOB) cable transmissions. OOB transmissions use the frequency bands that are mutually exclusive to the bands reserved for the traditional data transmissions. OOB provides auxiliary services, such as Set Top Box (STB) connectivity and management in cable access platforms [147]. The function separation in the CCAP platform makes the software and physical hardware upgrades in the R-PHY architecture modular and independent, resulting in improved availability and manageability [32, 33].

3.2.2.1 R-PHY Internals

The R-PHY architecture separates the CCAP into CCAP core functions that are implemented at a centralized location (e.g., headend or cloud), and into DOCSIS PHY

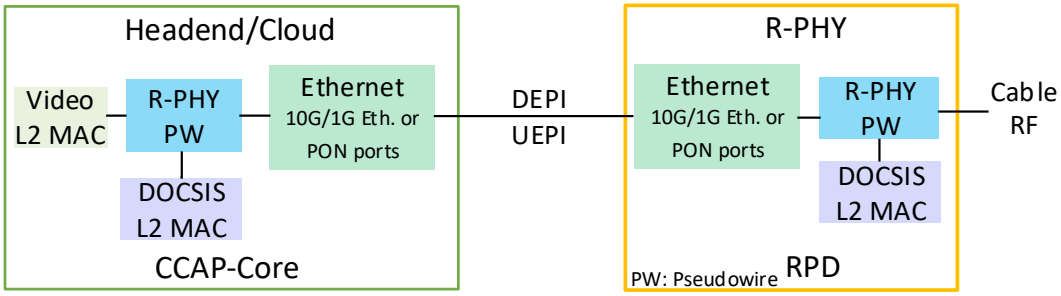

Figure 3.2: R-PHY Architecture: DOCSIS MAC is Implemented at the CCAP Core, Whereas, the DOCSIS PHY is Implemented at a Remote-PHY Device (RPD)

functions that are implemented at the RPD, as shown in Fig. 4.2. The CCAP core in an R-PHY architecture consists of the CMTS for DOCSIS (which in turn consists of the DOCSIS MAC and upper layers) and an edge QAM (EQAM) [146] MAC for video. The DOCSIS upper layers include control signaling functions, downstream and upstream bandwidth schedulers, as well as DOCSIS framing. The RPD connects to the CCAP cores through a network interface and connects to the CMs through an RF interface. An RPD also supports the Layer 1 PHY conversion, Layer 2 MAC conversion, and Layer 3 pseudowires (PWs) [4]. An IP PW is a logical interface, such as an IP tunnel, that seamlessly transports the DOCSIS frames between the CCAP core and the RPD.

The RPD receives the downstream DOCSIS signals from the CCAP core over a digital medium, such as Ethernet or PON. The RPD then essentially functions as a physical layer converter that converts the received digital signals to analog signals for RF transmissions over the coaxial cable. In the upstream direction, the RPD converts the DOCSIS analog signals received from the CMs of a service group (SG) to digital frames. These digital frames are then transported to the CCAP core at the headend/cloud for further processing.

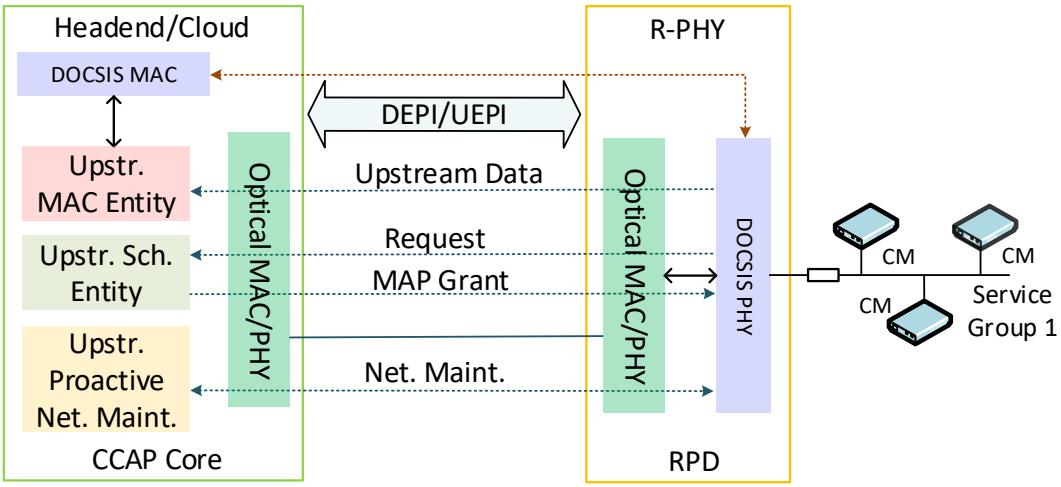

Figure 3.3: DEPI and UEPI Protocol Mechanisms Create Multiple Pseudowires (PWs) between CCAP Core and RPD to Transport the DOCSIS PHY Frames in the Downstream and MAC Frames in Upstream Directions.

3.2.2.2 R-PHY Transport Mechanisms

The Downstream External PHY Interface (DEPI) [148] and Upstream External PHY Interface (UEPI) [149] provide the transport mechanisms between the RPD and the CCAP core. DEPI and UEPI are based on the Layer 2 Tunneling Protocol version 3 (L2TPv3) i.e., RFC 3931 [150]. The L2TPv3 transparently transports Layer 2 protocols over a Layer 3 network creating the PWs. As illustrated in Fig. 4.3, the DEPI consists of multiple PWs between the DOCSIS MAC module at the CCAP core and the PHY module in the RPD so as to create independent paths for signalling and data transmissions between RPD and CCAP core. The signalling transmissions include control frames for setting up, maintaining, and tearing down of sessions. The data transmissions include DOCSIS data frames, video packets, and OOB packets. In addition, the DEPI supports the Packet Streaming Protocol (PSP) [151] for advanced services, such as DOCSIS 3.1. Similar to DEPI, the UEPI also creates PWs between the CCAP core and RPD, supporting independent control and data transmissions in the upstream direction.

More specifically, the downstream operation at the RPD involves DOCSIS framing of the payloads that are extracted from the traffic received by the DEPI interface, the RF modulation of DOCSIS frames, and the RF signal transmissions over the cable interface. When the signal is received from the coax cable in the upstream direction, the operations at the R-PHY include the RF demodulation, the digitization of the received analog RF signals, and the extraction of DOCSIS frames. The resulting frames are then encapsulated by the UEPI for transmissions via the network interface to the CCAP core. In order to support the DOCSIS MAC, the RPD extracts the bandwidth requests from the DOCSIS frames that arrive from the CMs. The RPD then encapsulates and sends the requests with priority over a separate PW. In particular, the routers and switches in the CIN support Differentiated Services Code Points (DSCPs) and can be configured with Per Hop Behaviors (PHBs) [11] such that control signalling traffic is prioritized. That is, the DOCSIS control packet traffic is forwarded with priority to achieve low latency while traversing the CIN [12].

3.2.2.3 R-PHY Variants

The CIN network between CCAP core and RPD is typically either an active Ethernet network or an optical network. The DOCSIS MAC can be implemented either at the headend (i.e., CCAP core) or in remote data centers (i.e., cloud). Additionally, the DOCSIS scheduler can be implemented either at the headend or RPD, i.e., the scheduler could be separated from the MAC [4, Section 10.1, Annex B1]. Thus, a variety of combinations of CIN type, vMAC location, and DOCSIS scheduler location are possible. We consider the DOCSIS MAC and scheduler to be co-located throughout. More specifically, we focus in this study on two common variants of R-PHY with Ethernet CIN: *i*) DOCSIS MAC and scheduling in the headend, and *ii*) DOCSIS MAC and scheduling implemented in the cloud (vMAC).

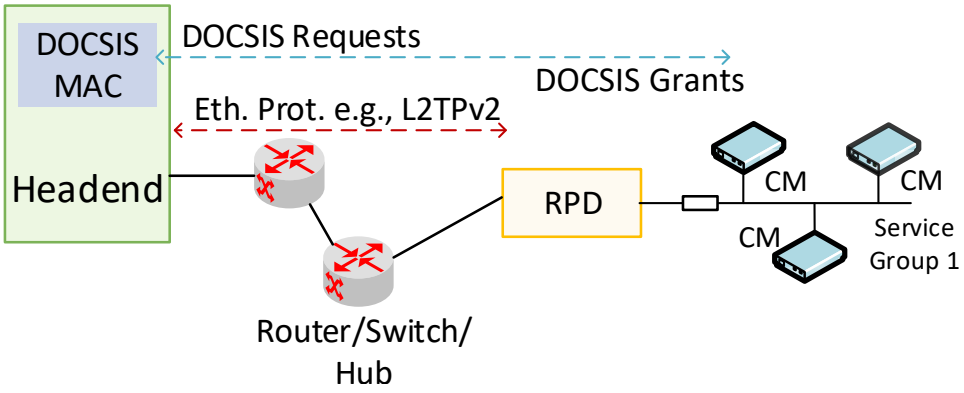

(a) R-PHY with MAC/Scheduling in Headend

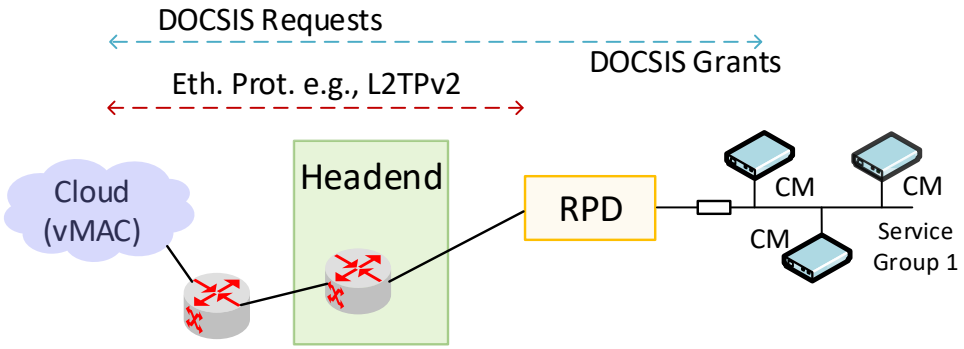

(b) R-PHY with vMAC in cloud

Figure 3.4: (a) R-PHY with Ethernet CIN and MAC/Scheduling in Headend (Section 3.2.2.3): Ethernet Links Provide the CIN Connectivity between the RPD and Headend. The CCAP Core is Located at the Headend and Implements the DOCSIS MAC and Scheduling. (b) R-PHY with Ethernet CIN and vMAC in cloud (Section 3.2.2.3): DOCSIS MAC and Scheduling are Implemented at a Cloud Location. An Ethernet Connection Spans From the Cloud to the RPD, Enabling the Communication between DOCSIS vMAC and RPD.

R-PHY with Ethernet CIN and MAC/Scheduling in Headend The R-PHY with Ethernet variant connects the RPD with the CCAP core through IEEE 802.3 [152] links over switches and routers in the CIN. The CCAP core implements the DOCSIS MAC and scheduler in the headend as show in Fig. 3.4(a). DEPI and UEPI interfaces establish the L2TPv3 tunnels so that the DOCSIS request (REQ) and grant (GNT) control messages traverse the CIN between the CCAP core at the headend and the RPD over prioritized L2TPv2 sessions.

R-PHY with Ethernet CIN and Cloud vMAC The virtualization of the DOCSIS MAC and scheduling in a cloud vMAC effectively shifts the MAC and scheduling implementation to a remote datacenter or cloud. Therefore, the DEPI and UEPI sessions are established between the cloud location and the RPD, as illustrated in Fig. 3.4(b). The headend functions as a switch or router supporting the L2TPv3 mechanisms. The DOCSIS REQ and GNT messages traverse all the way between the remote cloud location and the RPD, resulting in longer request-grant delay compared to an R-PHY with DOCSIS MAC and scheduler at the headend.

3.2.3 Remote-MACPHY (R-MACPHY) Architecture

The Remote-MACPHY (R-MACPHY) architecture moves both the DOCSIS MAC and PHY layers out to the remote node, which is referred to as Remote MACPHY Device (RMD) [153]. The connection between the CCAP core and the RMD is essentially a Layer 2 Ethernet connection. In the downstream direction, an RMD accepts data from a headend L2 aggregation device, i.e., the RMD accepts data, video, and digitized signal sequences from an external OOB converter [3]. In the upstream direction, the RMD collects data from cable modems and set-top boxes (STBs), and forwards the data to the headend and STB control system. Thus, the RMD transparently converts the optical data frames on the headend-to-RMD network to RF data frames on the broadcast cable network and vice versa.

The R-MACPHY design can vary based on the implementation of the remaining CCAP functions, i.e., the CCAP functions that do not belong to DOCSIS CMTS MAC and PHY. These remaining CCAP functions can be either implemented at the headend or in the cloud. Common to all design variants is that the MAC and PHY are implemented on the same RMD physical device.

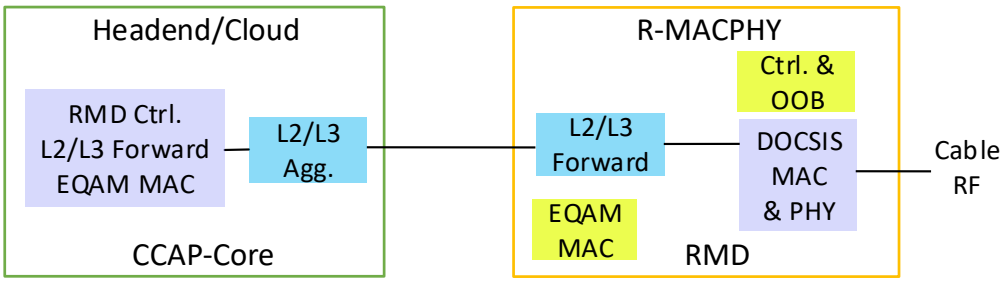

Figure 3.5: Illustration of R-MACPHY Architecture: DOCSIS MAC and PHY are Implemented at the Remote MACPHY Device (RMD). The Upper DOCSIS Layers are Implemented at the Headend

3.2.3.1 R-MACPHY Internals

Figure 4.4 highlights the components that are common to the variety of options. Distributed architectural variations of R-MACPHY can be mainly classified into: *i*) RMD with minimal configuration, i.e., only the DOCSIS MAC is implemented at the RMD, *ii*) RMD with embedded edge-QAM (EQAM) [146], i.e., the MAC for both video and DOCSIS data are implemented at the RMD, *iii*) Remote CCAP (R-CCAP), which implements all CCAP functions at the remote nodes, and *iv*) R-CCAP with centralized controller. Our evaluation considers the implementation of the MAC scheduler at the remote node, which is common to the variations of the R-MACPHY architecture.

3.2.3.2 R-MACPHY Transport Mechanisms

With the DOCSIS MAC implemented at the RMD, only the upper layer (i.e., L3 and above) DOCSIS data must be transported to the CCAP core located at the headend for further processing. The request-grant delay is much shorter compared to R-PHY, since the exchange of REQ and GNT messages occurs over much shorter distances, namely between RMD and CMs. While the RPD in the R-PHY architecture must prioritize the REQ packet transmissions over normal payload data traffic on the CIN,

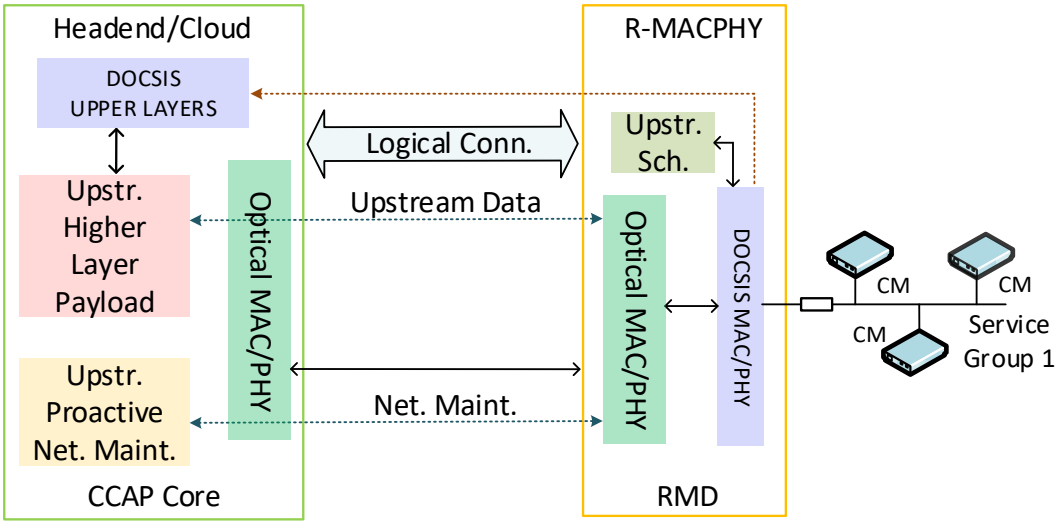

Figure 3.6: A Generic Interface Can Be Used to Transport the DOCSIS Upper Layer Data From RMD to DOCSIS Upper Layers, Which Are Implemented at the CCAP Core.

the RMD does not require any such prioritization.

Typically, the headend and RMD are connected through a Layer 2 digital transport connection over optical fiber. Thus, RMD traffic can be transported by optical Gigabit Ethernet CINs or EPON/GPON CINs [154]. Logical connections, such as L2/L3 tunnels (interfaces) provide transparent flow level connections between RMD and headend, as described in Fig 4.5.

3.2.3.3 R-MACPHY with Ethernet CIN

An Ethernet CIN composed of routers and switches can interconnect the RMD and the headend, i.e., the CIN in Figure 3.7 is composed of an active Ethernet network. The RMD essentially forwards the L2/L3 packets to the CCAP core. A layer 2 or 3 level connection, such as Layer 2 Virtual Private Network (L2VPN) or L2TPv3 is established between the RMD and headend.

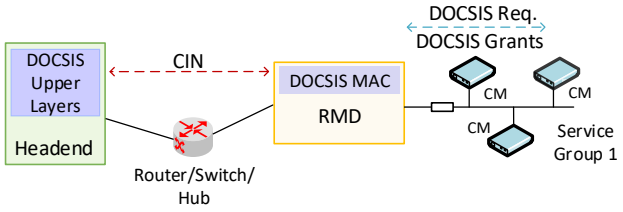

Figure 3.7: DOCSIS Request and Grant Messages Are Exchanged Over Coaxial Cable Between Remote-MACPHY Device (RMD) and CM.

3.3 Distributed Cable Access Protocols

DOCSIS implements a centralized reservation-based allocation of the cable upstream bandwidth for the CM transmissions. Periodically, the headend sends a bandwidth allocation MAP (MAP) to inform attached CMs of the start time and duration of their next upstream transmission windows. Also, the allocation MAP defines the slots available for contention transmission and the slots available for new CMs to join the network [15]. More specifically, CMs can acquire bandwidth for upstream data transmission through requests sent with contention or with piggybacking onto data transmissions. Piggybacking avoids contentions, since the requests are transmitted along with the upstream payload data [22].

3.3.1 Background on Dynamic Bandwidth Allocation

We categorize and identify the dynamic bandwidth allocation (DBA) algorithms in the polling based DOCSIS MAC protocol using the three design dimensions, i) grant scheduling framework which characterizes the event triggering the scheduling and bandwidth allocation as well as the overall structure of the granting and scheduling process, ii) grant sizing policy which determines the size of the upstream transmission window allocated to each CM, and iii) grant scheduling policy which arranges the order of the different scheduled transmission windows [155–158]. A dynamic bandwidth allocation (DBA) algorithm in the DOCSIS scheduler sizes (dimensions) the upstream

transmission windows (grants) based on the reports received by the CMs and sends the grants via MAP messages to the respective CMs.

3.3.1.1 Grant Scheduling Framework

Offline Grant transmission windows are allocated after REPORTs from all CMs have been received at the CMTS. That is, the schedule for the entire granting cycle of CM upstream transmissions is generated when the REPORT message from the last CM is received.

Double Phase Polling (DPP) CMs in a SG are partitioned into two independent DPP groups. Within each DPP group, the granting and scheduling is triggered by the receipt of REPORTs from all CMs in the group. Each DPP group is scheduled independently in an offline manner.

3.3.1.2 Grant Sizing Policy

In DOCSIS 3.1, grant sizes are allocated to the CMs in terms of number of minislots. Each minislot corresponds to a set of specific frequency subcarriers for a specific transmission time duration. An OFDM symbol is the fundamental unit of the minislot, and the number of OFDM symbols for each minislot in a given SG is defined as per the specifications in [143]. The grant sizing policy determines the grant sizes in terms of minislots such that the CM transmissions are orthogonal. By maintaining orthogonality, each CM gets exclusive access (without collisions) to the cable broadcast channel for its upstream transmissions. Effectively, a group of minislots that are reserved for the transmissions of a given CM can be abstracted to a variable transmission (bandwidth) bitrate channel.

The grant sizing policy determines the transmission window size (in terms of number of OFDM minislots) based on the CM upstream transmission request (in

terms of bytes of data queued for upstream transmission). We consider two widely considered grant sizing policies for the comparison of the R-PHY and R-MACPHY architectures:

Gated The Gated grant sizing mechanism grant the CMs their full amount of requested bandwidth [155, 158–160].

Limited with Excess Share Based on the requested transmission windows, the CMs sharing a cable channel are segregated into a group of underloaded CMs and a group of overloaded CMs [161, 162]. A CM is considered to be underloaded if the reported queue size (requested transmission window) is less than or equal to a prescribed maximum grant size divided by the number of CMs. An overloaded CM requested a transmission window larger than the maximum grant size. In the excess share mechanism, the total excess bandwidth is the sum of the remaining (unused) bandwidth of all underloaded CMs, which is then shared by the overloaded CMs. The grant for an overloaded CM becomes the maximum grant size plus the share of the total excess bandwidth divided by the number of overloaded CMs.

3.3.1.3 Grant Scheduling Policy

The grant scheduling policy determines how multiple CM transmission windows (minislots) are arranged during a granting cycle. We employ the Shortest Propagation Delay First (SPD) scheduling policy [163] which arranges the CM grants in ascending order of their round-trip propagation delay from the MAC module. In particular, we follow a hybrid allocation of minislot resources [164] across the frequency and time dimensions such that the earliest available (in the time dimension) minislots are allocated in a greedy manner to the CMs with the shortest round-trip propagation delays.

3.3.2 UEPI Pseudowire (PW) Overhead Evaluation

The R-PHY architecture incurs overhead for two reasons: *i*) UEPI protocol on CIN, as well as *ii*) REQ and maintenance frames. In contrast to the R-PHY architecture, the R-MACPHY architecture implements the DOCSIS MAC at the remote node. Thus, the R-MACPHY architecture does not need additional CIN transport mechanisms through UEPI interfaces and PWs. Therefore, the R-MACPHY does not experience the PW overheads for transporting the data information blocks from the remote node to the headend for the upper layer processing. In the remainder of this section, we evaluate the UEPI PW overhead incurred in the R-PHY architecture.

The RPD receives the upstream analog RF transmissions from the CMs in terms of DOCSIS frames over the cable link. These DOCSIS frames are processed to extract the REQ message and data payload. The UEPI protocol establishes multiple PWs for the transport of DOCSIS frame information to the headend (vMAC) with different priorities. The UEPI protocol uses standard IEEE 802.3 based Ethernet as the underlying technology for the transport of the DOCSIS frames in the digital format to the headend. For each UEPI packet, the 802.3 Ethernet header is 22 bytes, the IPv4 header is 20 bytes, the L2TPv2 header is 4 bytes, the Packet Streaming Protocol (PSP) subheader is 4 bytes, and the CRC is 4 bytes, resulting in a total overhead of 54 bytes per Ethernet frame. Thus, the overhead factor $\mathcal{O}$ due to the UEPI protocol for each Ethernet frame can be evaluated as $\mathcal{O} = 54/\mathcal{E}$, where, $\mathcal{E}$ is the Ethernet frame size. Although CableLabs specifications define the UEPI protocol, the actual framing of UEPI packets is implementation specific.

A given DOCSIS frame is typically mapped to several UEPI packets, separating payload data and REQ information for prioritization. Additionally, payload data

and REQ information are mapped to UEPI packets based on the criteria of minimum and maximum UEPI Ethernet frame sizes. That is, large information blocks, such as payload data may be fragmented, and short information blocks, such as REQs, may be opportunistically aggregated across several SGs to conform with the prescribed minimum and maximum Ethernet frame sizes. Therefore, an accurate estimation of the overhead requires detailed knowledge of the distribution of the UEPI packet sizes resulting from the Ethernet frame sizes $\mathcal{E}$. For UEPI packets based on the maximum Ethernet frame size $\mathcal{E}_{\max}$ = 1900 bytes [149], the overhead factor is $O_{\min}^{\text{UEPI}}$ = 54/1900 = 0.02842, i.e., the overhead is 2.8 % of the UEPI frame. Note that this is the overhead due to the UEPI interface, which is specific to R-PHY. For smaller Ethernet frame sizes $\mathcal{E}$ and correspondingly smaller UEPI packets, the overhead O^{UEPI} increases proportionally. For instance, for $\mathcal{E}$ = 950 bytes, the overhead is O^{UEPI} = 5.7 %, while for $\mathcal{E}$ = 425 bytes, the overhead due to UEPI climbs to O^{UEPI} = 11.4 %. Note that this overhead due to UEPI affects only the transmission over the CIN, which has typically abundant transmission bit rate R_i, compared to the transmission bit rate of the cable network R_c. Therefore, the overhead due to UEPI is negligible when the cable network is the bottleneck.

In terms of the overhead due to DOCSIS REQ and maintenance frames over the CIN link, an entire UEPI packet carrying a single (or multiple) REQ(s) and maintenance frames can be considered as an overhead on a given CIN link. However, evaluating how many UEPI packets would carry REQ and maintenance frames within a given time duration is complex. The complexity arises from the required estimation of the UEPI packet size distribution. In an actual deployment, the UEPI interface implementation decides the UEPI packet size distribution. We model the number UEPI packets with the variables $P_{\text{data}}^{\text{UPEI}}$ and $P_{\text{non-data}}^{\text{UPEI}}$ denoting the number of UEPI packets required to carry the data, as well as the request and maintenance information

blocks within one t_{MAP} duration, respectively. The total number of UEPI packets P^{UPEI} required to transport the DOCSIS PHY frames to the vMAC at the headend within a single t_{MAP} duration is, $P^{\text{UPEI}} = P^{\text{UPEI}}_{\text{data}} + P^{\text{UPEI}}_{\text{non-data}}$. With $\mathcal{E}^{\text{non-data}}$ and $\mathcal{E}_{\text{avg}}$ denoting the average frame sizes of the non-data UEPI packets and all UEPI packets (i.e., inclusive of data and non-data packets), respectively, the overhead $\mathcal{O}^{\text{RM}}$ from the REQ and maintenance UEPI packets on the CIN link, for a single t_{MAP} duration is

$$\mathcal{O}^{\text{RM}}_{\text{avg}} = \frac{P^{\text{UPEI}}_{\text{non-data}} \times \mathcal{E}^{\text{non-data}}_{\text{avg}}}{(P^{\text{UPEI}}_{\text{data}} + P^{\text{UPEI}}_{\text{non-data}}) \times \mathcal{E}_{\text{avg}}}. \tag{3.1}$$

The utilization impact of REQ and maintenance frames over the CIN link can be estimated as

$$\mathcal{U}^{\text{RM}}_{\text{avg}} = \frac{P^{\text{UPEI}}_{\text{non-data}} \times \mathcal{E}_{\text{max}}}{R_i \times t_{MAP}}. \tag{3.2}$$

Suppose we consider the maximum UEPI Ethernet frame, i.e., 1900 bytes, the CIN data rate $R_i = 1$ Gbps, and one REQ frame corresponding to one SG in the duration of $t_{MAP} = 2$ ms. The resulting utilization $\mathcal{U}_{\text{RM}}$ of the CIN link for a single REQ and maintenance frame is $(1 \times 1900)/(1 \times 10^9 \times 0.002) = 9.5 \times 10^{-4}$, which is a very small fraction of the CIN link capacity R_i. Thus, the overheads due to conducting the DOCSIS MAC REQ and maintenance in the R-PHY architecture over the CIN are essentially negligible.

3.4 DOCSIS Cable Polling Delay Analysis

This section presents a delay analysis of the DOCSIS polling protocol for upstream transmissions over the cable broadcast network. To the best of our knowledge, prior delay analyses of the DOCSIS protocol have mainly focused on the contention of bandwidth request (REQ) messages on the contention slots of the upstream MAC frames [20, 21, 45, 126–129]. We consider piggybacking of the REQ messages on upstream data transmissions; thus, contention does not arise in our model (future work

Table 3.2: Model Parameters

	Network Structure
R_c	Cable upstream transmission bit rate [bit/s] (CM to Remote Node (RN)) = 1 Gbps
R_i	CIN upstream transmission bit rate [bit/s] (RN to headend/cloud) = 10 Gbps
M	Number of CMs at considered RN
δ	One-way propagation delay from a CM to RN [s]
τ	One-way propagation delay between headend/cloud and RN [s]
$t_{\mathrm{M}p}^{\mathrm{R}-PHY}$	$= \delta + \tau + t_{\mathrm{MAP}}/2$; Mean MAP and prop. delay for one-way R-PHY network polling traversal, see Eq. (3.3)
$t_{\mathrm{M}p}^{\mathrm{R-MAC}}$	$= \delta + t_{\mathrm{MAP}}/2$; Mean MAP and prop. delay for one-way R-MACPHY network polling traversal
	Traffic Model
λ_c	Total packet generation rate [packets/s] of the M CMs at considered RN
λ_i	Base packet generation rate [packets/s] for CIN
$\bar{L}$	Mean packet size [bit]
σ_L^2	Variance of packet size [bit^2]
ρ_c	$= \bar{L}\lambda_c/R_c$ Relative cable traffic load (intensity) [unitfree]
ρ_i	$= \bar{L}\lambda_i/R_i$ Relative CIN base traffic load (intensity) of CIN [unitfree]
	Polling Protocol
t_{MAP}	Duration of bandwidth allocation MAP = 2 ms
G_n	Size of upstream transmission window [bit] granted to considered CM (or group of CMs) in cycle n
Z	Polling cycle duration [s]

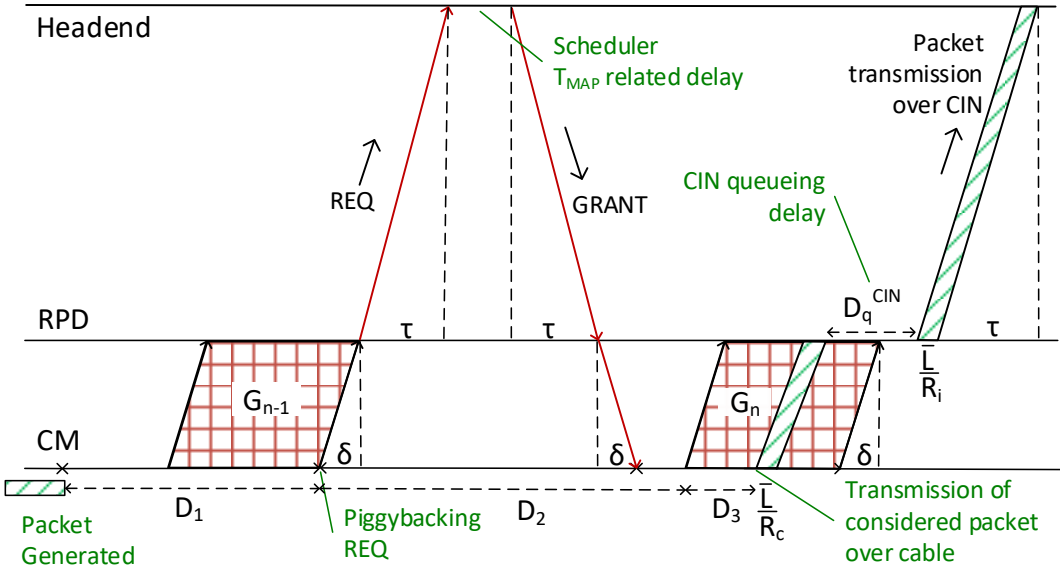

Figure 3.8: Illustration of Polling Cycle Timing for Cable Modem (CM) in R-PHY Architecture.

could combine prior contention models with our polling model). Polling protocols have been extensively analyzed for access networks based on passive optical networks (PONs), see e.g., [134–142].

3.4.1 Polling in R-PHY Architecture

In this section we present a basic timing analysis of the R-PHY bandwidth polling and upstream transmission dynamics. The goal of this timing analysis is to capture the main aspects of the DOCSIS protocol [143, Section 7.2] that govern the upstream transmission delays. Specifically, our goal is to gain insights into the elementary polling dynamics in the R-PHY architecture. For tractability, we focus on a single CM that is attached via a single RPD to a headend. We consider the Gated bandwidth allocation (grant sizing), which grants the CM its full request. Figure 3.8 illustrates the cyclical polling protocol exchanges between the considered CM and the DOCSIS MAC implemented at the headend (or cloud in the vMAC variant). In a given cycle, the headend sends a MAP message that is forwarded by the RPD

to the attached CM. As illustrated in Figure 3.8, the CM send its requests via the RPD to the headend/cloud, where the DOCSIS bandwidth allocation decisions are made. The corresponding grant is sent in a MAP message from the headend/cloud via the RPD to the CM. The CM in turn transmits its upstream data as instructed and piggybacks its next bandwidth request. In detail, a generated packet is reported via request that is piggybacked on the CM upstream payload data transmission and forwarded by the remote PHY device (RPD) via the prioritized UEPI pseudowire (PW) for request (control) traffic to the headend. The headend allocates bandwidth and communicates the allocation via the MAP/grant DEPI to the RPD and onwards to the CM. According to the scheduled bandwidth allocation in the MAP, the CM sends its payload data, including the considered packet, upstream to the RPD. The RPD sends the data via the upstream data UEPI over the CIN to the headend.

3.4.1.1 One-way R-PHY Network Traversal Delay

As ground work towards modeling the upstream packet delay, we first model the round-trip propagation delay of the R-PHY network as twice the one-way R-PHY network traversal delay $t_{\mathrm{Mp}}^{\mathrm{R-PHY}}$. In particular, we define for convenience (to reduce clutter) $t_{\mathrm{M}p}^{\mathrm{R-PHY}}$ as the constant delay components due to physical propagation over the cable and CIN network, plus half the MAP period t_{MAP}. We consider half the t_{MAP} to model that a given arbitrary data packet may be generated at any (uniformly distributed) time instant during the MAP period. Thus, the packet experiences on average half the MAP period as delay from packet generation to next reporting. We apply similar reasoning for the grant transmission from headend to CM and then the actual CM data transmission. That is, we model that the propagation delays across the CIN and cable network are not specifically synchronized to the MAP periods, which appears realistic for real deployments with varying propagation delays. Thus, we include half the t_{MAP} for each transmission in a given direction over the network,

resulting in the mean one-way R-PHY network traversal delay

$$t_{\mathrm{Mp}}^{\mathrm{R-PHY}} = \delta + \tau + \frac{t_{\mathrm{MAP}}}{2}. \tag{3.3}$$

We neglect the overhead due to the transmission delay of the request message over the cable and the CIN network in this analysis (but consider the request message transmission delays in the simulations in Section 4.4). Also, we assume that the request UEPI has negligible queueing delay in the RPD. Moreover, we neglect the schedule computation delay in the headend. For a refined analysis these neglected delay components could be included in refined model for the network traversal delay $t_{\mathrm{Mp}}^{\mathrm{R-PHY}}$.

3.4.1.2 Polling Cycle Duration

The polling cycle corresponds to the round-trip propagation delay from CM to headend and back to the CM for the request and grant as well as the transmission time for the accumulated generated traffic over the cable link to the RPD, i.e., transmission time G_n/R_c for an accumulated data amount G_n. With the modeling of the one-way R-PHY network traversal delay in Eqn. (3.3), the mean cycle duration $E[Z]$ follows from [135, Eqn. (7)]:

$$E[Z] = \frac{2t_{\mathrm{Mp}}^{\mathrm{R-PHY}}}{1-\rho_c}. \tag{3.4}$$

Note that the mean cycle duration is governed by the load (traffic intensity) on the cable network and is independent of the load on the CIN network. This is because the request and grant messages are transmitted with priority over the respective UEPI and DEPI CIN PW links. If these PWs achieve negligible transmission and queueing delays for the request and grant control messages over the CIN (relative to the round-trip propagation delay $t_{\mathrm{Mp}}^{\mathrm{R-PHY}}$ and the cable upstream data transmission delay G_n/R_c), then the CIN load has no significant effect on the cycle duration.

3.4.1.3 Upstream Packet Delay Components

We adapt the general polling protocol analysis from [135] to the R-PHY polling as illustrated in Figure 3.8. Following [135], we define the delay from the instant of packet generation to the piggybacked reporting at the end of the next upstream transmission as D_1. This delay D_1 corresponds to the residual life time of the polling cycle. According to general residual life time analysis [165, p. 173], the mean residual life time is

$$E[Z] = \frac{E[Z^2]}{2E[Z]}. \tag{3.5}$$

Applying Eqn. (3.5) to our setting by re-tracing the steps leading to [135, Eqn. (35)] gives the mean of delay component D_1 as:

$$E[D_1] = \frac{t_{\text{Mp}}^{\text{R–PHY}}}{1-\rho_c} + \frac{\rho_c}{2R_c(1-\rho_c^2)}\left(\frac{\sigma_L^2}{\bar{L}} + \bar{L}\right). \tag{3.6}$$

We define the delay component D_2 as the time period between the CM report transmission and the beginning of the corresponding upstream data transmission. The delay component D_2 models the mean round-trip propagation delays (including the MAP delays) for the request from CM to the headend and the corresponding grant (MAP) from the headend to the CM. Accordingly,

$$E[D_2] = 2t_{\text{Mp}}^{\text{R–PHY}}. \tag{3.7}$$

The delay component D_3 models the time period from the starting instant of the cable upstream data transmission that contains the considered packet to the starting instant of the transmission of the considered packet. This D_3 delay corresponds to the transmission delay of the packets that were generated for the upstream transmission in cycle n before our considered packet. This time period of packet generation

for cycle n before our packet corresponds to the backward recurrence time of a cycle. This backward recurrence time and the mean residual lifetime are equivalent for the considered steady state operation [166, Chapter 5.5]. That is, this packet generation time period has mean duration $E[Z^2]/(2E[Z])$, see Eqn. (3.5), during which packets are generated at rate λ. Each of the generated packets requires a mean transmission time of $\bar{L}/R_c$ over the cable link. Thus, the mean of delay component D_3 is

$$E[D_3] = \frac{\lambda \bar{L} E[Z^2]}{2R_c E[Z]} = \rho_c E[D_1]. \tag{3.8}$$

In addition to the delay components D_1, D_2, and D_3, the considered packet incurs the upstream transmission delay over the cable $\bar{L}/R_c$, the queueing delay D_q^{CIN} for the CIN transmission, the transmission delay over the CIN $\bar{L}/R_i$, and the one-way propagation delay $t_{\text{Mp}}^{\text{R-PHY}}$. Modeling the CIN queue with an M/G/1 model, we obtain for the mean waiting time in the CIN queue:

$$E[D_q^{\text{CIN}}] \;=\; \frac{\rho_i \left(\frac{\sigma_L^2}{\bar{L}} + \bar{L} \right)}{2R_i(1-\rho_i)}. \tag{3.9}$$

Combining all delay components, we obtain for the overall mean packet delay:

$$\begin{aligned} E[D] = {} & 2t_{\text{Mp}}^{\text{R-PHY}} \frac{2-\rho_c}{1-\rho_c} + \bar{L}\left(\frac{1}{R_c} + \frac{1}{R_i}\right) \\ & + \frac{1}{2}\left(\frac{\sigma_L^2}{\bar{L}} + \bar{L}\right)\left(\frac{\rho_c}{R_c(1-\rho_c)} + \frac{\rho_i}{R_i(1-\rho_i)}\right). \end{aligned} \tag{3.10}$$

3.4.2 R-MACPHY Timing Analysis

The R-MACPHY polling cycle starts with when piggybacked CM request reaches the remote R-MACPHY (RMD) node via the cable link. The RMD processes the request and grants the bandwidth allocation to the CM. After the corresponding data packet transmission has reached the RMD, the packet is queued for CIN upstream transmission, and then transmitted from the RMD to the headend. The R-MACPHY

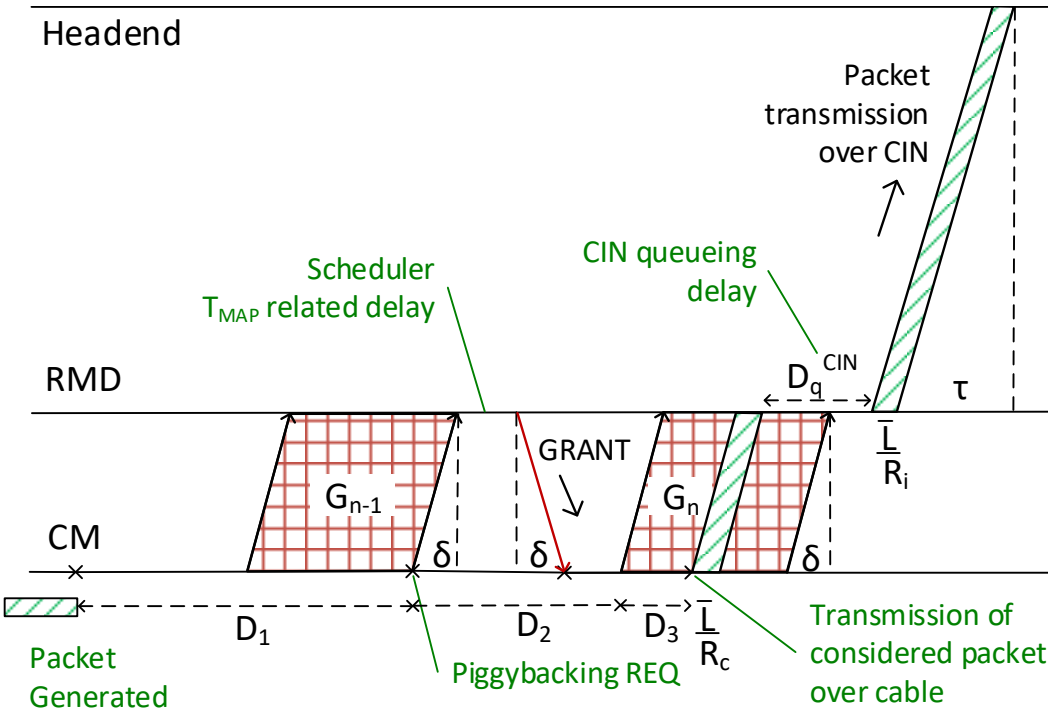

Figure 3.9: Illustration of Polling Cycle Timing for R-MAC Architecture

polling cycle includes only the propagation delay of the cable link δ, as illustrated in Figure 3.9. The potentially long propagation delay τ from the remote node to the headend does not arise for the R-MACPHY polling. Thus, we set the one-way propagation delay for the R-MACPHY polling analysis to $t_{\mathrm{Mp}}^{\mathrm{R-MAC}} = \delta + t_{\mathrm{MAP}}/2$. The R-MACPHY polling dynamics are essentially the same as for the R-PHY architecture and we can re-trace the R-PHY delay analysis with the shorter $t_{\mathrm{Mp}}^{\mathrm{R-MAC}}$ to obtain the mean packet delay for R-MACPHY. However, this re-traced analysis does not include the one-way CIN propagation delay τ. Thus, the total mean delay for R-MACPHY is the delay expression (3.10), evaluated with $t_{\mathrm{Mp}}^{\mathrm{R-MAC}} = \delta + t_{\mathrm{MAP}}/2$ plus the one-way CIN propagation delay τ.

3.4.3 R-PHY vs. R-MACPHY Analysis Comparison

For low traffic loads $\rho_c \to 0$, $\rho_i \to 0$, the mean R-PHY packet delay (3.10) approaches

$$\lim_{\rho_c \to 0, \rho_i \to 0} E[D^{\text{R-PHY}}] = 4\left(\delta + \tau + \frac{t_{\text{MAP}}}{2}\right) + \frac{\bar{L}}{R_c} + \frac{\bar{L}}{R_i}. \tag{3.11}$$

In contrast, the mean R-MACPHY packet delay approaches

$$\lim_{\rho_c \to 0, \ \rho_i \to 0} E[D^{\text{R-MAC}}] = 4\left(\delta + \frac{t_{\text{MAP}}}{2}\right) + \tau + \frac{\bar{L}}{R_c} + \frac{\bar{L}}{R_i}. \tag{3.12}$$

Thus, R-MACPHY reduces the mean packet delay at low loads by 3τ compared to R-PHY. Recall that the parameter τ represents the one-way CIN propagation delay. Thus, for a given CIN infrastructure, the parameter is constant. However, when comparing different CIN options, the parameter τ is variable. The range of the parameter τ corresponds directly to the CIN one-way propagation distance. Additional delays may be incurred on the CIN due to queueing and store-and-forward in intermediate switches.

Although we focus on upstream data packet transmission in this study, we briefly note that both R-PHY and R-MACPHY have essentially equivalent downstream packet delays. The downstream delay is mainly composed of the CIN queueing delay, which can be modeled analogous to Eqn. (3.9), the packet transmission delays over the CIN and cable networks, plus the one-way network traversal delay $t_{\text{M}p}$ (3.3).

3.5 Numerical Performance Comparison

3.5.1 Simulation Setup

3.5.1.1 Overview

We developed a simulation model of the link layer DOCSIS protocol operating in the R-PHY and R-MACPHY architectures using the discrete event simulator OMNET++. We simulate the broadcast cable based access network illustrated in Fig. 4.1 for a single remote node serving one SG of multiple CMs. The digital Ethernet CIN

network between the simulated remote node and the headend is loaded by the traffic from the simulated remote node as well as a CIN base traffic load ρ_i. The CIN base traffic load ρ_i could originate from other remote nodes (servicing other SGs) or from other access networks. We focus on simulating one remote node with its attached CMs in detail in order to gain insights into the polling dynamics with a remote node operating as either a Remote PHY node (RPD, see Fig. 4.3) or a Remote MACPHY node (RMD, see Fig. 4.5).

Although DOCSIS 3.1 can support different QoS levels for different applications [41], we focus on best-effort service [167] in this first comparative evaluation of the R-PHY and R-MACPHY architectures. Moreover, we focus on the DOCSIS data services and do not consider EQAM video services.

3.5.1.2 Cable Network

For typical broadcast cable deployment scenarios, the average number of HouseHolds Passed (HHP) for a given remote node can be up to 450 CMs, which may belong to several SGs. A typical average number of CMs connected to a remote node is around 200 CMs [168]. A given set of physical resources are commonly shared among all the CMs in a given SG. The resource allocation to each individual CM in a given SG is controlled by the scheduler (see Sec. 4.3.3). Under high utilization scenarios the number of CMs per SG can reach up to 400 CMs [169]. Therefore, we consider SG sizes $\boldsymbol{M}$ ranging from 200 to 400 CMs in our simulations.

The recent DOCSIS 3.1 version supports both upstream and downstream data peak throughputs on the order of Gbps [17]. DOCSIS 3.1 includes Orthogonal Frequency Division Multiplexing (OFDM) for the physical layer modulation over the broadband spectrum to achieve high spectral efficiency [16, 170, 171]. DOCSIS 3.1 also incorporates high levels of QAM modulation (up to 16K), Low Density Parity

Check (LDPC) Forward Error Correction (FEC), and a wide spectrum of 1.2 GHz in the downstream and 204 MHz in the upstream [16]. We set the transmission bit rate of the cable uplink channel to R_c = 1 Gbps. The upstream transmissions from all CMs attached to the remote node share the upstream cable transmission bit rate R_c.

The distance from the CMs to the remote node, i.e., the RPD or RMD, can be estimated based on the number of Actives (RF amplifiers) in the cable link. Typically, a single coaxial broadcast cable segment can run up to a distance of 600–900 feet. Additionally, there can be a cascade depth of 4 to 5 Actives from a remote node to the CMs. Five Actives support five coaxial segments reaching up to the distance of, say, 5×600 = 3000 feet in total. We consider the CM-to-remote node one-way distance to be uniformly distributed between 1 and 2 km in our simulations and set the one-way cable propagation delay δ accordingly.

Throughout, we assume that 20 % of the cable transmission bit rate R_c is occupied with contention and maintenance slots. Thus, only 80 % of the cable transmission bit rate R_c are available for data transmissions. In each cycle, each CM sends a request message of 64 bytes upstream in piggybacked manner to communicate its queue occupancy to the MAC module.

3.5.1.3 CIN Network

We vary the CIN distance from the remote node (RPD or RMD) to the headend from 10 to 2000 miles, considering that a WAN digital Ethernet link can span for long distances to cloud locations. In our simulations, we model the logical Ethernet CIN link over the CIN network as an infinite-sized queue that is drained by a link with transmission bit rate R_i = 10 Gbps and has one-way propagation delay τ leading to the headend.

3.5.1.4 Traffic Model

Following widely used traffic models for access networks, we consider self-similar traffic [172]. We vary the level of burstiness of the self-similar traffic from Hurst parameter value $H = 0.5$, corresponding to Poisson traffic, to $H = 0.925$, which corresponds to highly bursty traffic. Each CM independently generates self-similar data packet traffic, whereby the packet sizes are distributed as follows: 60 % 64 byte packets, 4 % 300 byte packets, 11 % 580 byte packets, and 25 % 1518 byte packets, i.e., the mean packet size is $\bar{L} = 494$ bytes. Initially, we assume that each CM has unlimited buffering, i.e., there are no losses and the long-run throughput is equal to the offered traffic load (for the considered stable network operating scenarios); finite CM buffers are considered in Section 3.5.5. We vary the aggregate data packet generation rate λ_c of the CMs attached to the simulated remote node to achieve prescribed levels of cable network traffic (load) intensity $\rho_c = \lambda_c \bar{L}/R_c$ (see Table 3.2). All CMs at the simulated remote node contribute equally to the aggregate packet generation rate λ_c.

We load the CIN network with a base traffic load $\rho_i = \lambda_i \bar{L}/R_i$ that we keep fixed at $\rho_i = 0.5$ for $R_i = 10$ Gbps throughout the evaluations presented in this section. This CIN base traffic has always the same Hurst parameter as the traffic in the cable network. Note that the total CIN traffic load is the base CIN load plus the traffic from the one simulated cable network, i.e., the total CIN traffic intensity is $(\lambda_c + \lambda_i)\bar{L}/R_i$.

3.5.1.5 Performance Metrics

We define the packet delay as the time period from the time instant of packet generation at a CM to the time instant of the complete packet delivery to the headend (CCAP core). The average of the packet delays sampled from over 300 s of simulated

network operation forms the mean packet delay reported in Sections 4.4.2– 4.4.4. The packet loss rate considered in Section 3.5.5 is defined as the long-run ratio of the number of lost packets to the number of generated packets.

3.5.2 Offline Scheduling with Gated Bandwidth Allocation

Initially, we cross-validate the analytical delay model from Section 3.4 with the simulation model. We consider offline scheduling with Gated bandwidth allocation, see Section 4.3.3. A single CM generating Poisson traffic is attached to the considered RPD/RMD.

3.5.2.1 Single Cable Modem (CM) with Poisson Traffic

Fig. 3.10 shows the mean packet delay of the R-PHY and R-MACPHY networks as a function of the traffic intensity ρ_c on the cable upstream link. More specifically, Figs. 3.10(a), (b), and (c) consider relatively short one-way CIN distances between the RPD/RMD and the headend of 12.5, 50, and 100 miles. The 50 miles distance corresponds to the CM-to-CMTS distance for conventional (non-modular) DOCSIS 3.1 networks [143], while DOCSIS 3.0 has a limit of 100 miles [173]. The longer distances of 500, 1000, and 2000 miles, which arise with cloud vMAC operation, see Section 3.2.2.3, are considered in Figs. 3.10(d), (e), and (f). We observe from Fig. 3.10(a) that the analytical model has relatively large deviations from the simulations for the very short CIN distance of 12.5 miles. These discrepancies appear to be due to our assumption that each traversal across the network incurs the $t_{\mathrm{M}p}$ delay due to physical propagation and the waiting time until the next MAP period (whereby the MAP period is denoted by t_{MAP}), see Section 3.4 and in particular Eqn. (3.3).

In order to examine the impact of this assumption we have varied the factor associated with $t_{\mathrm{M}p}$ in Eqn. (3.10) as well as the divisor of t_{MAP} in Eqn. (3.3). We

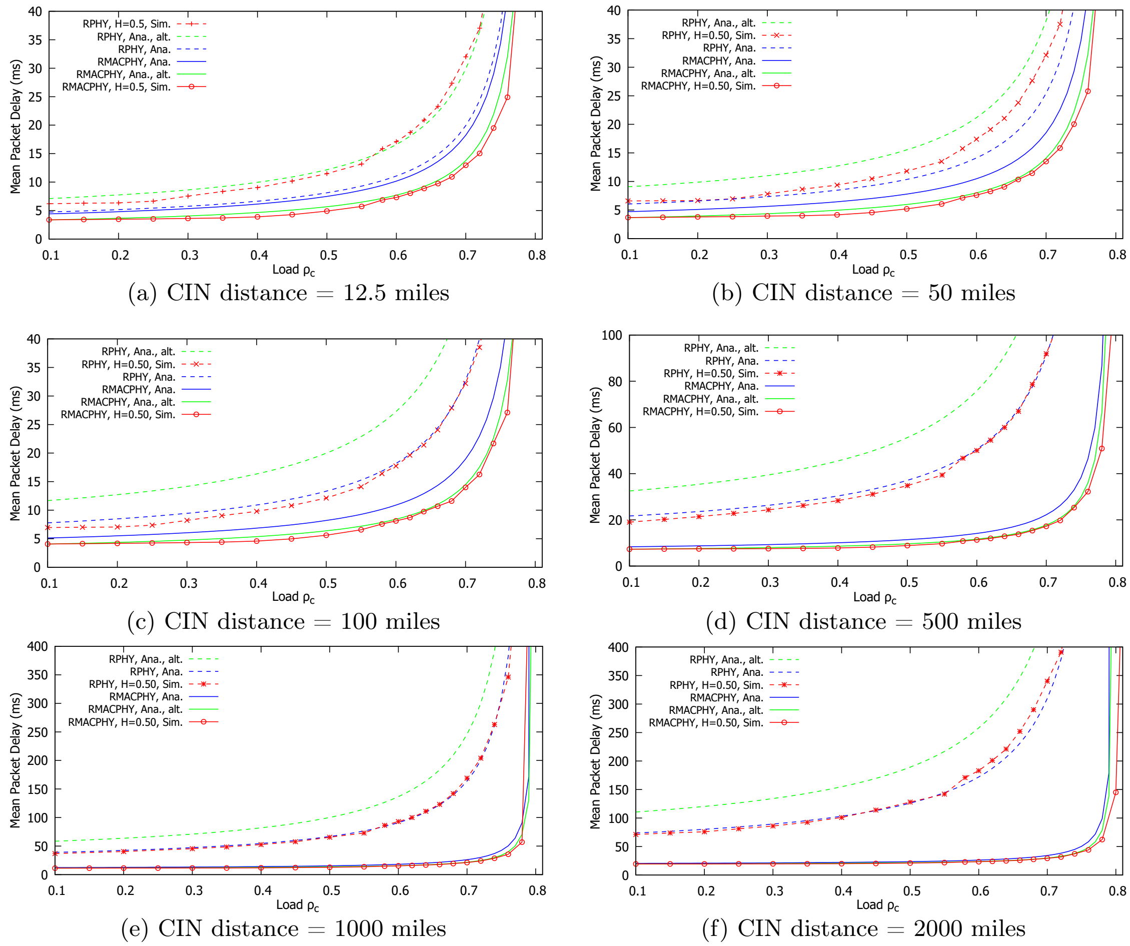

(a) CIN distance = 12.5 miles

(b) CIN distance = 50 miles

(c) CIN distance = 100 miles

(d) CIN distance = 500 miles

(e) CIN distance = 1000 miles

(f) CIN distance = 2000 miles

Figure 3.10: R-PHY vs. R-MACPHY Mean Packet Delay as a Function of Cable Link Traffic Intensity ρ_c for CIN One-Way Distances Ranging From 12.5 to 2000 Miles; Fixed Parameters: CIN Base Traffic Intensity $\rho_i = 0.5$, One CM, Gated Bandwidth Allocation, 20 % of Cable Capacity for Contention and Maintenance.

found that alternate factors/divisors may lead to a closer match between analysis and simulation. Specifically, we found that the combinations of factor 3 and divisor 2 for R-PHY, as well as factor 3 and divisor 4 for R-MACPHY, which are plotted as "alt." in Fig. 3.10 give relatively close matches for the short CIN scenarios. The improvement in accuracy with these alternate factors/divisors is likely due to a particular alignment of the MAP period boundaries with the typical arrival and dispatch times of control messages. That is, these alignments are possibly not uniformly random, but follow some different distribution. Future research could further explore

the underlying reasons for these modeling discrepancies in more detail. However, we note that the discrepancies have relatively small magnitude and are visible only for short CIN scenarios. Importantly, we observe from Fig. 3.10(c) for the longer 100 miles CIN distance and particularly from Figs. 3.10(d), (e), and (f) for the distances above 100 miles that the analytical and simulation models achieve relatively close correspondence.

We observe from the initial evaluation results in Figs. 3.10(c)–(f) that R-MACPHY achieves significantly lower mean packet delays than R-PHY for long CIN distances and for moderate to high traffic load levels ρ_c on the cable link. For instance, for a CIN distance of 500 miles and ρ_c = 0.6, R-PHY incurs over twice the delay of R-MACPHY. The lower mean packet delay with R-MACPHY is due to the "localized" MAC scheduling in the remote node (RMD), which avoids the long round-trip delay over the CIN for the request-grant signalling.

Throughout the evaluations in Fig. 3.10, contention and maintenance slots take up 20 % of the MAP. Thus, effectively only 80 % of the cable upstream transmission bit rate R_c is available for upstream data packet transmissions. We observe that R-PHY has generally pronounced delay increases well before approaching the effective upstream capacity (stability limit) of $0.8R_c$. In contrast, R-MACPHY continues to provide low delays for moderate to high loads that quite closely approach the stability limit. R-MACPHY then has sharply increasing delays very close to the stability limit. This R-MACPHY behavior is a positive feature: R-MACPHY consistently provides very low delays across the entire load range, up to very close to the stability limit. R-MACPHY gives substantial delay increases only when the system is loaded very close to the stability limit.

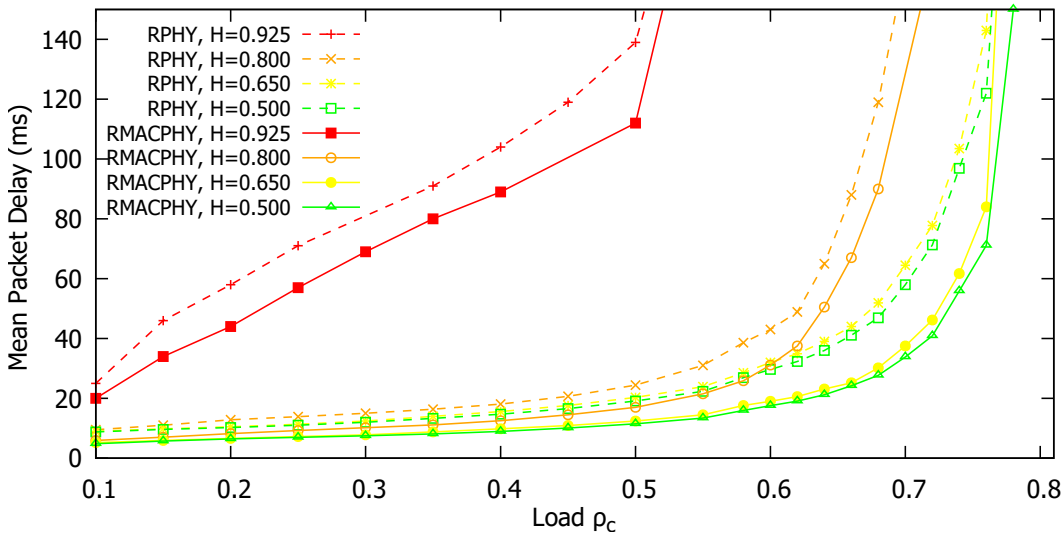

(a) Different Hurst parameters for CIN dist. = 50 miles, M = 200 CMs

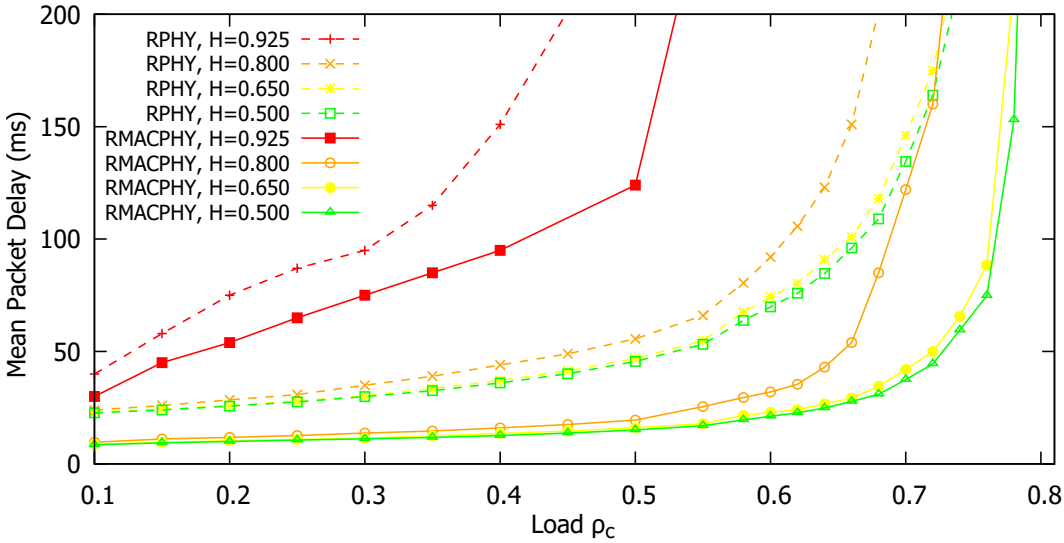

(b) Different Hurst parameters for CIN dist. = 500 miles, M = 200 CMs

Figure 3.11: R-PHY vs. R-MACPHY Mean Packet Delay as a Function of Cable Link Traffic Intensity ρ_c for Different Levels of Traffic Burstiness (i.e., Different Hurst parameters) for Different CIN One-Way Distances; Fixed Parameters: CIN Base Traffic Intensity ρ_i = 0.5, Gated Bandwidth Allocation, 20 % of Cable Capacity for Contention and Maintenance.

3.5.2.2 Multiple Cable Modems (CMs) with Self-Similar Traffic

We proceed to compare the performance of R-PHY and R-MACPHY for multiple CMs attached to a given remote node and for different levels of traffic burstiness in

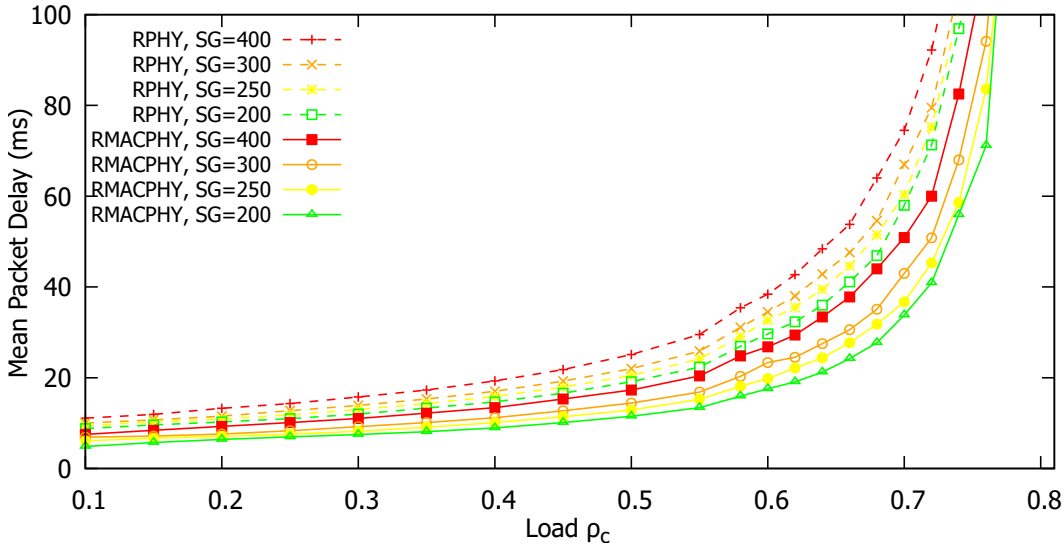

(a) Different SG sizes M for CIN dist. = 50 miles, H = 0.5 traffic

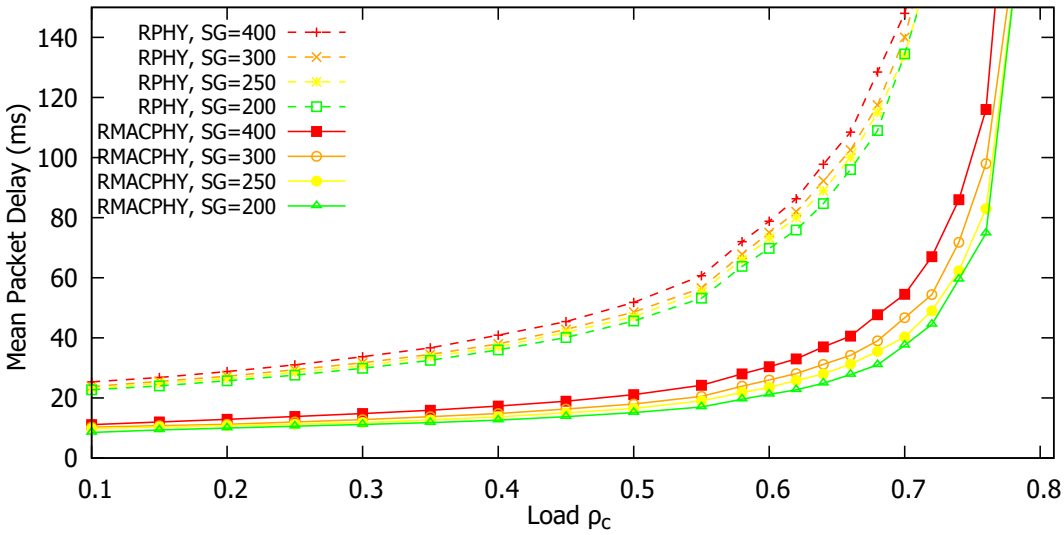

(b) Different SG sizes M for CIN dist. = 500 miles, H = 0.5 traffic

Figure 3.12: R-PHY vs. R-MACPHY Mean Packet Delay as a Function of Cable Link Traffic Intensity ρ_c for Different Numbers of CMs in a Service Group Attached to a Given Remote Node for Different CIN One-Way Distances; Fixed Parameters: CIN Base Traffic Intensity $\rho_i = 0.5$, Gated Bandwidth Allocation, 20 % of Cable Capacity for Contention and Maintenance.

Fig. 3.11. Figs. 3.11(a) and (b) show the mean upstream packet delay as a function of the traffic intensity on the cable upstream channel ρ_c for different levels of traffic burstiness for a fixed number of $M = 200$ CMs that are attached to the considered remote node. We consider a CIN distance of 50 miles as representative for the R-

PHY variant with MAC processing in the headend (see Section 3.2.2.3) and the CIN distance of 500 miles (τ = 4.05 ms) as representative of cloud vMAC processing (see Section 3.2.2.3). We increase the traffic burstiness by increasing the Hurst parameter H of the self-similar traffic. We observe from Figs. 3.11(a) and (b) that the delay differences between R-PHY and R-MACPHY follow the same general pattern as for Poisson traffic in Fig. 3.10. However, pronounced delay differences occur at lower loads. For instance, for Poisson traffic, we observed very pronounced higher R-PHY delay compared to R-MACPHY at load ρ_c = 0.7, see Figs. 3.10(b) and (d). For bursty self-similar traffic, the delay differences become very pronounced at lower loads, e.g., ρ_c = 0.6, especially for the long 500 miles CIN distance, see Fig. 3.11(b) (in comparison to the corresponding Fig. 3.10(d)).

We also observe from Figs. 3.11(a) and (b) that the effects of the traffic burstiness are especially pronounced for the highly bursty traffic with H = 0.925. For H = 0.925, we observe significant delay differences between R-PHY and R-MACPHY of around 10 ms already for low loads above ρ_c = 0.15. For a CIN distance of 500 miles, for instance, R-PHY achieves mean delays below 100 ms only for loads up to around ρ_c = 0.3, whereas R-MACPHY achieves delays below 100 ms for loads up to around ρ_c = 0.4 for this highly challenging H = 0.925 traffic. These pronounced effects of high levels of burstiness are in agreement with earlier studies in access networks, e.g., [174]. We conclude that for the highly bursty H = 0.925 traffic, the faster dynamic bandwidth allocation in the remote RMD node in the R-MACPHY architecture can significantly reduce the mean packet delay already for low network loads. In contrast, for traffic with lower levels of burstiness in the short 50 miles CIN setting (see Fig. 3.11(a)), R-PHY and R-MACPHY give very similar mean packet delays up to moderate load levels.

Figs. 3.12(c) and (d) evaluate the mean packet delay for R-PHY and R-MACPHY nodes with respect to the number M of CMs connected to the remote node for Poisson (i.e., $H = 0.5$) traffic. We observe from Figs. 3.12(c) and (d) that increasing numbers M of CMs slightly increase the mean packet delays. The delay increases are most pronounced in the moderately high load range for ρ_c ranging from 0.6 to 0.75 and are very similar for both R-PHY and R-MACPHY. The delay increases with increasing CM numbers are due to the overhead for the request messages. In our simulations, each CM sends a 64 byte request message in each cycle (piggybacked onto upstream data transmission, or separately if CM has no data to send). With M denoting the number of CMs and Z denoting the cycle duration, these request message increase the relative cable channel load by

$$\text{Request Message Overhead} = \frac{64 \times 8 \times M}{0.8 \times R_c \times Z}. \tag{3.13}$$

The resulting delay increases are most pronounced in the moderately high load range where (i) the cycle durations Z are still short enough so that the request messages cause a noticeable additional load, and (ii) the cable channel has high enough load ρ_c from the payload traffic that the additional load from the request messages results in noticeable delay increases. As the traffic load approaches the $0.8R_c$ available cable channel transmission bit rate, the cycle duration Z of the Gated allocation considered in Figs. 3.12(c) and (d) grows very long, resulting in a negligible load increase due to the request messages.

3.5.3 Double-Phase Polling (DPP) with Excess Share Bandwidth Allocation

In this section we compare the performance of R-PHY and R-MACPHY for double-phase polling (DPP) with excess bandwidth sharing [157, 175]. The simulation evaluations for DPP with excess bandwidth sharing are motivated as follows. DOCSIS protocol versions 3.0 and 3.1 permit multi-thread scheduling (or pipelined schedul-

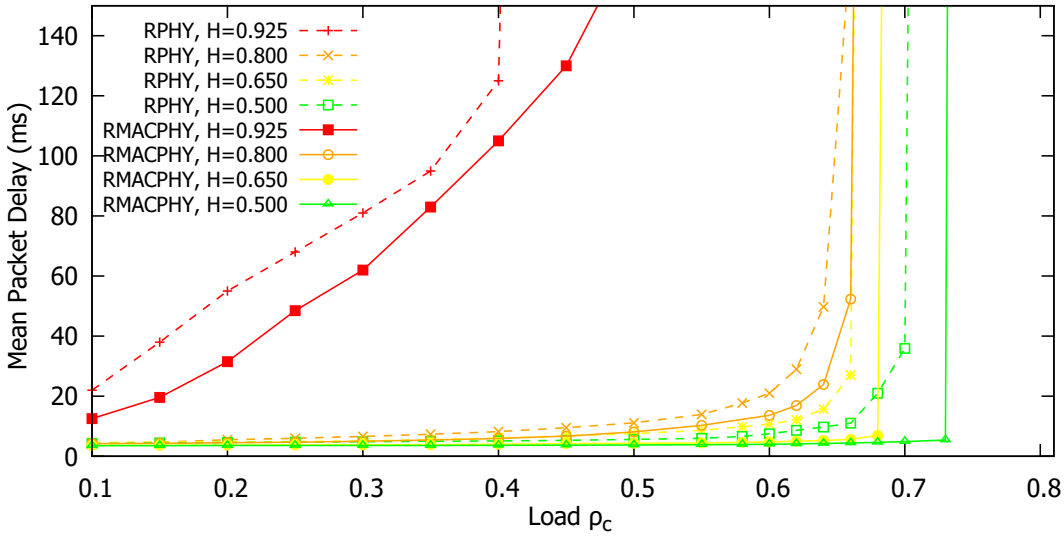

(a) Different Hurst param. for CIN dist. = 50 miles, M = 200 CMs

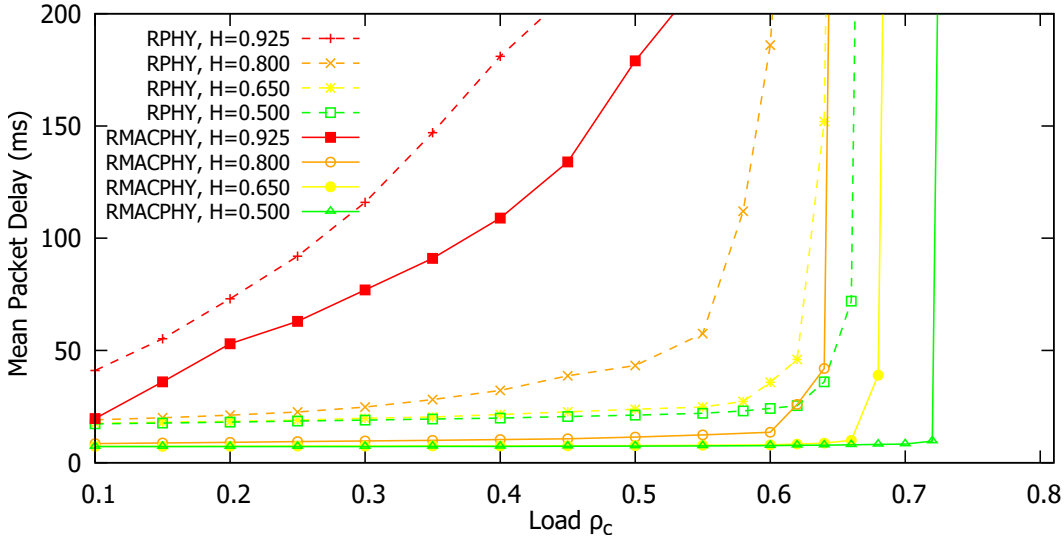

(b) Different Hurst param. for CIN dist. = 500 miles, M = 200 CMs

Figure 3.13: R-PHY vs. R-MACPHY Mean Packet Delay as a Function of Cable Link Traffic Intensity ρ_c for Different Levels of Traffic Burstiness (i.e., Different Hurst parameters) for Different CIN One-Way Distances; Fixed Parameters: CIN Base Traffic Intensity ρ_i = 0.5, DPP Bandwidth Allocation, 20 % of Cable Capacity for Contention and Maintenance.

ing) [13] using multiple outstanding requests as described in [143, Sec. 7]. A CM may have multiple outstanding requests, i.e., the CM can send additional requests without having received a grant or grant-pending in the form of an acknowledgment for an earlier request.

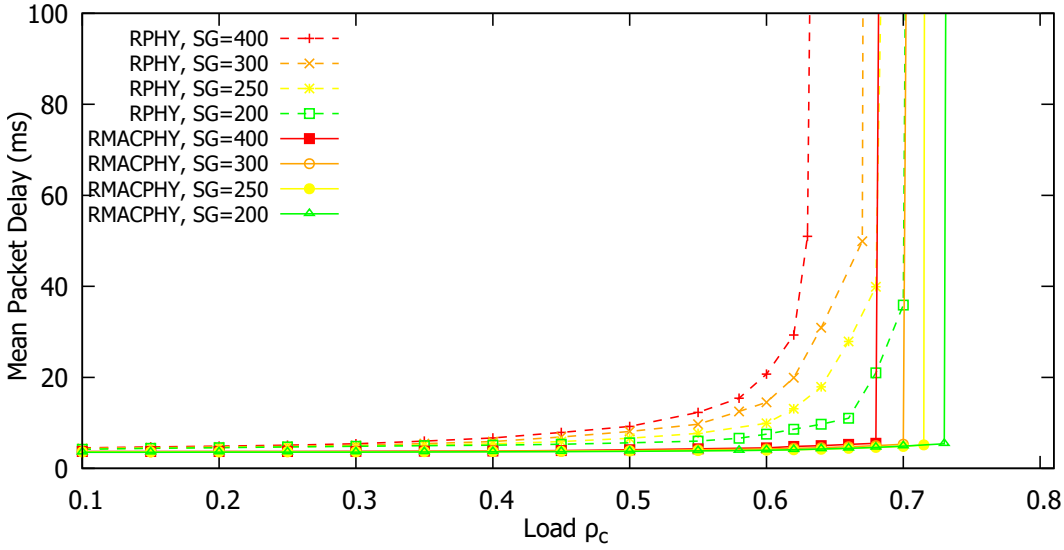

(a) Different SG sizes M for CIN dist. = 50 miles, $H = 0.5$

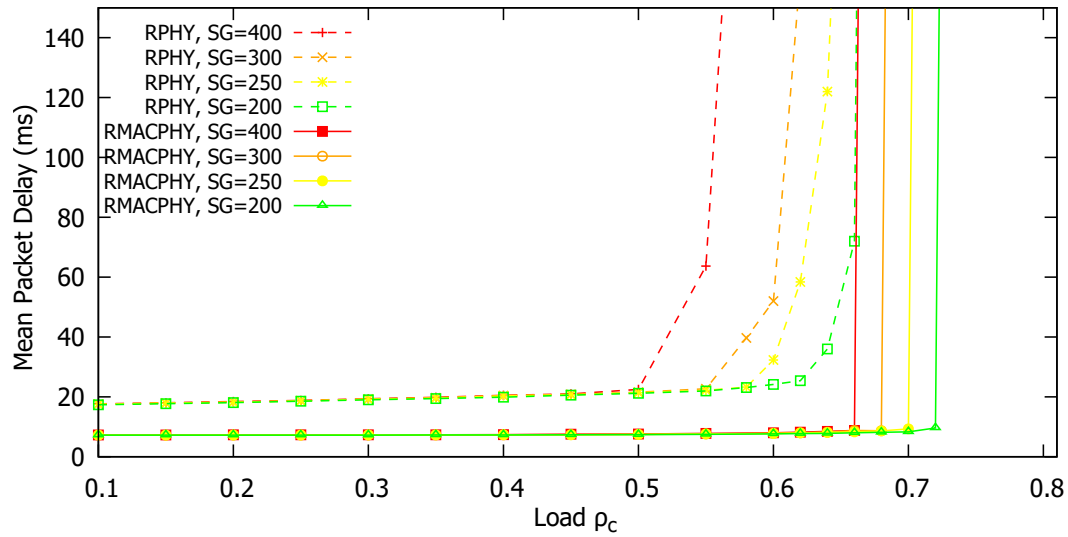

(b) Different SG sizes M for CIN dist. = 500 miles, $H = 0.5$

Figure 3.14: R-PHY vs. R-MACPHY Mean Packet Delay as a Function of Cable Link Traffic Intensity ρ_c for Different Numbers of CMs in a Service Group Attached to a Given Remote Node for Different CIN One-Way Distances; Fixed Parameters: CIN Base Traffic Intensity $\rho_i = 0.5$, DPP Bandwidth Allocation, 20 % of Cable Capacity for Contention and Maintenance.

Multi-thread (pipelined) scheduling is generally well suited to mask the long propagation delays in polling MAC systems covering long distances [176, 177]. However, multi-thread polling is also quite complex and requires complex thread tun-

ing [178]. A recent study [179] has demonstrated that the simple double phase polling scheduling with excess bandwidth sharing DBA [157, 175] gives essentially equivalent performance to the complex multi-thread polling in long-propagation delay polling systems.

A critical aspect of polling-based MAC is masking the idle times that may arise due to the long propagation delays between the CM transmission of a request message and the arrival of the corresponding grant message to the CM. In the DPP mechanism, the polling cycle of one CM group is interleaved with the transmissions of the other CM group so as to mask the idle times between request and transmission. In order to enable this masking, we set the maximum aggregate grant size $G_{\max}$ [bit] for a DPP group to mask the round-trip propagation delay between the CMs and the scheduler. In particular, we set $G_{\max}$ such that the transmission time of the maximum grant size $G_{\max}$ upstream over the cable link (with $0.8R_c$ available transmission bit rate for data) corresponds to the smallest integer multiple of the MAP duration t_{MAP} that exceeds the mean round-trip propagation (network traversal) delay $2t_{Mp}$, i.e.,

$$G_{\max} = 0.8R_c \left\lceil \frac{2t_{Mp}}{t_{MAP}} \right\rceil t_{MAP}. \tag{3.14}$$

Thus, when one DPP polling group has enough data traffic to utilize the maximum permitted grant size $G_{\max}$, the upstream data transmission time $G_{\max}/(0.8R_c)$ of this DPP group will mask the round trip propagation delay for the requests and grants of the other DPP group. We note that in order to mask the worst case round-trip propagation (network traversal) delay $2(t_{MAP} + \delta + \tau)$, a correspondingly larger $G_{\max}$ setting would be needed. However, we found that the $2(t_{MAP} + \delta + \tau)$ worst-case delay occurs very rarely and the larger $G_{\max}$ would make DPP bandwidth allocation slightly less responsive; therefore, we consider the $G_{\max}$ setting based on the mean network traversal delay as per Eqn. (3.14).

Comparing Figs. 3.13(a) and (b) with Figs. 3.12(a) and (b), we observe that for the highly bursty $H = 0.925$ traffic, DPP gives about the same or slightly higher mean packet delays than Gated allocation; whereas for the lower traffic burstiness levels $H \leq 0.8$, DPP achieves significant mean delay reductions compared to Gated allocation. For the highly bursty $H = 0.925$ traffic, a single (or very few) CM(s) may have a very large traffic burst at a time, while all other CMs have no traffic. If only CMs in one DPP polling group have data traffic, the other polling group cannot effectively mask the propagation delay. Rather, the limitation of the DPP cycle duration (to approx. $Z_{DPP} = 2t_{Mp} + G_{\max}/(0.8R_c)$) introduces frequent request messages that increase the overhead compared to Gated allocation, which requires only one request message for an arbitrarily large traffic burst (i.e., has no grant size limit).

For low to moderate traffic burstiness, e.g., for $H \leq 0.8$, the traffic burst are typically spread over CMs from both DPP polling groups. For such balanced loading of the two DPP polling groups, the upstream transmissions of one group can effectively mask the round-trip propagation delay for the request and grant messages of the other group, resulting in significant reductions of the mean packet delays compared to Gated allocation. This masking effect of DPP can effectively extend the operating range of R-PHY for low-delay applications, e.g., we observe from Fig. 3.13(b) that for load $\rho_c = 0.58$ of $H = 0.65$ traffic, R-PHY achieves a mean packet delay of 27.3 ms, whereas Gated gives a corresponding mean packet delay of 67.6 ms in Fig. 3.12(b). Importantly, we observe from Fig. 3.14(a) that for traffic with low to moderate levels of burstiness ($H \leq 0.8$) and cable traffic loads up to a moderately high level of $\rho_c = 0.6$ (which corresponds to 0.6/0.8 = 75 % effective utilization of the available data upstream transmission bitrate), both R-PHY and R-MACPHY give very similar performance when DPP is employed up to the CIN distance of 50 miles. In particular,

both R-PHY and R-MACPHY achieve mean packet delays below 20 ms for up to 75 % effective utilization of the available transmission bitrate (and delays below 10 ms for effective utilizations up to 0.5/0.8 = 62.5 %; below 6 ms for up to 0.25/0.8 = 31 % effective utilization).

Figs. 3.14(c) and (d) evaluate the effects of SG size M on the mean packet delay for the R-PHY and R-MACPHY architectures with DPP. Comparing the DPP mean packet delays in Figs. 3.14(c) and (d) with the corresponding Gated delays in Figs. 3.12(c) and (d), we observe that with Gated, the delays increase gradually with increasing load; whereas with DPP, the delays are essentially constant up to a "knee point" and then increase abruptly. This "knee point" behavior is particularly pronounced for R-MACPHY, which in Fig. 3.14(d) gives essentially constant 7.3 ms mean delay up to knee points located at approximately $\rho_c = 0.66$ for 400 CMs and roughly at $\rho_c = 0.72$ for 200 CMs. For the 500 Mile CIN distance, the DPP maximum grant size is set to $G_{\max} = 6t_{MAP} \times 0.8R_c$ for R-PHY and $G_{\max} = t_{MAP} \times 0.8R_c$ for R-MACPHY, according to Eqn. (3.14). Correspondingly, R-MACPHY has roughly a six times higher DPP request message frequency and overhead compared to R-PHY. The frequent request messages and "localized" bandwidth allocation in the remote RMD node make R-MACPHY with DPP highly responsive, ensuring low delay packet service up to data (plus request message) traffic loads very close to the $0.8R_c$ available cable upstream transmission bit rate. [The frequent request messages with R-MACPHY increase the overhead and result in higher packet loss rates than R-PHY for very high load levels (beyond the practically relevant load range), see Fig. 3.16 and Section 3.5.5.] In contrast, the R-PHY architecture is less responsive due to the bandwidth allocation at the headend, leading to a more gradual delay increase than for R-MACPHY. Nevertheless, R-PHY with DPP achieves significant mean packet delay reductions compared to Gated allocation. For instance, for 500

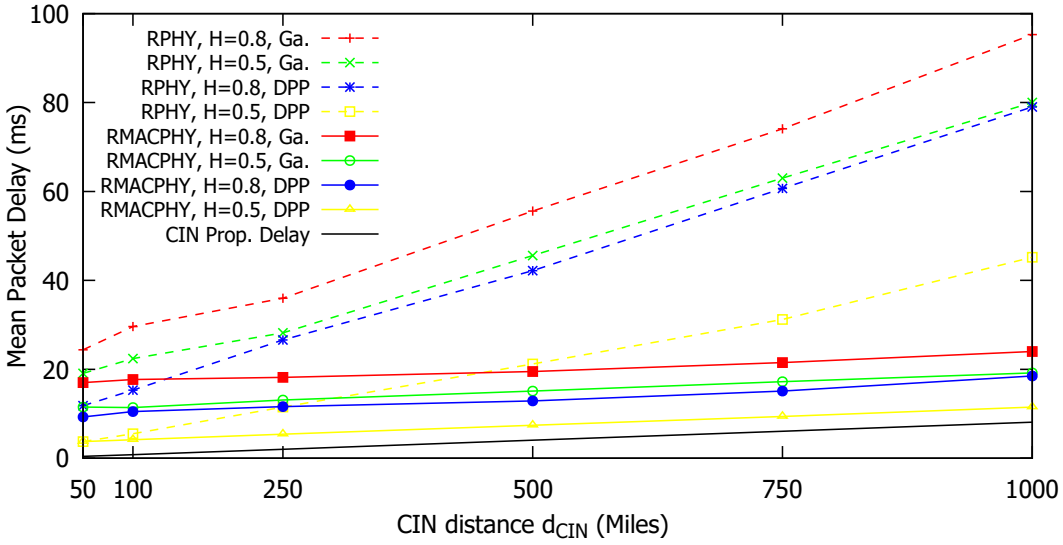

Figure 3.15: R-PHY vs. R-MACPHY Mean Packet Delay Performance for Self-Similar ($H = 0.8$) and Poisson ($H = 0.5$) Traffic as a Function of CIN Distance; Fixed Parameters: Cable Link Traffic Intensity $\rho_c = 0.5$, CIN Base Traffic Intensity $\rho_i = 0.5$, 200 CMs, 20 % of Cable Capacity for Contention and Maintenance.

miles CIN distance and $\rho_c = 0.5$ load, the mean packet delay of 48.6 ms for $M = 300$ CMs with Gated (Fig. 3.12(d)) is reduced to 21.6 ms with DPP (Fig. 3.14(d)). For the 50 miles CIN, we observe from Fig. 3.14(c) that R-PHY and R-MACPHY give very similar mean packet delays for all considered numbers of CMs up to a moderately high load of $\rho_c = 0.6$ (whereby the delays are below 6 ms for loads up to $\rho_c = 0.5$).

3.5.4 Mean Delay as a Function of CIN Distance

In order to gain further insight into the impact of the CIN distance, which is a key parameter considered in the planning of R-PHY and R-MACPHY networks, we examine the mean packet delay as a function of CIN distance in Fig. 3.15. From Fig. 3.15 we observe that R-MACPHY achieves a very significant reduction of average packet delay as compared to R-PHY. As the maximum CIN propagation delay is increased, the performance differences between R-MACPHY and R-PHY become more pronounced. For the CIN distance of 1000 miles, the R-PHY mean packet delay is over four times

higher than the R-MACPHY mean packet delay.

Examining the results for R-PHY and Poisson traffic ($H = 0.5$), in Fig. 3.15 more closely, we observe that DPP with excess bandwidth sharing achieves a substantially lower mean packet delays than Gated scheduling. For instance, when the CIN distance is 100 miles, the Gated scheduling yields an average mean packet delay of 22.4 ms, while DPP yields an average mean delay of 5.5 ms which is a 75 % decrease, illustrating the impact of the scheduling mechanism. In addition, the mean packet delay for DPP with excess bandwidth sharing for bursty traffic ($H = 0.8$) is lower than the delay for Gated scheduling of Poisson traffic.

We proceed to contrast our results to the results presented in Chapman et al. [13] who examined the impact of the CIN distance on the R-PHY architecture. Fig. 20 of [13] considers the REQ-GRANT scheduler, which closely follows the protocol of our Gated and DPP mechanisms, at 50% load (i.e., $\rho_i = 0.5$). Fig. 3.15 shows a linear increase in the mean packet delay with respect to CIN distances for both the R-PHY and R-MACPHY architectures. For example, the mean packet delay varies linearly from 3.5 ms to 21.5 ms for Poisson traffic and DPP scheduling in the R-PHY architecture for CIN distances between 50 and 500 miles. In Fig. 20 of [13] the corresponding mean packet delays roughly ranges from 5 ms to 20 ms which are comparable to our results. The near linear increase of the R-PHY DPP mean packet delay has significantly higher slope than the corresponding R-MACPHY DPP delay. Thus, R-PHY gives significantly higher delays than R-MACPHY for long CIN networks.

Importantly, we observe from Fig. 3.15 that self-similar traffic gives substantially higher slopes of the mean packet delay as a function of CIN distance than Poisson traffic. For instance, we observe that the mean packet delay for self-similar

traffic with $H = 0.8$ increases near linearly to close to 80 ms for the 1000 miles CIN distance in R-PHY. In contrast, the slope for $H = 0.8$ for DPP is very low for R-MACPHY and the mean packet delay stays below 20 ms for a 1000 miles CIN distance. Thus, the mean packet delay of R-PHY is four times higher than the R-MACPHY mean packet delay for a 1000 miles CIN. One-way mean packet delays on the order of 80 ms may negatively impact the QoS of real-time packet traffic that has to traverse two access networks as well as a long-distance core network on the end-to-end path. Thus, R-MACPHY appears better suited to provide real-time QoS for access networks with long CIN distances.

3.5.5 Packet Loss Rate

We compare the packet loss rates of the R-PHY and R-MACPHY architectures by simulating a limited buffer (with First-In-First-Out (FIFO) queuing and tail drop) in each CM. We considered typical CM buffer capacities, including 12.5 kbyte and 64 kbyte as considered in [41]. Due to space constraints, we present only plots for the 12.5 kbyte buffer capacity, which exhibits the typical packet loss dynamics, in Fig. 3.16. We observe from Fig. 3.16 that for both 50 and 500 miles CIN distance, the loss rates stay below 1 % for the moderately bursty ($H = 0.8$) traffic up to a cable traffic load of $\rho_c = 0.64$ (resp. below 3 % for R-PHY for 500 miles); additional evaluations found less then 1 % loss rate for up to $\rho_c = 0.66$ for 64 kbyte CM buffers. We also observe from Fig. 3.16 that for loads of bursty $H = 0.8$ traffic below $\rho_c = 0.66$, R-PHY has very slightly higher losses than R-MACPHY, which are due to the less responsive (higher delay) MAC protocol dynamics in R-PHY.

In contrast, we observe from Fig. 3.16(b) that R-PHY achieves significantly lower loss rates than R-MACPHY for high cable traffic loads above $\rho_c = 0.66$. These lower R-PHY loss rates are due to the lower request overhead of R-PHY for the

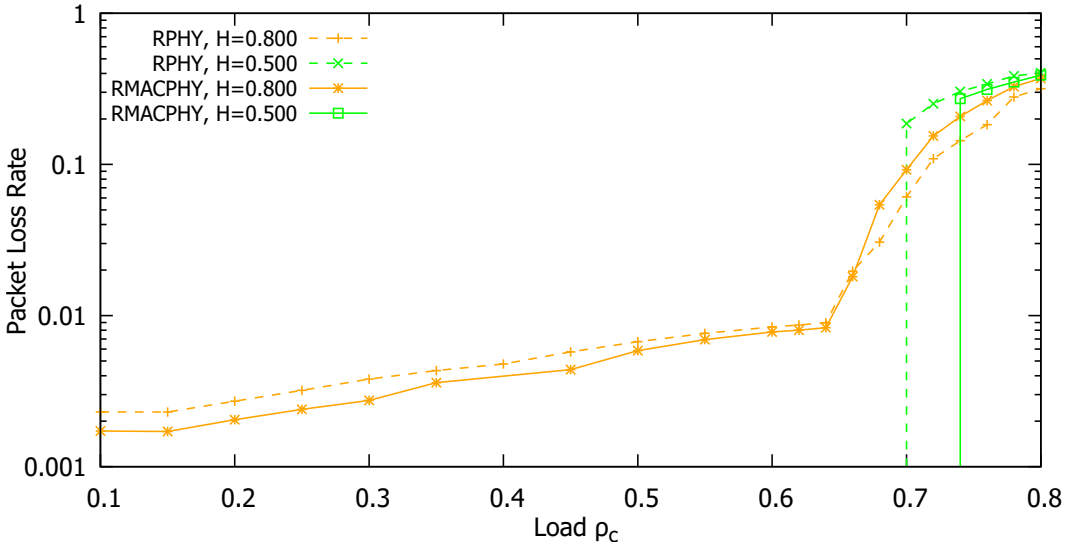

(a) CIN distance = 50 miles

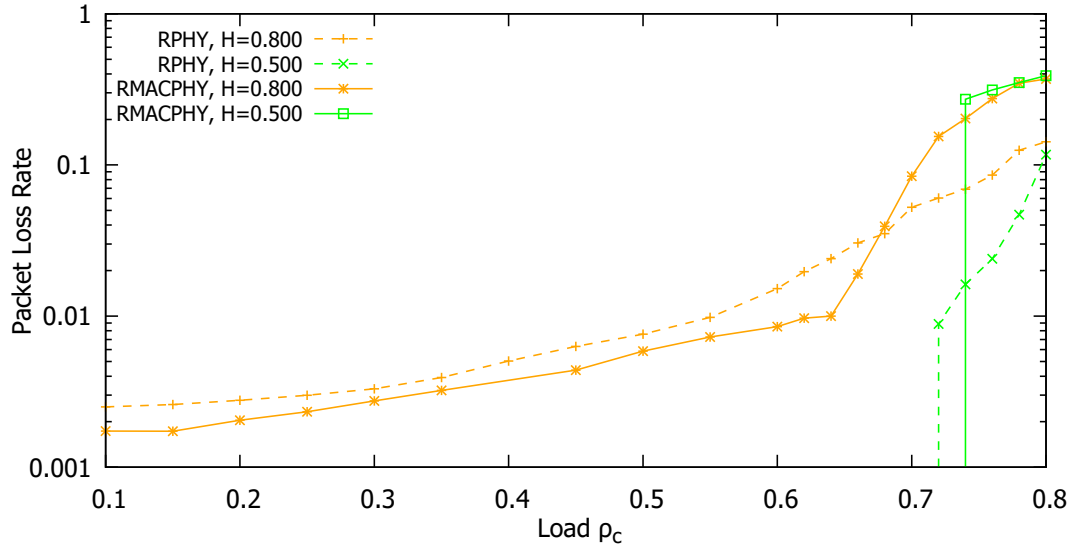

(b) CIN distance = 500 miles

Figure 3.16: R-PHY vs. R-MACPHY Packet Loss Rate for Double Phase Polling (DPP) Scheduling WIth Excess Share Grant Sizing, as a Function of Cable Link Traffic Intensity ρ_c Different CIN One-Way Distances; Fixed Parameters: CM Buffer Size 12.5 kbyte, CIN Base Traffic Intensity ρ_i = 0.5, 200 CMs, 20 % of Cable Capacity for Contention and Maintenance.

long CIN distance. In particular, for the 500 miles CIN distance, R-PHY has five times larger DPP maximum grant size $G_{\max}$ to mask the long round-trip propagation delay. Accordingly, R-MACPHY has about five times higher request frequency and correspondingly higher overhead due to CM request messages, which lead to higher

losses. Referring back to the mean packet delays in Figs. 3.13(a) and 3.13(b), we observe that the delays shoot up to very large values above 100 ms for cable loads ρ_c above 0.66 for 50 miles, resp. for loads above 0.64 for 500 miles. Any further load increases result in loss rates that rapidly grow above 1 % in Fig. 3.16. This region of high mean packet delays above 100 ms and high losses is generally not of practical interest for an operational network.

Overall, our evaluations for typical operating scenarios indicate that cable traffic loads up to ρ_c = 0.64 (which corresponds to a utilization level of 0.64/0.8 = 80 % of the available cable upstream transmission bitrate) can be supported by both R-PHY and R-MACPHY architectures with the packet losses below 1 % with a 12.5 kbyte CM buffer in a 50 miles CIN network.

CHAPTER 4

DESIGN OF FUNCTIONAL SPLIT IN EPON BASED DISTRIBUTED CABLE ACCESS

4.1 Introduction

Distributed cable access network architectures pass on some cable headend functions to remote nodes that are located close to the broadcast cable links reaching the cable modems (CMs) in the subscriber homes and businesses. In the Remote-PHY (R-PHY) architecture, a Remote PHY Device (RPD) node conducts the physical layer processing for the analog RF cable transmissions, while the headend runs the DOCSIS medium access control (MAC) for the upstream transmissions of the distributed CMs over the shared cable link. In contrast, in the Remote MACPHY (R-MACPHY) architecture, a Remote MACPHY Device (RMD) node conducts both the physical and MAC layer processing. [1–5, 96].

In this article we contribute the first analysis and design of EPON based R-PHY and R-MACPHY distributed cable access architectures. We investigate the open research challenges in the context of dynamic bandwidth allocation mechanisms for both EPON and distributed cable architectures. We performed extensive simulations to evaluate the performance of EPON based R-PHY and R-MACPHY architectures. We find that the R-MACPHY architecture significantly reduces the mean packet delays especially for long propagation distances.

We examine the MAP duration effect on R-PHY and R-MACPHY architectures. We conduct extensive simulation evaluations for both R-PHY and R-MACPHY architectures. We find that R-MACPHY achieves significantly lower average packet delays than R-PHY for short polling cycle duration at low loads. However, R-PHY and R-MACPHY give very similar average packet delays at moderate to high loads.

Table 4.1: Summary of Main Acronyms

CCAP	Converged Cable Access Platform (CCAP core implements CMTS headend functions)
CIN	Converged Interconnect Network (between RN and CMTS)
CM	Cable Modem
CMTS	Cable Modem Termination System (DOCSIS cable headend)
DEPI	Downstream External PHY Interface (downstream CCAP core to RPD PWs)
DOCSIS	Data Over Cable Service Interface Specification
MAP	Bandwidth Allocation MAP
PW	Pseudowire (logical link between RN and CCAP core)
RMD	Remote MACPHY Device
RN	Remote Node (either RMD or RPD)
RPD	Remote PHY Device
SG	Service Group (group of CMs)
UEPI	Upstream External PHY Interface (upstream RPD to CCAP core PWs)
vMAC	virtual MAC (implemented in cloud)

The remainder of this paper is organized as follows. In Section 4.2, we present related work focused on the cable architectures. Section 4.3 introduces R-PHY and R- MACPHY cable access networks, giving an overview of the remote architectures, protocols, and bandwidth allocation mechanisms. Section 4.4 presents the performance comparisons of R-PHY and R- MACPHY with respect to wide set of network parameters. The main acronyms used in this article are summarized in Table 4.1.

4.2 Background and Related Work

4.2.1 General Background on Cable Access Networks

The Converged Cable Access Platform (CCAP) integrate the data and video QAM modulators [144] into a one QAM for the cable headend physical layer connection to the customer premises. The Data over Cable Service Interface Specification (DOCSIS) standards specify the PHY and MAC layers [26] for communication between the client CMs and the headend centralized cable modem termination system (CMTS).

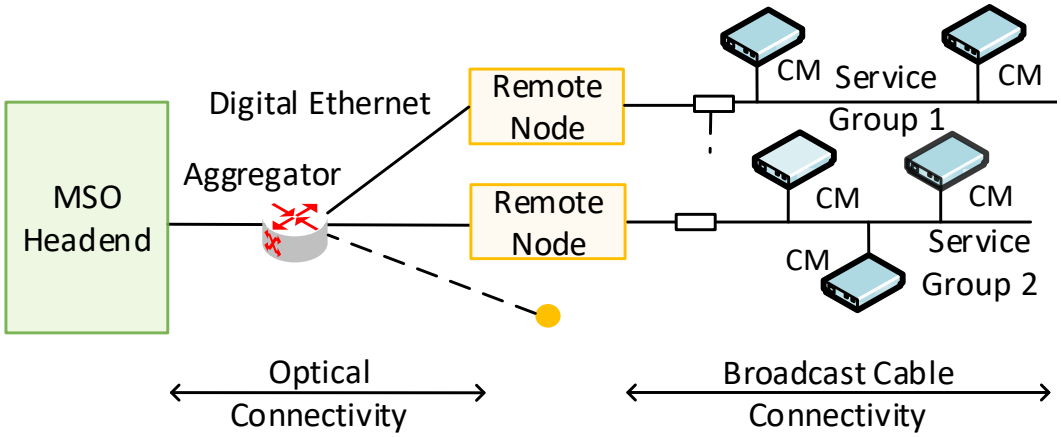

Figure 4.1: The Distributed Access Architectures (DAAs) Moves Some CCAP Functions From the Headend to Remote Nodes.

Traditionally, the cable industry have used analog optics at the cable headend to transmit signals. These analog optical signals underwent amplitude modulation to carry the information to a fiber node located at the remote node. These signals are then received by remote cable node that converts them to radio frequency signal to be transmitted to the client CMs via hybrid fiber coaxial access networks [145, 146]. However, the headend and remote nodes are connected through analog fiber, which suffers from attenuation in as the link distance is increased.

The Distributed CCAP (DCCAP) overcomes the analog signal attenuation by splitting the CCAP functionality between the remote nodes and the headend. The remote nodes are connected through a digital fiber to the cable headend. The use of digital fiber link between the headend and the remote node leads to eliminating the optical signal attenuation and deeper remote node deployments into the coaxial network. All the traditional CMTS functions excluding those implemented at the remote node are contained at the head-end at the core of CCAP or the cloud.

The DOCSIS standard gives support to different digital fiber protocols, such as 802.3 family of Ethernet (EPONs, IEEE 802.3ah, IEEE 802.3av). Fig. 4.1 illus-

trate the high level DCCAP architecture. The Headend/CCAP core is connected via a digital Ethernet fiber network to the remote nodes [8]. The cable Distributed access architecture specify two DCCAP architectures: Remote-PHY and Remote-MACPHY.

4.2.2 Related Work

Several studies have investigated broadcast cable access networks in the course of IEEE 801.14 protocol mechanisms development [97–105], and afterward impacted the DOCSIS specification [109–111]. The basic DOCSIS mechanisms have undergone evaluation by several studies. Subsequent research have examined and developed the DOCSIS mechanisms. Development of DOCSIS Simulation models has been covered in [15, 26, 27], DOCSIS upstream throughput analysis has been evaluated in [112–115], and DOCSIS MPEG and IPTV video transmissions has been studied in [123–125].

Design of QoS DOCSIS dynamic MAP allocations have been Initially discussed in [19]. A CM located at the user premises content for the upstream channel with other CMs in the same service group to transmit bandwidth requests to the headend CMTS. The performance analysis and examination of DOCSIS request contention has been investigated in [20, 45, 126–129]. Several studies begun to explore the issues arising from contention and how to improve DOCSIS MAC protocols [21–25, 28]. However, these studies have examined traditional cable access architectures that locates all the functionality in the headend. DOCSIS MAC have been based on the general polling protocols [131–133], these protocols have been extensively studied and analyzed in a variety of other network settings [134–142]. We have considered a CMs bandwidth request thats piggyback on the data upstream transmissions [143] and focused our analysis on the MAC polling dynamics as we adjust existing polling and delay strategies for the cable MAC protocol.

The traditional Passive Optical Network (PON) connects an Optical Line Terminal (OLT) with multiple distributed Optical Network Units (ONU). Moreover, the OLT in a PON network can be extended to support DOCSIS networking and management functions. DOCSIS Provisioning of EPON (DPoE) [46] is an mechanism for existing EPON whereby DOCSIS functions are provisioned through the PON. Emmendorfer et al. [49] have extensively discussed PON deployments for DOCSIS management in both centralized and distributed architectures. The PON deployments increase the fiber distance between headend and customers. The IEEE has defined a new project, EPON Protocol over Coax (EPoC) 802.3bn, to enable 1G/10G EPON services over HFC networks. Bhumika et al. [50] have discussed the design issues and challenges of the EPoC networks. Complementary to DOCSIS networks, PON technology also plays a significant role in Digital Subscriber Line (DSL) networks. Mercian et al. [52, 53] have presented an approach to control the upstream buffer occupancies at the drop-point devices (DPDs) or the ONUs. In their approach, the DPD, which is similar to a remote node in the D-CCAP architecture is connected to OLT in the headend and schedules upstream transmissions for DSL modems which are connected to DPDs.

Effective management and control of the shared hybrid upstream transmission channel is important to serve ONUs with minimum packet delay while avoiding congestion in the network. Several studies investigated the dynamic bandwidth allocation mechanisms that have been developed for the hybrid EPON upstream access. The DBA mechanisms can operate in offline mode, i.e., OLT will collect all the report messages from ONUs before granting the upstream transmission allocations, or in the online mode the OLT can make the grant decisions after receiving each ONU individual report message. Double-Phase Polling (DPP) mechanism is simple and robust bandwidth allocation mechanism and have been proven to have beneficial

performance characteristics. In DPP, each ONU is assigned to one of two separate polling groups and each DPP polling group implements an offline scheduling framework. [54, 110, 157, 161, 180–185]

In this study we investigate the Converged Cable Access Platform architectures where remote nodes perform distributed headend functionality. Earlier work on distributed cable access architectures mostly have been qualitative in essence, these studies explored the advantages unlocked by renovating the cable architecture [1, 13, 32–34, 130]. Recent studies have studied the R-PHY(Physical layer functions in the remote node) and R-MACPHY (Physical and MAC layer functions in the remote node) modular cable architectures and provided an extensive performance analysis of both remote architectures for the Converged Interconnect Network (CIN).

4.3 Distributed Cable Access Architectures

DOCSIS CMs upstream bandwidth transmissions are based on a centralized reservation which are traditionally implemented at the MSO headend. Periodically, the DOCSIS scheduler will transmit to all CM bandwidth allocation MAP which contain the time and duration of transmission of each CM during the next transmission windows. The allocation MAP describes the available slots for contention and also indicate the slots for new CMs to join the network [15]. More specifically, CMs can attain bandwidth for data transmission over requests through contention or with piggybacking at end of data transmissions. Piggybacking evades delays from contentions, since the bandwidth requests are sent along with the payload data [22].

4.3.1 Remote PHY (R-PHY) Architecture

Remote-PHY (R-PHY) [4] architecture moves the DOCSISPHY layer functionality to the remote node. Specifically, R-PHY architecture splits the DOCSIS PHY roles from the traditional CCAP. DOCSIS upper layers are still implemented centrally at

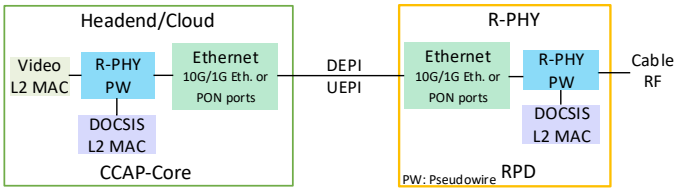

Figure 4.2: R-PHY Architecture: DOCSIS PHY is Implemented at a Remote-PHY Device (RPD) and DOCSIS MAC is Implemented at CCAP Core

the headend or pushed to the cloud. Splitting CCAP functions lead to achieving several advantages, such as independent scaling of video delivery, and flexibility in management of DOCSIS and out-of-band (OOB) transmissions. The CCAP platform function split will lead to making hardware and software upgrades modular and independent, which will result in improved Network availability and manageability [32, 33].

The R-PHY architecture splits the CCAP into CCAP MAC and upper layer functions that are located at a centralized location (e.g., headend or cloud), and the DOCSIS PHY layer functions that are implemented at the RPD, as shown in Fig. 4.2. The CCAP headend in an R-PHY architecture comprises of the DOCSIS CMTS for data transmission and an edge QAM (EQAM) [146] MAC for video transmission. The CMTS upper layers include upstream and downstream bandwidth schedulers, control signaling functions in addition to DOCSIS framing. The RPD links to the CCAP core over a network interface and connects to the CMs over an RF interface. An RPD also provisions the Layer 1 PHY conversion, Layer 2 MAC conversion, and Layer 3 pseudowires (PWs) [4]. An IP pseudowires are a logical interface, similar to an IP tunnel, that seamlessly transports the DOCSIS frames between the CCAP core and the RPD. The Upstream External PHY Interface (UEPI) [149] and Downstream External PHY Interface (DEPI) [148] offer the transport mechanisms between the CCAP core and the RPD. UEPI and DEPI are based on the Layer 2 Tunneling

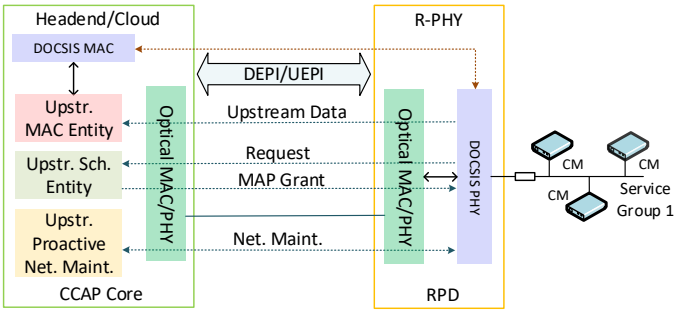

Figure 4.3: DEPI and UEPI Protocol Between CCAP Core and RPD to Transport the DOCSIS PHY Frames in Downstream and MAC Frames in Upstream Directions.

Protocol version 3 (L2TPv3) i.e., RFC 3931 [150]. The RPD receives the DOCSIS downstream transmission from the CCAP core over a digital fiber, such as Ethernet PON. The RPD fundamentally functions as a converter for physical layer signals that have been received through digital fiber to analog for RF transmissions over the coaxial cable. In the upstream link, the RPD converts the CM analog signals received from the service group (SG) to digital frames and then transmit them to the CCAP core located at the headend/cloud for further processing.

4.3.2 Remote-MACPHY (R-MACPHY) Architecture

The Remote-MACPHY (R-MACPHY) architecture splits both the DOCSIS PHY and MAC layers from CCAP core to the remote node, which is referred to as Remote MACPHY Device (RMD) [153]. The CCAP core connection and the RMD is essentially a Layer 2 Ethernet connection. In the downstream direction, the CCAP core will transmit data, video, and digitized OOB signals through a L2 aggregation device to the RMD [3]. In the upstream direction, the RMD will collect data transmissions from all the cable modems and set-top boxes (STBs) connected to it, and then will forwards the data to the CCAP core and STB control system. Hence, the RMD converts transparently the digital optical data frames from the headend to RF signals to be transmitted on the broadcast cable network.

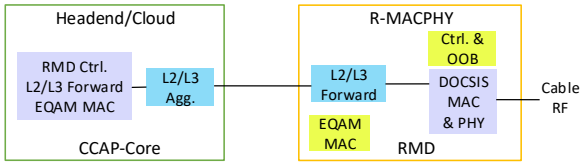

Figure 4.4: R-MACPHY Architecture: DOCSIS PHY and MAC Implemented at the Remote MACPHY Device (RMD) and Upper DOCSIS Layers are Implemented at Headend

The design of R-MACPHY architecture can differ based on the execution of the remaining CCAP functions not belonging to DOCSIS CMTS MAC and PHY. These outstanding CCAP functions can then be either executed at the headend or in the cloud. Shared between all design variants are the PHY and MAC layers that are implemented on the RMD physical device. Figure 4.4 highpoints the essential components that are common to the variety of options. Distributed R-MACPHY architectural variations can be primarily classified into: *i*) RMD with minimal configuration, where only the DOCSIS MAC and PHY are implemented at the RMD, *ii*) RMD with embedded edge-QAM (EQAM) [146], where the MAC for both video and DOCSIS data are implemented at the RMD, *iii*) Remote CCAP (R-CCAP), which implements all CCAP functions at the remote nodes, and *iv*) R-CCAP with centralized controller.

As DOCSIS MAC layer are implemented at the RMD the remaining DOCSIS upper layer (i.e., L3 and above) must be transported to the CCAP core at the headend for further processing. The request-grant delay of R-MACPHY is reduced much when compared to R-PHY, since the exchange of Request and Grant messages only travel between RMD and CMs for much shorter distances. While in the R-PHY architecture the RPD prioritize all the CMs Requests over payload data traffic on the CIN to ensure low delays and QoS for all CMs, the RMD does not require any such prioritization.

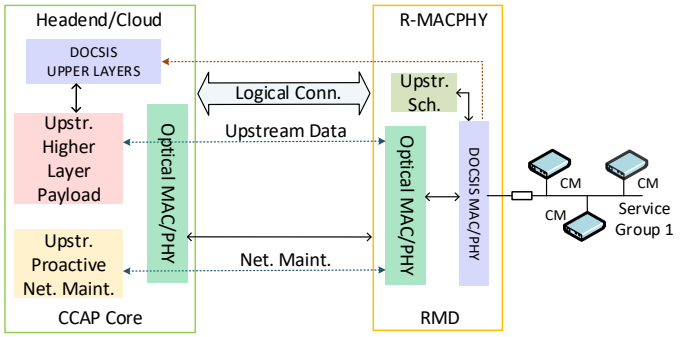

Figure 4.5: Generic Interface to Transport DOCSIS Data Between RMD and DOCSIS Upper Layers

Typically, the CCAP core connects to the RMD through a Layer 2 digital transport connection over optical fiber. Thus, RMD traffic can be seemly transported by optical Gigabit EPON/GPON CINs [154]. Logical connections, such as L2/L3 tunnels interfaces provide transparent flow level connections between RMD and CCAP core, as described in Fig 4.5.

4.3.3 DOCSIS Dynamic Bandwidth Allocation

We categorize and identify the dynamic bandwidth allocation (DBA) algorithms in the polling based DOCSIS MAC protocol using the three design dimensions, i) grant scheduling framework which characterizes the event triggering the scheduling and bandwidth allocation as well as the overall structure of the granting and scheduling process, ii) grant sizing policy which determines the size of the upstream transmission window allocated to each CM, and iii) grant scheduling policy which arranges the order of the different scheduled transmission windows [155–158]. A dynamic bandwidth allocation (DBA) algorithm in the DOCSIS scheduler sizes (dimensions) the upstream transmission windows (grants) based on the reports received by the CMs and sends the grants via MAP messages to the respective CMs.

4.3.3.1 Grant Scheduling Framework

Offline Grant transmission windows are allocated after REPORTs from all CMs have been received at the CMTS. That is, the schedule for the entire granting cycle of CM upstream transmissions is generated when the REPORT message from the last CM is received.

Double Phase Polling (DPP) CMs in a SG are partitioned into two independent DPP groups. Within each DPP group, the granting and scheduling is triggered by the receipt of REPORTs from all CMs in the group. Each DPP group is scheduled independently in an offline manner.

4.3.3.2 Grant Sizing Policy

In DOCSIS 3.1, grant sizes are allocated to the CMs in terms of number of minislots. Each minislot corresponds to a set of specific frequency subcarriers for a specific transmission time duration. An OFDM symbol is the fundamental unit of the minislot, and the number of OFDM symbols for each minislot in a given SG is defined as per the specifications in [143]. The grant sizing policy determines the grant sizes in terms of minislots such that the CM transmissions are orthogonal. By maintaining orthogonality, each CM gets exclusive access (without collisions) to the cable broadcast channel for its upstream transmissions. Effectively, a group of minislots that are reserved for the transmissions of a given CM can be abstracted to a variable transmission (bandwidth) bitrate channel.

The grant sizing policy determines the transmission window size (in terms of number of OFDM minislots) based on the CM upstream transmission request (in terms of bytes of data queued for upstream transmission). We consider two widely

considered grant sizing policies for the comparison of the R-PHY and R-MACPHY architectures:

Gated The Gated grant sizing mechanism grant the CMs their full amount of requested bandwidth [155, 158–160].

Limited with Excess Share Based on the requested transmission windows, the CMs sharing a cable channel are segregated into a group of underloaded CMs and a group of overloaded CMs [161, 162]. A CM is considered to be underloaded if the reported queue size (requested transmission window) is less than or equal to a prescribed maximum grant size divided by the number of CMs. An overloaded CM requested a transmission window larger than the maximum grant size. In the excess share mechanism, the total excess bandwidth is the sum of the remaining (unused) bandwidth of all underloaded CMs, which is then shared by the overloaded CMs. The grant for an overloaded CM becomes the maximum grant size plus the share of the total excess bandwidth divided by the number of overloaded CMs.

4.3.3.3 Grant Scheduling Policy

The grant scheduling policy determines how multiple CM transmission windows (minislots) are arranged during a granting cycle. We employ the Shortest Propagation Delay First (SPD) scheduling policy [163] which arranges the CM grants in ascending order of their round-trip propagation delay from the MAC module. In particular, we follow a hybrid allocation of minislot resources [164] across the frequency and time dimensions such that the earliest available (in the time dimension) minislots are allocated in a greedy manner to the CMs with the shortest round-trip propagation delays.

4.4 Performance Evaluation

4.4.1 Simulation Setup

4.4.1.1 Overview

We extended our OMNET++ R-PHY and R-MACPHY architectures simulator [186, 187] to include Ethernet Passive Optical Networks. We simulate the EPON based cable network illustrated in Fig. 4.1 for a single ONU/RN serving only one service group (SG). The EPON network between the ONU/RN and the OLT/headend is loaded by the traffic from the simulated cable SG traffic as well as EPON traffic load ρ_i which could be from different RN's or other services. In this paper we only focus on simulating one cable SG in detail to acquire insights into Remote PHY, Remote MACPHY, and overall EPON polling dynamics.

4.4.1.2 Cable Network

Similar to [186, 187], In our simulations we model the coaxial broadcast cable segment as link with transmission bit rate R_c = 1 Gbps and has one way propagation delay δ to the cable headend. We uniformly distribute the CM distance to the remote node (RPD or RMD) from 1 to 2 Km. Throughout, we reserve 20 % of the cable transmission bit rate R_c for contention and maintenance slots. Thus, throughout the simulation that only 80 % of R_c the cable transmission bit rate are accessible for data transmissions.

4.4.1.3 EPON Network

The EPON network has one-way propagation delay τ leading to the headend. We vary the distance from the ONU/RN (RPD or RMD) to the OLT from 10 to 500 Miles, considering that the EPON link can extend for longer distances to reach cloud locations. We model the EPON network with a total number of ONU= 32 and Upstream transmission bit rate R_i = 10 Gbps. Throughout, the EPON network

apply a Double Phase Polling with Excess share scheduling mechanism [157]. Each ONUs report their queue depths with a REPORT message (64 Bytes) and set the guard time to $t_g = 1\ \mu s$.

4.4.1.4 Traffic Model

The simulator uses the self-similar traffic generator [172]. The self similar traffic burstiness level is set by the Hurst parameter value H. Hurst parameter value $H = 0.5$, corresponds to Poisson traffic, and the traffic burstiness level increases for increasing H. Traffic generated by each CM in the upstream direction is modeled as self-similar traffic with the corresponding H parameter and 494 byte average packet size. The packet sizes distribution are as follows: 25 % 1518 Byte packets, 11 % 580 Byte packets, 4 % 300 Byte packets, and 60 % 64 Byte packets. Each CM will generate data packets with a generation rate λ_c to reach the cable network traffic (load) intensity $\rho_c = \lambda_c \bar{L}/R_c$. Each of the remote node connected CMs contribute equally to the overall packet generation rate λ_c. The EPON network is loaded with a traffic load $\rho_i = \lambda_i \bar{L}/R_i$ and the EPON and Cable traffic have the same Hurst parameter value.

4.4.2 Offline Scheduling with Gated Bandwidth Allocation

This section focuses on presenting the performance of the R-PHY and R-MACPHY architectures over EPON for CMs with Gated bandwidth allocation for different levels of traffic burstiness. Fig. 4.6 shows the mean upstream packet delay as a function of the traffic intensity on the cable upstream channel ρ_c for different levels of traffic burstiness for a fixed number of $M = 200$ CMs that are attached to a remote node. Fig. 4.6 considers gated bandwidth allocation for both stages of polling, i.e., between CM and remote node (cable), and between remote node and headend (EPON OLT) to coordinate the upstream transmissions over the cable and optical segments, respectively. We consider an EPON distance of 50 Miles ($\tau = 0.405$ ms)and the EPON

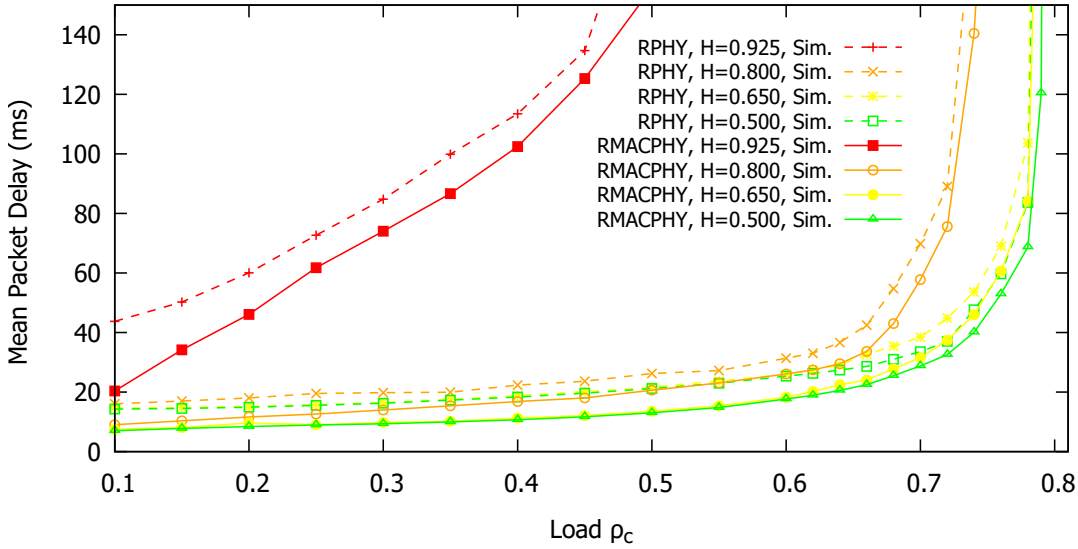

(a) EPON CIN distance = 50 Miles

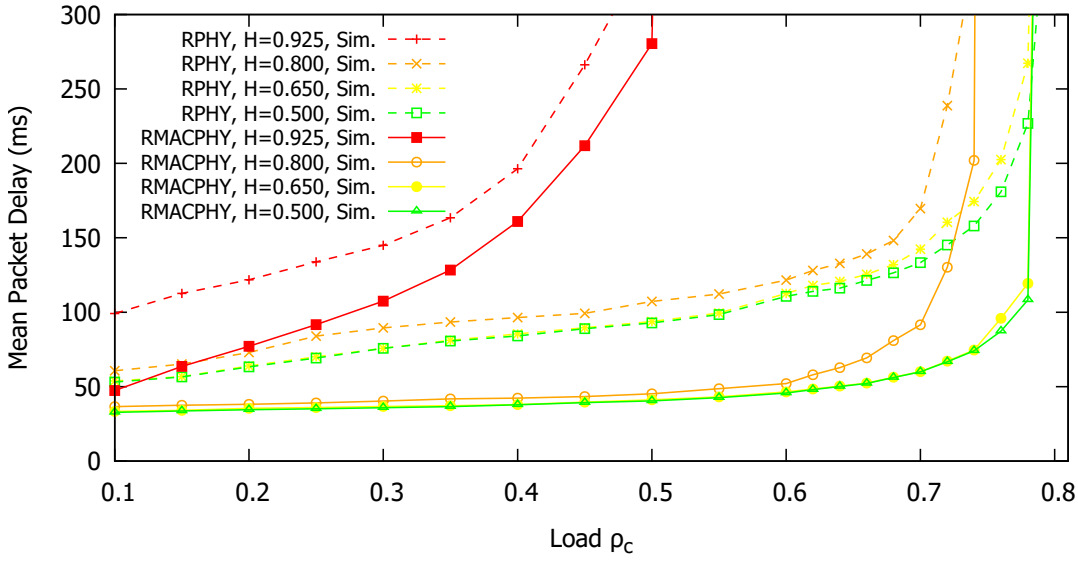

(b) EPON CIN distance = 500 Miles

Figure 4.6: R-PHY vs. R-MACPHY Mean Packet Delay as Function of Cable Link Traffic Intensity ρ_c for EPON One-Way Distance of 50 and 500 Miles; Fixed Parameters: EPON Traffic Intensity ρ_i = 0.5, 200 CMs, Gated Bandwidth Allocation, 20 % of Cable Capacity for Contention and Maintenance.

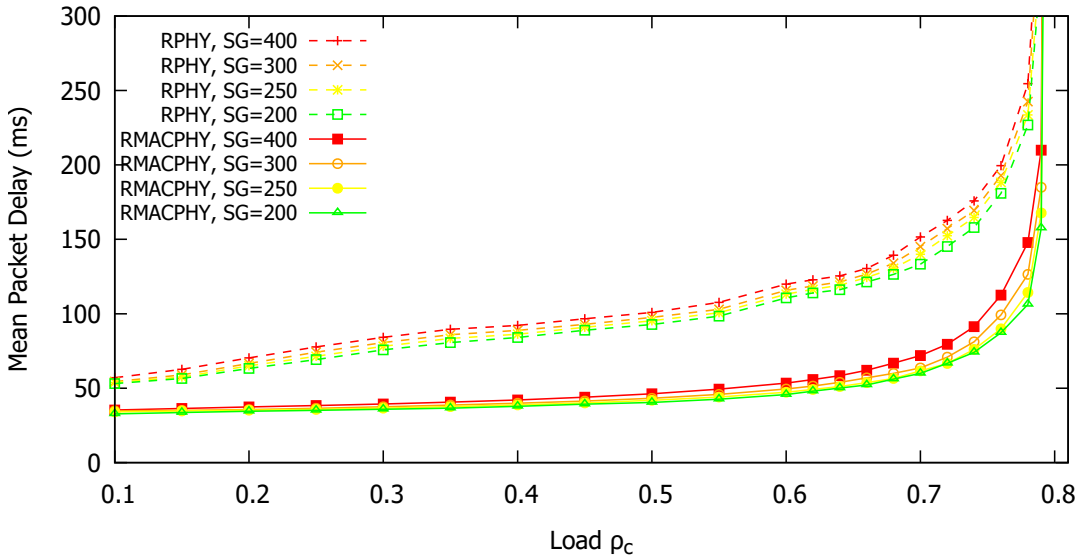

(a) EPON CIN distance = 50 Miles

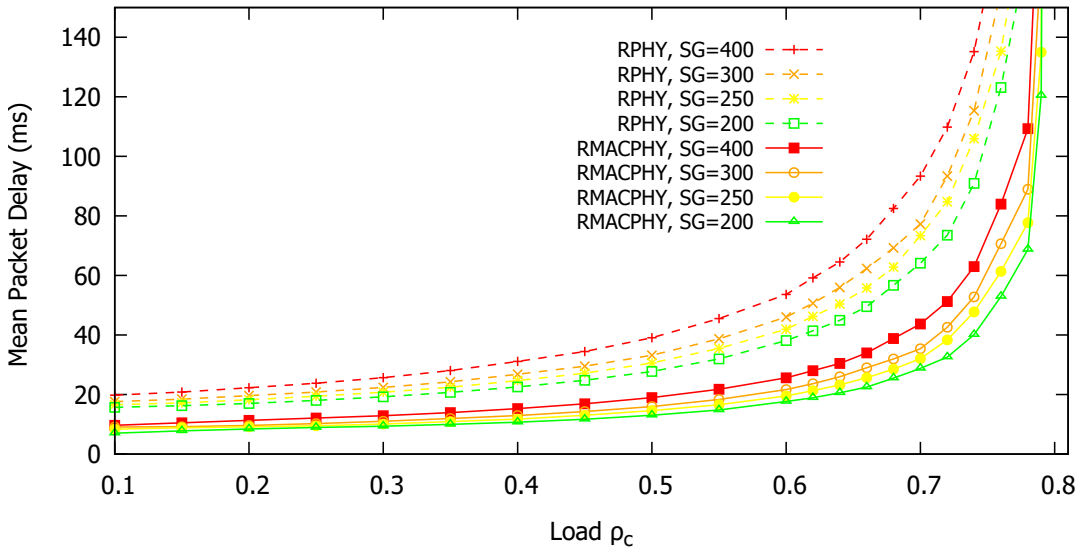

(b) EPON CIN distance = 500 Miles

Figure 4.7: R-PHY vs. R-MACPHY Mean Packet Delay as Function of Cable Link Traffic Intensity ρ_c for Different Number of CMs Attached to a Given Remote Node and Different EPON One-Way Distances; Fixed Parameters: EPON Traffic Intensity ρ_i = 0.5, Gated Bandwidth Allocation, 20 % of Cable Capacity for Contention and Maintenance.

distance of 500 Miles (τ = 4.05 ms). We increment the self-similar traffic burstiness by increasing the self-similar traffic Hurst parameter H. We observe from Fig. 4.6 that the delay differences between R-PHY and R-MACPHY follow the same general pattern as for Poisson traffic H = 0.5, whereas the EPON CIN show significantly larger delay as the Hurst parameter H is increased. For example, for ρ_c = 0.1, the delay for the EPON CIN is 14.3 ms, as shown in Fig. 4.6(a). The EPON CIN exhibits pronounced delay differences at low to moderate loads for bursty self-similar traffic. For the long 500 Miles EPON CIN distance, the delay differences become very pronounced at low to moderate loads, e.g., ρ_c = 0.6.

For the highly bursty traffic with H = 0.925, as expected, Fig. 4.6(a) and (b) show the pronounced effects compared to Poisson traffic (H = 0.5). We observe a considerable performance differences between R-PHY and R-MACPHY of about 20 ms for highly bursty traffic low loads above ρ_c = 0.1. For instance, R-PHY with an EPON distance of 500 Miles achieves packet delays below 100 ms only for up to cable traffic loads ρ_c = 0.35, whereas R-MACPHY accomplish 100 ms or less delays for cable traffic loads up to ρ_c = 0.425 for the very highly challenging bursty traffic H = 0.925. In contrast, R-PHY and R-MACPHY yields a lower packet delays up to moderate load levels for EPON distance of 50 Miles and a lower cable traffic burstiness levels (see Fig. 4.6(a)). We can conclude that for the highly bursty traffic H = 0.925, the R-MACPHY quicker dynamic bandwidth allocation located the remote RMD node can significantly trim the cable traffic delays for low network loads.

Fig. 4.7 evaluates the mean packet delay for R-PHY and R-MACPHY nodes for the EPON CIN with respect to the number M of CMs connected to a remote node for Poisson (i.e., H = 0.5) traffic. We observe from Fig. 4.7 that as we increase the numbers of CMs we slightly increase the mean packet delays. These increases

are more noticeable for moderate to high cable traffic loads range and occur for both R-PHY and R-MACPHY architectures. The increment in delay with increasing the numbers of CMs are as a result of the extra request messages overhead which increase the relative cable channel load on R_c. These delay are most detectable for high enough load ρ_c as a result of the polling duration been relatively short so that the additional requests cause a detectable extra load.

4.4.3 Double-Phase Polling (DPP) with Excess Share Bandwidth Allocation

For the evaluation of DPP scheduling mechanism with the EPON CIN, we have considered DPP at both stages, i.e., the cable and the EPON segment. Comparing Fig. 4.8 with Fig. 4.6 for gated EPON, for highly bursty traffic $H = 0.925$, we observe that DPP gives only slightly lower mean packet delays than Gated allocation for EPON. Whereas, for the lower traffic burstiness levels $H \leq 0.8$, DPP allocation attains a significant decrease in the average delay in comparison with Gated allocation.

For a low to moderate traffic burstiness level $H \leq 0.8$, we observe that the generated traffic bursts are distributed over diffrent CMs from both polling groups. The CMs upstream transmissions of one DPP polling group can mask the the request and grant round-trip propagation delay of the other group, which as a result reduces the average packet delay when compared to Gated bandwidth allocation. As a result, the DPP can reduce the average packet delay drastically, e.g., Fig. 4.8(b) at load point $\rho_c = 0.58$ with $H = 0.65$ traffic, we observe that R-PHY with DPP DBA has an average packet delay of 20.1 ms, where in Fig. 4.6(b) Gated has a corresponding average packet delay of 52.5 ms.

Fig. 4.8(a) shows for traffic with low burstiness level ($H \leq 0.65$) and moderately high cable traffic loads $\rho_c = 0.6$, R-PHY and R-MACPHY with DPP allocation have a very similar performance and achieves an average packet delays below 10 ms

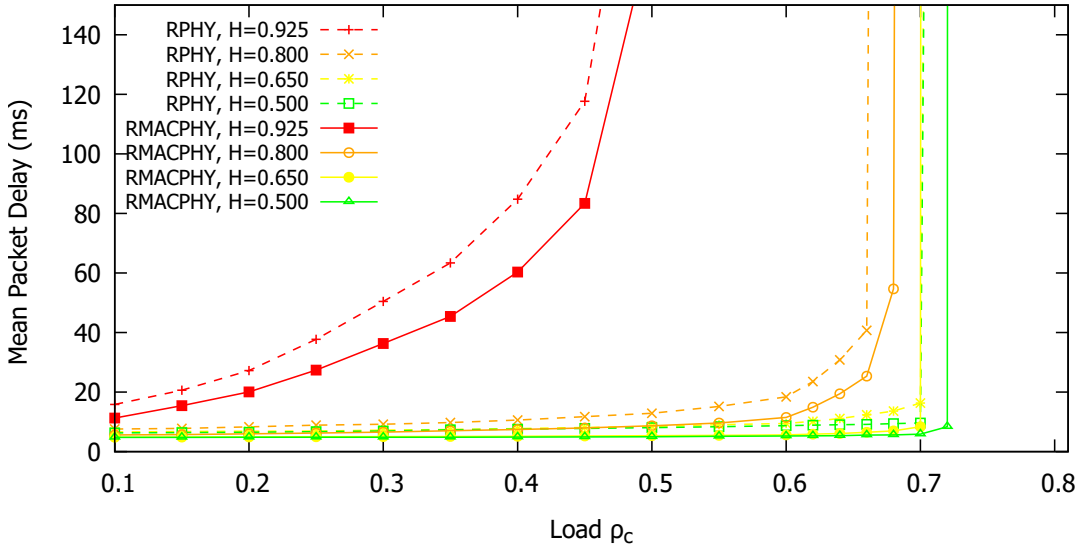

(a) EPON CIN distance = 50 Miles

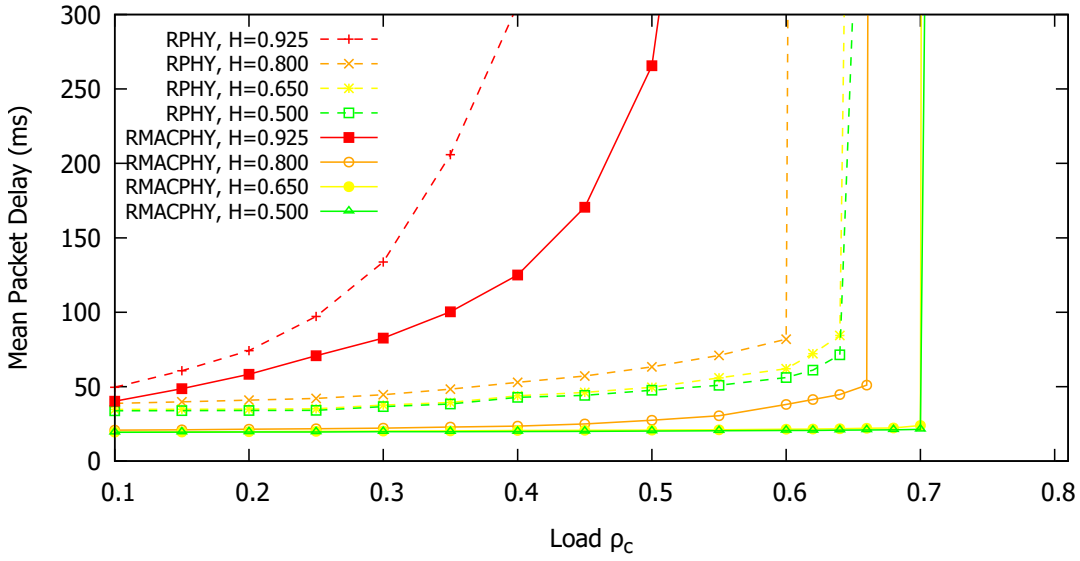

(b) EPON CIN distance = 500 Miles

Figure 4.8: R-PHY vs. R-MACPHY Mean Packet Delay as Function of Cable Link Traffic Intensity ρ_c for EPON One-Way Distance of 50 and 500 Miles; Fixed Parameters: EPON Traffic Intensity $\rho_i = 0.5$, 200 CMs, DPP Bandwidth Allocation, 20 % of Cable Capacity for Contention and Maintenance.

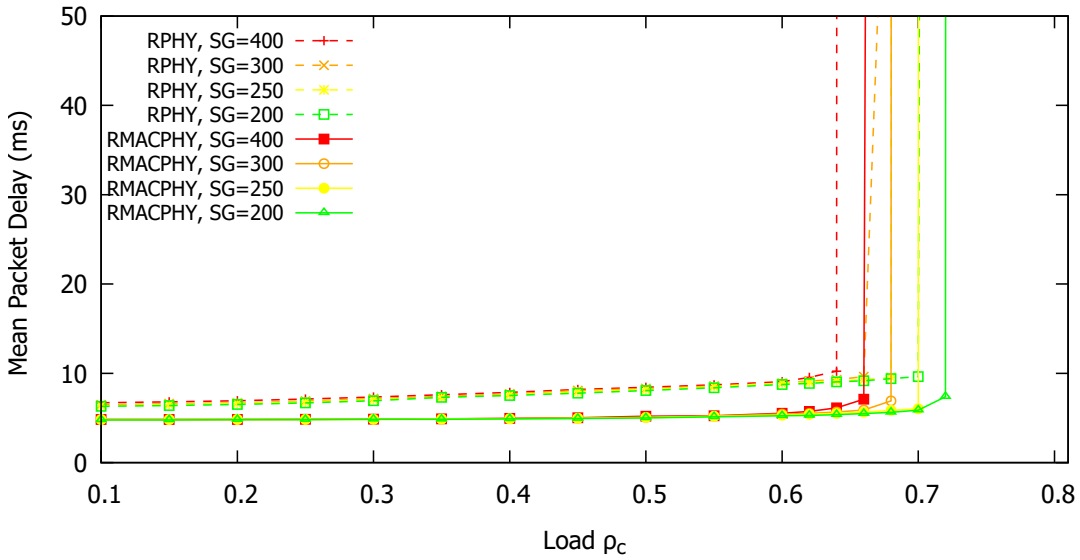

(a) EPON CIN distance = 50 Miles

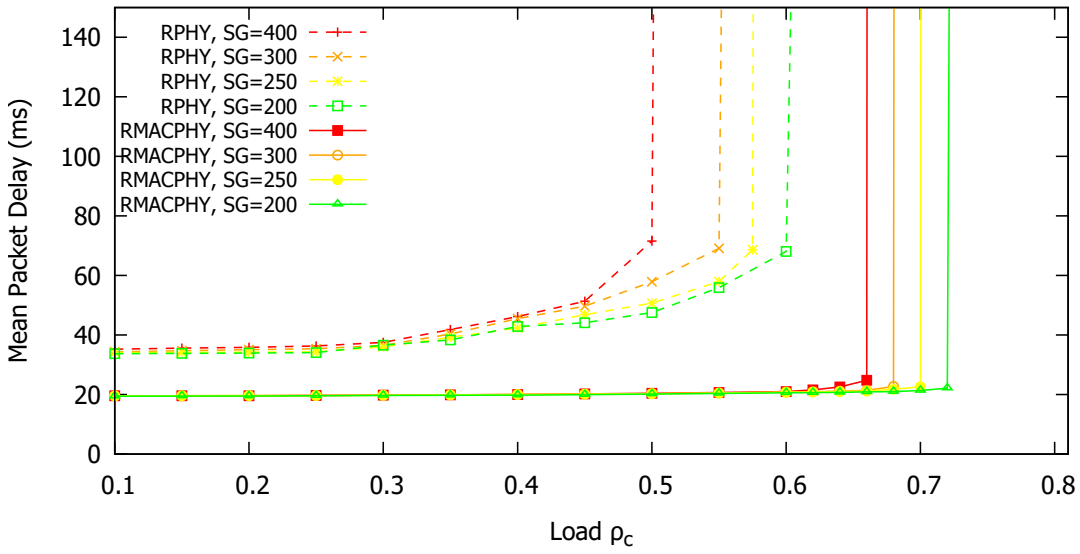

(b) EPON CIN distance = 500 Miles

Figure 4.9: R-PHY vs. R-MACPHY Mean Packet Delay as Function of Cable Link Traffic Intensity ρ_c for Different Number of CMs Attached to a Given Remote Node and Different EPON One-Way Distances; Fixed Parameters: EPON Traffic Intensity ρ_i = 0.5, DPP Bandwidth Allocation, 20 % of Cable Capacity for Contention and Maintenance.

for possion traffic and for $H = 0.8$ a delay below 20 ms.

Fig. 4.9 assess the significance of the SG size M on the packet average delay for the EPON with DPP scheduling R-PHY and R-MACPHY. Comparing the DPP allocation average packet delays in Fig. 4.9 with the Gated allocation corresponding delay in Fig. 4.7, we observe that with the Gated allocation, the mean packet delay increase step by step with rising load; on the contrast with DPP allocation, the delay remain in essence constant until it reachs a "knee point" and then the delay abruptly increase. This behavior is especially noticeable for R-MACPHY, e.g., in Fig. 4.9(b) RMACPHY delay remains basically constant at 6 ms up to $\rho_c = 0.66$ for 400 CMs and to $\rho_c = 0.72$ for 200 CMs. The localized bandwidth alloction behavior of RMD node leads the R-MACPHY with DPP to be very responsive and ensures low average packet delay.

On the other hand, the R-PHY architecture suffers from sudden change in the network due to the headend centerlized bandwidth allocation, which leads to gradual delay increase in comparison with R-MACPHY. However, R-PHY with DPP allocation achieves considerable reduction in the mean packet delay when compared to the Gated allocation. For example, In the 500 Miles EPON distance scenario (Fig. 4.7(b)) with Gated allocation and load $\rho_c = 0.5$, yields an average packet delay of 94.5 ms for $M = 300$ CMs. The delay is reduced by almost 45 % to 53 ms by implmenting a DPP alocation as can be observed in Fig. 4.9(b).

4.4.4 Mean Delay as a Function of CIN Distance

We investigate the average mean packet delay as a function of EPON distance in Fig. 4.10 with either DPP or Gated scheduling mechanisms for the cable segment of the network. Fig. 4.10 shows significant reduction in the average packet delay for R-MACPHY as compared to R-PHY. As the distance between the remote node and

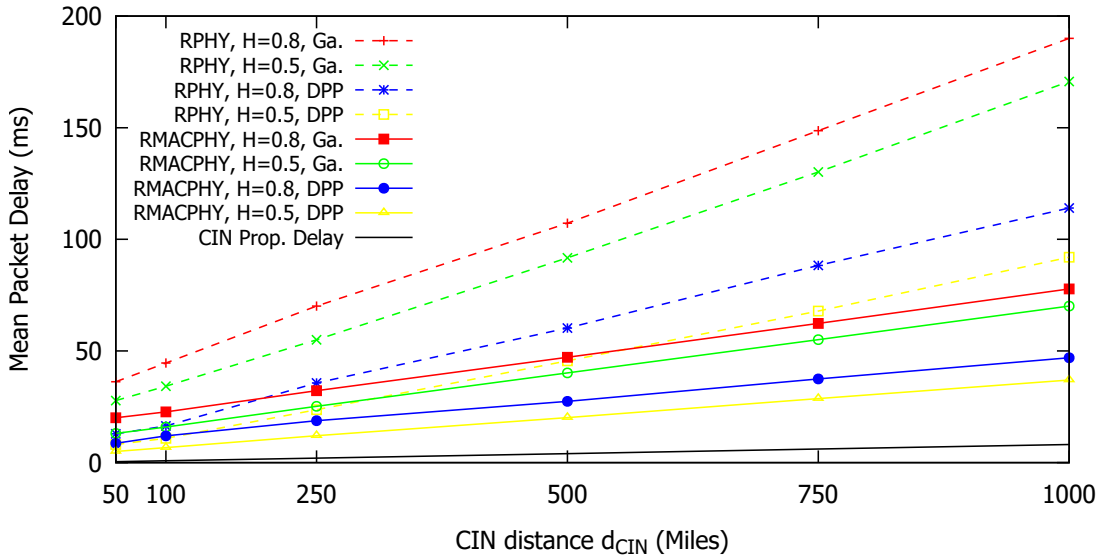

Figure 4.10: R-PHY vs. R-MACPHY Mean Packet Delay Performance for Self-Similar (H = 0.8) and Poisson (H = 0.5) Traffic as a Function of EPON CIN Distance; Fixed Parameters: Cable Link Traffic Intensity ρ_c = 0.5, EPON Traffic Intensity ρ_i = 0.5, 200 CMs, 20 % of Cable Capacity for Contention and Maintenance.

the headend is increased, the variations in operational performance between R-PHY and R-MACPHY architectures become more noticeable. For the EPON distance of 1000 Miles, the R-PHY R-MACPHY mean packet delay differences are much higher as compared to the EPON distance of 100.

We observe from Fig. 4.10 that the delay differences between R-PHY and R-MACPHY for EPON CIN show significantly larger delay. For example, in Fig. 4.10 when EPON distance is 100 Miles, R-PHY average mean packet delay is almost 10.8 ms while the delay for R-MACPHY is 6.7 ms. The increase in delay of almost 60% is due to the R-PHY cascaded scheduling at two stages from headend to CM, and especially from the long round trip propagation delays between headend and remote node. On the other hand, R-MACPHY shows a lower delay, this occurs because of

the separation of the two polling dynamics.

For R-PHY, while evaluating the performance of mean delay with respect to EPON distance as showen in Fig. 4.10, we observe that Double-Phase Polling attains a substantially lower packet average delays than the Gated scheduling mechanism. For example, when the EPON distance is 100 Miles, the Gated scheduling renders a packet mean delay of 34.2 ms, while DPP achieves a packet average delay of 10.85 ms which is a 75% decrease, exemplify the scheduling mechanism impact. Furthermore, the averge packet delay bursty traffic ($H = 0.8$) with DPP scheduling is lower than the delay for Poisson traffic with Gated scheduling .

Fig. 4.10 shows an additive increase in the average packet delay with regard to EPON distance for both the R-PHY and R-MACPHY architectures. The R-PHY DPP mean packet delay has considerably larger slope than comparable R-MACPHY delay and as a result, R-PHY has significantly higher delays for long EPON networks. Importantly, we observe from Fig. 4.10 that self-similar traffic gives considerably bigger slope values for the mean packet delay than Poisson traffic as a function of EPON distance . For example, we observe that R-PHY self-similar traffic with $H = 0.8$ mean packet delay increases almost linearly to 80 ms for the 1000 Miles EPON distance. In comparison, the slope for R-MACPHY DPP for $H = 0.8$ is very low and the packet mean delay for a 1000 Miles CIN distance is below 45 ms.

4.4.5 Packet Loss Rate

CM Buffer Size of 64 KB Figure 4.11 shows the packet loss rate of R-PHY and R-MACPHY as a function of the cable link traffic intensity ρ_c for EPON CIN distances of 50 Miles and 500 Miles, respectively. The performance was evaluated for 200 CMs, CIN traffic intensity of 50%, As we can observe from Fig. 4.11 that for both 50 and 500 Miles EPON distance, for up to a cable load of $\rho_c = 0.6$ the packet loss rates

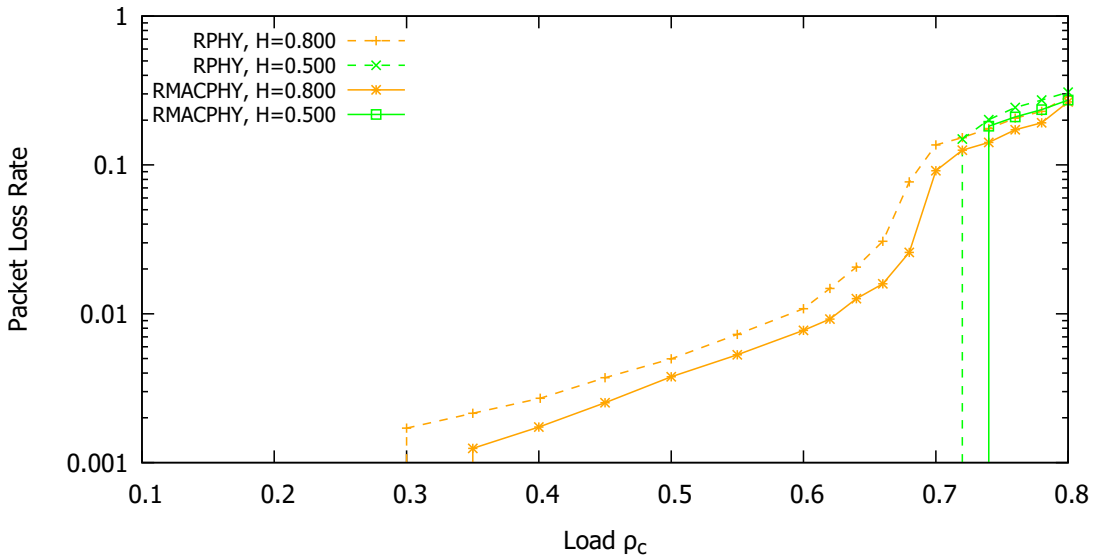

(a) EPON CIN distance = 50 Miles, CM Buffer Size = 64 KB

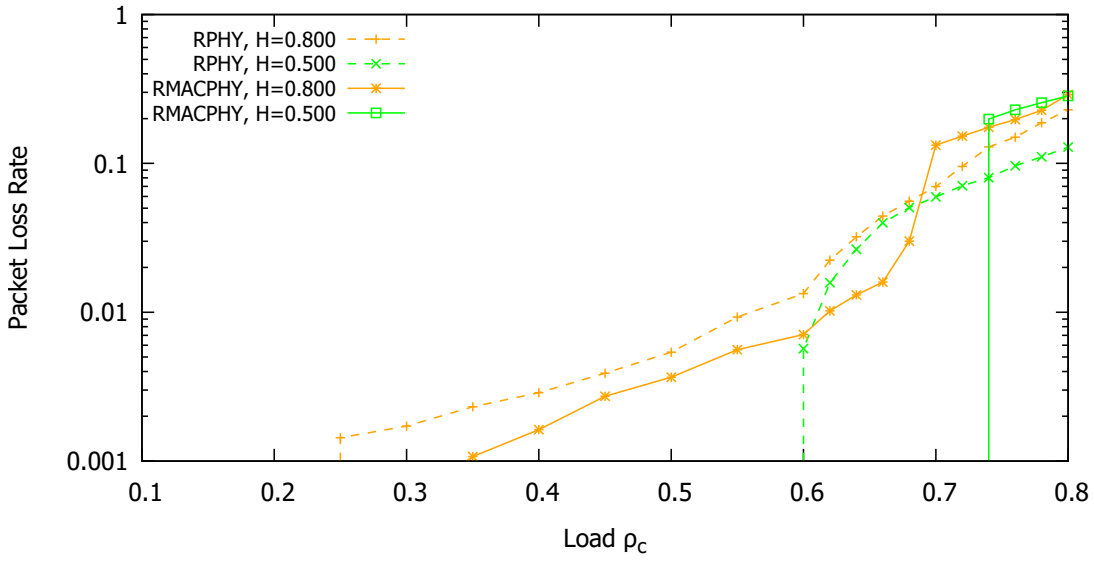

(b) EPON CIN distance = 500 Miles, CM Buffer Size = 64 KB

Figure 4.11: R-PHY vs. R-MACPHY Packet Loss Rate for Double Phase Polling (DPP) Scheduling with Excess Share Grant Sizing, as a Function of Cable Link Traffic Intensity ρ_c for Different EPON One Way Distances; Fixed Parameters: CM Buffer Size of 64 KB, EPON Traffic Intensity ρ_i = 0.5, 200 CMs, 20 % of Cable Capacity for Contention and Maintenance.

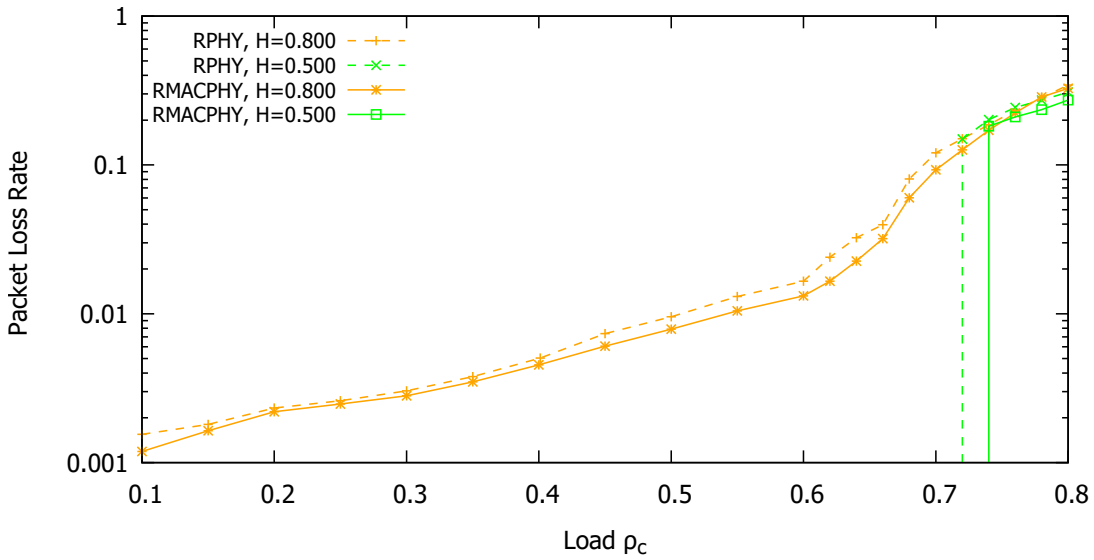

(a) EPON CIN distance = 50 Miles, CM Buffer Size = 12.5 KB

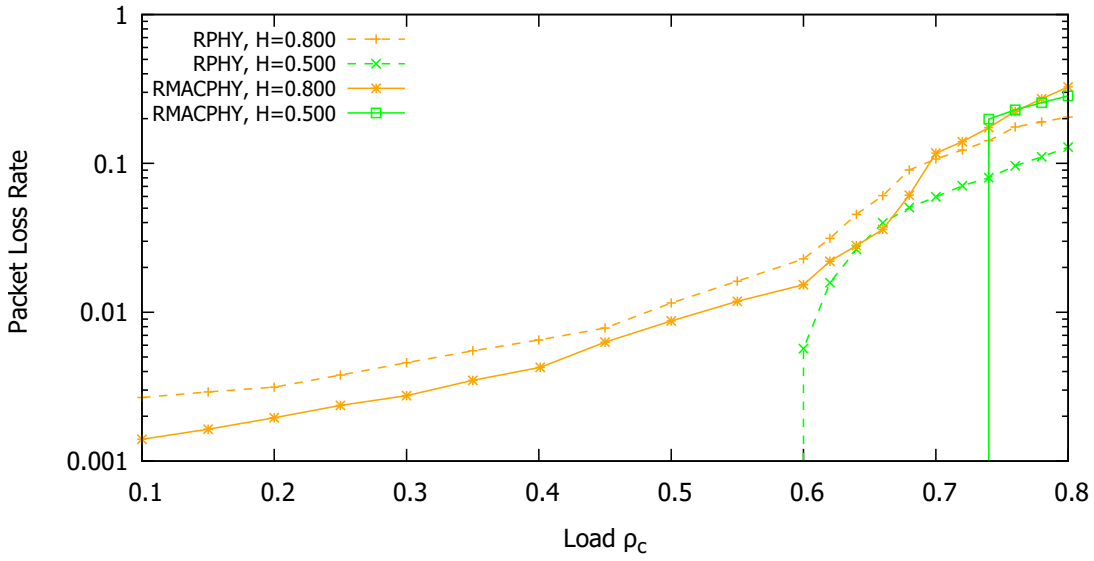

(b) EPON CIN distance = 500 Miles, CM Buffer Size = 12.5 KB

Figure 4.12: R-PHY vs. R-MACPHY Packet Loss Rate for Double Phase Polling (DPP) Scheduling with Excess Share Grant Sizing, as a Function of Cable Link Traffic Intensity ρ_c for Different EPON One Way Distances; Fixed Parameters: CM Buffer Size of 12.5 KB, EPON Traffic Intensity ρ_i = 0.5, 200 CMs, 20 % of Cable Capacity for Contention and Maintenance.

remain under 1 % for the bursty traffic (H = 0.8). Also, Fig. 4.11(a) shows that for bursty traffic R-PHY has a slightly higher packet losses than R-MACPHY, this is due to the R-PHY bandwiidth allocation protocol dynamics accrued delays. In contrast, we observe from Fig. 4.11(b) that R-PHY attain a lower packet loss rate for high cable loads above ρ_c = 0.66 as a result of the R-PHY lower request overhead for the long EPON distance. Also, we observe from Fig. 4.11 that for loads of bursty H = 0.8 traffic above ρ_c = 0.6, the delays shoot up to very large values, indicating the instability of the system after reaching the maximum capacity. That is, when the system reaches the maximum attainable capacity, any increase in the instantaneous packet rate simply results in the dropping of packets causing very high packet loss rate as observed in Fig. 4.11.

CM Buffer Size of 12.5 KB Figure 4.12 shows the packet loss rate performance of R-PHY and R-MACPHY as a function of the cable link traffic intensity ρ_c for EPON CIN distances 50 Miles and 500 Miles, respectively. In comparison to the buffer size of 64 KB, in Fig. 4.12, we observe the packet drop rates of both R-PHY and R-MACPHY for H = 0.8 are closely related and the small increase in the drop rate arises due to the higher delay of the R-PHY MAC protocol dynamics. As compared to the log-linearity in Figs. 4.11, we observe a higher slope in the packet loss rate from $0.3 < \rho_c$ because of the smaller CM buffer size. Whereas, when the EPON CIN distances of 50 Miles and 500 Miles are compared, as seen in Figs. 4.12(a) and (b), we observe earlier packet loss for the larger EPON CIN distance due to the request-to-grant delay. Also, we observe packet losses from $0.1 < \rho_c < 0.35$, which were not seen for the 64 KB CM buffer size, because of the limited buffer size.

Overall, we conclude the that EPON CIN and Ethernet CIN performance for R-PHY and R-MACPHY are comparable with small variations in the delay at

moderate CIN load ρ_i=0.5. However, R-PHY and R-MACPHY with EPON CIN observe sightly larger delays, especially R-PHY with larger EPON CIN distances, because of the cascaded scheduling between CM and remote node, as well as remote node and headend.

4.4.6 Mean Delay as a Function of EPON Traffic

This section presents the effect of the EPON traffic intensity on the R-PHY and R-MACPHY architectures performance. We examine the Cable packet delay as function of EPON traffic intensity considering Cable DPP scheduling mechanisms and a fixed Cable traffic intensity $\rho_c = 0.2, 0.6$. In Fig. 4.13 we illustrate the effect of EPON traffic proportion, i.e., that changing the EPON traffic intensity ρ_i can have on the Cable delay differentiation between R-PHY and R-MACPHY architectures.

We observe from Fig.4.13 that for low to intermediate traffic intensity ($\rho_i \leq 0.5$), only a small increment in the averge dely occurs. Also, as the load increases we can notice the performance difference of remote node architecture and the effect of EPON distance become more clearer. For the R-PHY architecture , the mean packet delay for the 500 Miles is higher than the corresponding 50 Miles R-PHY mean packet delay which is a result from the effect of EPON distance on R-PHY polling dynamics. We also observe that low cable traffic $\rho_c = 0.2$ achieves considerably lower average packet delays than high cable traffic $\rho_c = 0.6$. For example, when the network load is 0.3 and for the 50 Miles distance, the low cable traffic yields a mean packet delay of [6.1, 7.72] ms for traffic burstiness levels $H = 0.5, 0.8$. While when the network load is 0.7 the low cable traffic yields a mean delay of [7.11, 10.78] ms. This is almost a 15% and 29% increase for possion and bursty traffic respectively, illustrating the impact of the EPON traffic on the Cable mean delay. In addition, the low cable traffic can maintain network performance as the network load is increases until the EPON load reach [0.93,

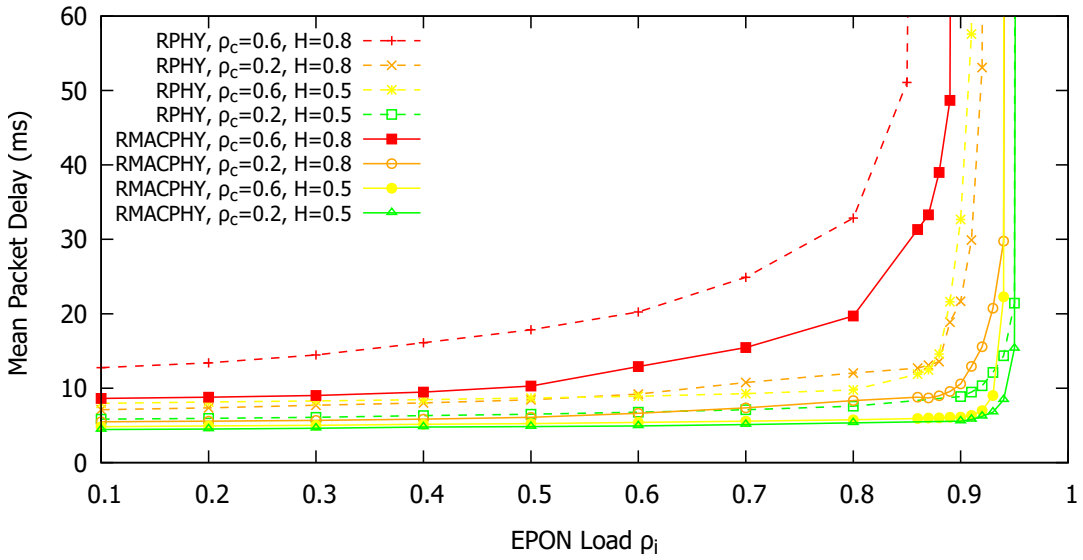

(a) EPON CIN distance = 50 Miles

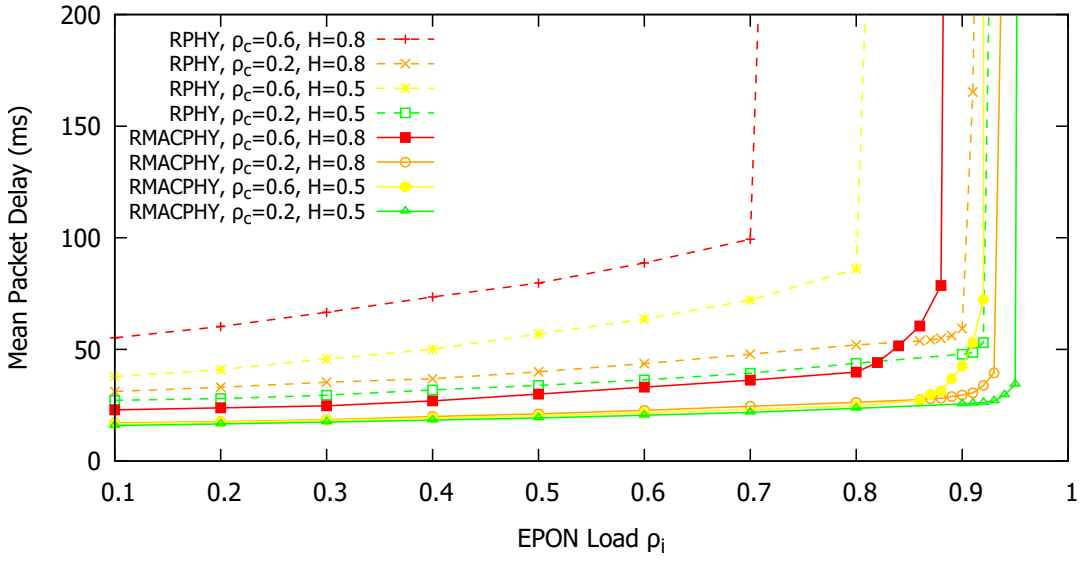

(b) EPON CIN distance = 500 Miles

Figure 4.13: R-PHY vs. R-MACPHY Mean Packet Delay as Function of EPON Link Traffic Intensity ρ_i for EPON One Way Distance of 50 and 500 Miles; Fixed Parameters: Cable Traffic Intensity $\rho_c = 0.2, 0.6$, 200 CMs, Cable DPP Bandwidth Allocation, 20 % of Cable Capacity for Contention and Maintenance.

0.9] load intensity for corresponding traffic burstiness levels $H = 0.5, 0.8$ and EPON 500 Miles distance. However, the high cable traffic delay increases exponentially as EPON load reach [0.8, 0.7] load intensity for corresponding traffic burstiness levels $H = 0.5, 0.8$, as a result of the increase of Cable traffic proportions in 500 Miles scenario.

For the R-MACPHY, as expected the change of EPON traffic intensity ρ_i only slightly increases the mean DOCSIS packet delays. We observe a small additive increment of the Cable traffic mean packet delay as the EPON traffic intensity ρ_i is increased until load reach 0.9 for possion traffic and 0.8 for high bursty traffic $H = 0.8$. After reaching that point the mean packet delay increase abruptly. Also, with the increase of Cable traffic proportions $\rho_c = 0.6$ the delay has higher delays than the scenario with low Cable traffic $\rho_c = 0.2$. For instance,In the 500 Miles scenario we observe that the mean packet delay for Low cable traffic for EPON network load of 0.8 increases nearly linearly to close to 23.5 ms for possion traffic and 26.35 ms for high bursty traffic $H = 0.8$. In contrast, the mean packet delay for the high cable traffic stays below 24.75 ms for possion traffic and 36.25 ms for high bursty traffic $H = 0.8$.

4.4.7 Mean Delay as a Function of MAP Duration

This section focuses on presenting the effect of MAP duration on the performance of R-PHY and R-MACPHY architectures over EPON, for different MAP lengths. We present the mean upstream packet delay as a function of Cable MAP duration and the traffic intensity on the cable upstream channel ρ_c for different levels of traffic burstiness for a fixed number of $M = 200$ CMs that are attached to a remote node. We consider a DPP bandwidth allocation for both stages of polling, i.e., between CM and remote node (cable), and between the remote node and headend (EPON) to

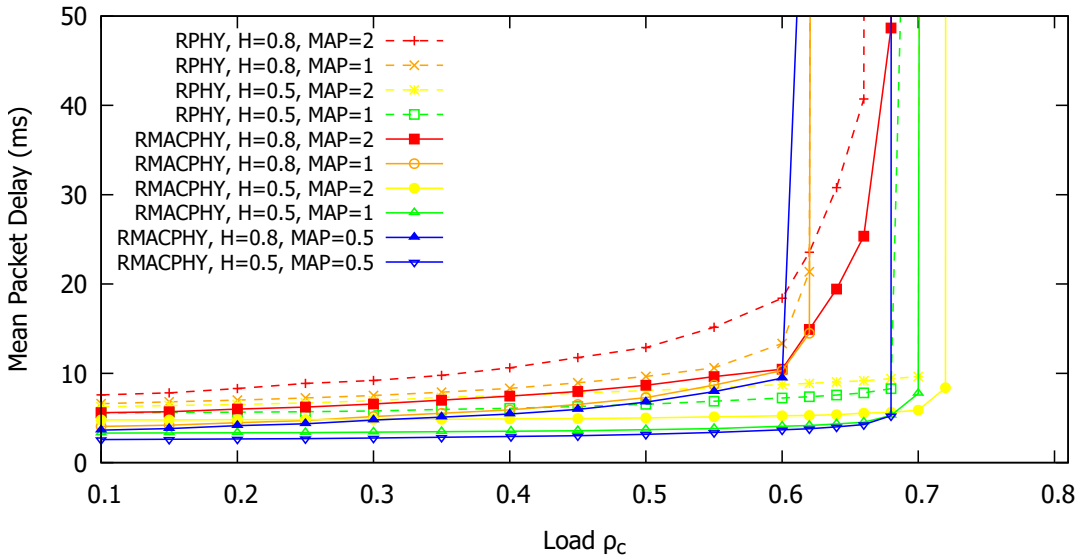

(a) EPON CIN distance = 50 Miles

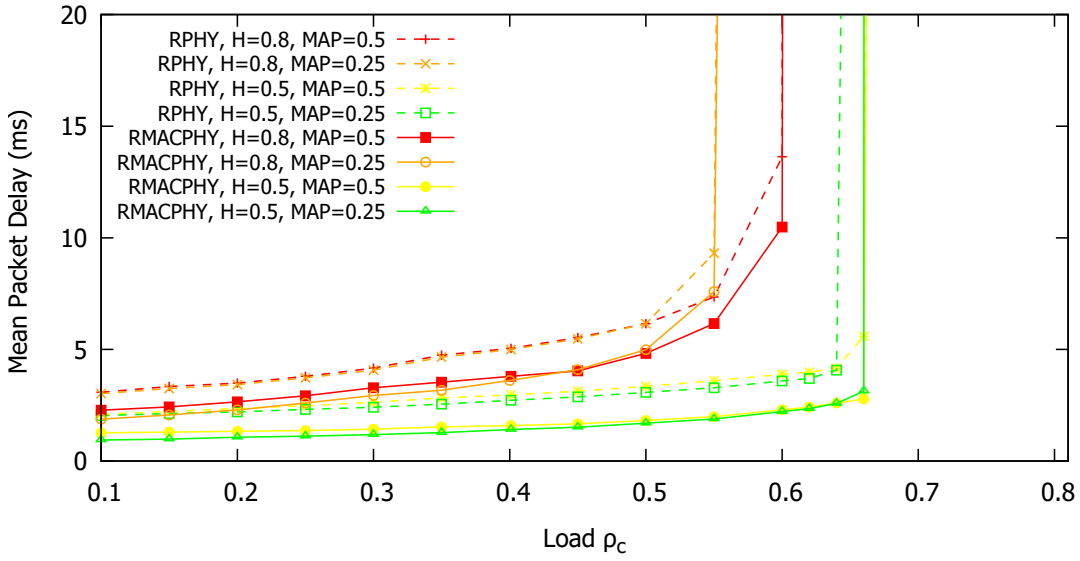

(b) EPON CIN distance = 10 Miles

Figure 4.14: R-PHY vs. R-MACPHY Mean Packet Delay as Function of Cable Link Traffic Intensity ρ_c for EPON One Way Distance of 50 and 10 Miles; FIxed Parameters: EPON Traffic Intensity $\rho_i = 0.5$, 200 CMs, DPP Bandwidth Allocation, 20 % of Cable Capacity for Contention and Maintenance.

coordinate the upstream transmissions over the cable and optical segments, respectively. We consider an EPON CIN distance of 50 Miles (τ = 0.405 ms)and the CIN distance of 10 Miles (τ = 0.081 ms). We vary the MAP duration and EPON cycle time between 2 ms and 1 ms in Fig. 4.14(a). Also, to demonstrate the flexibility of R-MACPHY we consider a MAP duration of 0.5 ms with an EPON cycle time of 1 ms. For the shorten distance of 10 Miles we can further reduce the MAP and EPON cycle time due to the reduced propagation delay. In Fig. 4.14(b), we vary the MAP duration and EPON cycle time between 0.5 ms and 0.25 ms.

Fig. 4.14(a) assess the significance of MAP duration reduction on the performance for the 50 Miles EPON cable network. We observe that the packet delay performance differences between R-PHY and R-MACPHY follow the similar general pattern as shown in Section 4.4.3, whereas the R-PHY show a larger delay when compared to the R-MACPHY. For R-PHY, as we reduce the MAP duration to 1 ms we can observe for cable load ρ_c = 0.5 that the averge packet delay for possion traffic is 6.53 ms which is reduction of almost 23% when compared to the 2 ms MAP duration R-PHY delay of 8.45. For the bursty traffic with $\boldsymbol{H}$ = 0.8, reducing the MAP to 1 ms also help reduce the delay by almost 25% to become 9.65 ms (compared to 12.9 ms delay for 2 ms MAP). For R-MACPHY, we find that the MAP duration reduction results in similar behavior to R-PHY,e.g., R-MACPHY with 1 ms MAP and cable load ρ_c = 0.5 yeilds a delay of 3.7 ms for possion traffic which is a 25 % delay reduction. As we further reduce the MAP duration to 0.5 ms, R-MACPHY achives a delay reduction of almost 35% and 25 % for possion and bursty traffic respectively (when compared to R-MACPHY with 2 ms MAP).

Fig. 4.14(b) presents the effect of MAP duration reduction for the 10 Miles EPON cable network. Due to the smaller propagation distance we can further reduce

MAP duration to consider 0.5 and 0.25 ms MAP. We observe a smaller reduction in cable traffic delay when compared to the results in Fig. 4.14(a). For example, when the cable load is $\rho_c = 0.4$, the R-PHY with 0.5 ms MAP renders a packet mean delay of [2.97, 5.05] ms for possion and bursty traffic respectively, while R-PHY with 0.25 ms MAP achieves a packet average delay of [2.73, 4.9] ms which result in a [9%, 3%] delay decrease, illustrating the MAP impact. Furthermore, when we consider the 1 ms MAP duration we observe a bigger delay reduction of 31% and 19% for possion and bursty traffic respectively. For R-MACPHY, while evaluating the performance effects of MAP Duration and while considering possion traffic, we observe that R-MACPHY with 0.25 MAP can attain an almost 12% and 35% delay reduction than in R-MACPHY with 0.5 and 1 ms MAP respectively for cable load $\rho_c = 0.4$. For the bursty traffic with $H = 0.8$, R-MACPHY with 0.25 ms achives a delay reduction of 10% and 16% when compared to R-MACPHY with 0.5 and 1 ms MAP.

CHAPTER 5

CONCLUSION

In this dissertation, we present an overview of the distributed converged cable access platform architecture, a shifting paradigm is a key step towards revolutionizing the Internet connectivity through the hybrid fiber cable network. However, the benefits of DCCAP, such as flexibility and high scalability, come with the price of associated challenges, which include the operator investment, the design of new remote PHY/MAC devices, and the deployment of new fiber nodes for the digital transmissions. One way to address the growing operator concerns towards the increased operational cost is by virtualizing the DCCAP functions which can be deployed in the Headend of the operator core. However, a careful study needs to be conducted to examine the impact of virtualization of DCCAP functions at the headend to ensure the user satisfaction while achieving cost reduction and maximizing the resource utilization.

In addition to virtualization of the CMTS and DOCSIS functions, a functional split based on PHY, MAC, or higher protocol layers can be made to achieve the desired levels of flexibility and scalability at the virtualized DCCAP. However, each split at the higher layers, i.e., higher than PHY, will increase the complexity at the remote nodes. Therefore, we propose a research study focusing on the trade-offs across multiple splits, whereby our studies have focused within the framework of the functional split in a *virtualized DCCAP*. In addition, the delay and throughput performance due to the physical distance, i.e., the separation between the remote PHY device from the CCAP core will be investigated.

In Chapter 3, we have compared the two main architectures of distributed cable access networks, namely Remote PHY (R-PHY) and Remote MACPHY (R-MACPHY). R-PHY processes the physical layer (PHY) in the remote node close to

the cable modems (CMs) while the medium access control (MAC) for the upstream transmissions is processed in a headend that is connected to the remote node via a Converged Interconnect Network (CIN). R-MACPHY processes both the PHY and MAC in the remote node. We adapted a general polling protocol delay model to analyze the mean upstream packet delays in the R-PHY and R-MACPHY architectures. We conducted extensive simulations to verify the analytical model and to provide a comprehensive performance comparison of the R-PHY and R-MACPHY architectures. We examined elementary offline Gated dynamic bandwidth allocation (DBA) as well as double phase polling (DPP) based DBA, which masks the propagation delays for MAC signalling control through two parallel polling groups.

We found that for CIN networks with long propagation delays above 100 Miles, which may arise when outsourcing the headend processing to a distant cloud, the R-MACPHY architecture achieves significantly lower mean packet delays than the R-PHY architecture. On the other hand, for CIN distances on the order of 50 Miles, which correspond to typical distances of the conventional (non-modular) DOCSIS 3.1 protocol, both the R-PHY architecture and the R-MACPHY architecture achieve comparable mean packet delays and packet loss rates. More specifically, for traffic with low to moderate levels of burstiness (Hurst parameter $H \leq 0.8$), DPP achieves mean packet delays below 10 ms up to an effective cable link utilization level of approximately 62.5 % (less than 20 ms for up to 75 % utilization) in both architectures.

In Chapter 4, we have examined the EPON based Remote PHY (R-PHY) and Remote MACPHY (R-MACPHY) distributed cable access networks. We have examined fiber-cable networks with short-range and long-range propagation in the fiber-based passive optical network (PON) part of the overall hybrid network. We found that for EPON networks with long propagation delays above 100 Miles R-

MACPHY architecture achieves significantly lower mean packet delays than the R-PHY architecture. On the other hand, for short-range EPON distances, we found that both the R-PHY architecture and the R-MACPHY architecture attain a comparable mean packet delays and packet loss rates with advantages to R-MACPHY. Through extensive simulations for a wide range of levels of traffic burstiness, we verified that DPP with Excess share outperforms Offline Gated DBA. More specifically, In the 500 Miles EPON distance scenario with Gated allocation and load $\rho_c = 0.58$ with $H = 0.65$, R-PHY yields an average packet delay of 52.1 ms for $M = 200$ CMs. The delay is reduced by almost 60 % to 20.1 ms by implementing a DPP allocation.

5.1 Future Direction

There are many important directions for future research on distributed cable access networks. One direction is to examine different functional splits between remote node and headend. For instance, moving some of the physical layer processing components of the R-PHY architecture to the headend may reduce the cost of the remote node and make it easier to update and control the physical layer processing routines that have been moved to the headend. Another interesting direction is to explore modular cable access architectures that support both conventional cable modems as well as small cell base stations that provide 5G wireless service and Internet of Things (IoT) applications. Future research should investigate the qual- ity of service and quality of experience achieved over the distributed network for 5G and IoT applications that require access network transport.

Techniques based on software defined networking (SDN), a key paradigm of centralized network control can be further investigated across the multitude of the distributed converged cable access platform architecture to coordinate the resource sharing mechanism among multiple RPD/RMDs and ensuring QoS to CMs. Addi-

tionally, the development of high level overall network management techniques to utilize the principles of SDN to focusing primarily on reducing the operational cost for the service providers.

REFERENCES

[1] ARRIS International Plc, "Looming challenges and potential solutions for future distributed CCAP architecture systems," 2015. [Online]. Available: https://www.arris.com/globalassets/resources/white-papers/arris_distributedccapchallenges_whitepaper_final.pdf

[2] CableLabs, "Converged Cable Access Platform Architecture Technical Report," May 2012.

[3] ——, "Distributed CCAP Architectures Overview Technical Report," Sep. 2015.

[4] ——, "Remote PHY Specificationg," Jan. 2017.

[5] ——, "Modular Headend Architecture v2 Technical Report," Jun. 2015.

[6] C. DeCusatis, "Optical interconnect networks for data communications," *IEEE/OSA Jour. of Lightwave Techn.*, vol. 32, no. 4, pp. 544–552, Feb. 2014.

[7] Y. Chen and S. J. Savage, "The effects of competition on the price for cable modem internet access," *The Review of Economics and Statistics*, vol. 93, no. 1, pp. 201–217, Feb. 2011.

[8] M. Kuzlu and M. Pipattanasomporn, "Assessment of communication technologies and network requirements for different smart grid applications," in *Proc. IEEE PES Innov. Smart Grid Techn.*, 2013, pp. 1–6.

[9] T. Kiravuo, M. Sarela, and J. Manner, "A survey of ethernet LAN security," *IEEE Commun. Sur. & Tut.*, vol. 15, no. 3, pp. 1477–1491, 2013.

[10] A. Triki, P. Gavignet, B. Arzur, E. L. Rouzic, and A. Gravey, "Efficient control plane for passive optical burst switching network," in *The International Conference on Information Networking 2013 (ICOIN)*, Jan 2013, pp. 535–540.

[11] F. Baker and G. Fairhurst, "IETF recommendations regarding active queue management," IETF, Tech. Rep., 2015.

[12] M. T. Barros, R. Gomes, M. S. de Alencar, and A. F. da Costa, "IP traffic classifiers applied to DiffServ networks," in *Proc. IEEE Symp. on Comp. and Commun.*, 2013, pp. 000 827–000 832.

[13] J. Chapman, G. White, and H. Jin, "Impact of CCAP to CM distance in a Remote PHY architecture," in *INTX Spring Techn. Forum Proc.*, May 2015.

[14] J. Martin and N. Shrivastav, "Modeling the DOCSIS 1.1/2.0 MAC protocol," in *Proc. IEEE Int. Conf. on Computer Commun. and Netw. (ICCCN)*, 2003, pp. 205–210.

[15] N. Shah, D. Kouvatsos, J. Martin, and S. Moser, "A tutorial on DOCSIS: protocol and performance models," in *Proc. Int. Working Conf. on the Performance Modelling and Eval. of Heterog. Netw.*, 2005.

[16] B. Hamzeh, M. Toy, Y. Fu, and J. Martin, "DOCSIS 3.1: Scaling broadband cable to gigabit speeds," *IEEE Commun. Mag.*, vol. 53, no. 3, pp. 108–113, Mar 2015.

[17] D. J. Rice, "DOCSIS 3.1® technology and hybrid fiber coax for multi-Gbps broadband," in *Proc. IEEE OFC*, Mar. 2015, pp. 1–4.

[18] M. Toy and H. ElBakoury, "Business metro Ethernet services over DOCSIS 3.1," in *Proc. IEEE Consumer Commun. and Netw. Conf.*, 2015, pp. 373–381.

[19] M. Droubi, N. Idirene, and C. Chen, "Dynamic bandwidth allocation for the HFC DOCSIS MAC protocol," in *Proc. IEEE Int. Conf. on Computer Commun. and Netw. (ICCCN)*, 2000, pp. 54–60.

[20] K.-C. Chang and W. Liao, "The contention behavior of DOCSIS in CATV networks," *IEEE Trans. Broadcasting*, vol. 53, no. 3, pp. 660–669, Sep. 2007.

[21] W.-K. Kuo, S. Kumar, and C.-C. J. Kuo, "Improved priority access, bandwidth allocation and traffic scheduling for DOCSIS cable networks," *IEEE Trans. Broadcasting*, vol. 49, no. 4, pp. 371–382, Dec. 2003.

[22] C. Heyaime-Duvergé and V. K. Prabhu, "Statistical multiplexing of upstream transmissions in DOCSIS cable networks," *IEEE Trans. Broadcasting*, vol. 56, no. 3, pp. 296–310, Sep. 2010.

[23] W. Liao and H.-J. Ju, "Adaptive slot allocation in DOCSIS-based CATV networks," *IEEE Trans. Multimedia*, vol. 6, no. 3, pp. 479–488, Jun. 2004.

[24] W. Liao, "The behavior of TCP over DOCSIS-based CATV networks," *IEEE Trans. Commun.*, vol. 54, no. 9, pp. 1633–1642, Sep. 2006.

[25] J. Martin, "The impact of the DOCSIS 1.1/2.0 MAC protocol on TCP," in *Proc. IEEE Consumer Commun. Netw. Conf.*, 2005, pp. 302–306.

[26] J. Martin and J. Westall, "A simulation model of the DOCSIS protocol," *Simulation*, vol. 83, no. 2, pp. 139–155, Feb. 2007.

[27] N. P. Shah, D. D. Kouvatsos, J. Martin, and S. Moser, "On the performance modelling and optimisation of DOCSIS HFC networks," in *Net. Perf. Eng.* Springer, 2011, pp. 682–715.

[28] L. Volkers, N. Barakat, and T. Darcie, "A simple DOCSIS simulator," *IEICE Trans. Commun.*, vol. 93, no. 5, pp. 1268–1271, May 2010.

[29] J.-Y. Jung, D.-J. Choi, and N. Hur, "Performance comparison of mixed modulation codewords and shortened codewords in DOCSIS 3.1 cable modem system," in *Proc. IEEE Int. Conf. on Consumer Electronics*, Jan 2015, pp. 647–648.

[30] T. Benhavan and K. Songwatana, "HFC network performance monitoring system using DOCSIS cable modem operation data in a 3 dimensional analysis," in *Proc. IEE Int. Conf. Info. and Commun. Techn. Ele. and Electri. Eng.*, March 2014, pp. 1–5.

[31] S. J. Ra, J. Song, J. Bae, J. Jung, D. J. Choi, N. Hur, and C. S. Kim, "Performance measurement of high-efficient OFDM based transmission system in commercial HFC network," in *Proc. IEEE Int. Symp. on Broadband Multimedia Systems and Broadcasting*, June 2016, pp. 1–2.

[32] A. Breznick, "Making the case for Remote-PHY," Feb 2016. [Online]. Available: http://www.casa-systems.com/assets/Casa-White-Paper-Distributed-Access-Architecture.pdf

[33] P. Sowinski, "The impact of Remote-PHY on cable service convergence," in *INTX Spring Techn. Forum Proc.*, May 2016.

[34] J. Chapman, "Remote PHY for converged DOCSIS, Video, and OOB," in *NCTA Spring Techn. Forum Proc.*, June 2014.

[35] J. H. Lee, D. J. Choi, S. I. Lee, and W. W. Kim, "A cable modem receiver supporting four upstream channels," *IEEE Trans. on Consumer Electronics*, vol. 57, no. 3, pp. 1105–1111, aug 2011.

[36] J. Bae, J. Song, S. J. Ra, D. J. Choi, and N. Hur, "A study on common phase rotation compensation for coaxial transmission systems in the HFC network," in *Proc. IEEE Int. Conf. Info. and Commun. Techn. Convergence*, Oct 2015, pp. 159–163.

[37] M. Dischinger, A. Haeberlen, K. P. Gummadi, and S. Saroiu, "Characterizing residential broadband networks," in *Proc. ACM Internet Measurement Comference (IMC)*, 2007, pp. 43–56.

[38] J. Gettys and K. Nichols, "Bufferbloat: Dark buffers in the internet," *Queue*, vol. 9, no. 11, p. 40, 2011.

[39] G. White and R. Pan, "A PIE-based AQM for DOCSIS cable modems," *IETF draft-white-aqm-docsis-pie-02*, 2015.

[40] J. Martin, J. Westall, T. Shaw, G. White, R. Woundy, J. Finkelstein, and G. Hart, "Cable modem buffer management in DOCSIS networks," in *Proc. IEEE Sarnoff Symposium*, Apr 2010, pp. 1–6.

[41] G. White, "Active queue management in DOCSIS 3.1 networks," *IEEE Communications Magazine*, vol. 53, no. 3, pp. 126–132, Mar 2015.

[42] G. Hong, J. Martin, and J. M. Westall, "On fairness and application performance of active queue management in broadband cable networks," *Computer Networks*, vol. 91, pp. 390–406, 2015.

[43] H. Mehmood, S. Rahman, and J. M. Cioffi, "Bit loading profiles for high-speed data in DOCSIS 3.1," *IEEE Communications Magazine*, vol. 53, no. 3, pp. 114–120, Mar. 2015.

[44] H. Gao, T. Best, R. Pendse, and M. E. Sawan, "Traffic classification and observer design of cable networks," in *Proc. IEEE Int. Wksp. Techn. Committee on Commun. Quality and Reliab.*, 2012, pp. 1–6.

[45] ——, "Theoretic performance analysis of cable networks with strategic subscribers," in *Proc. IEEE Int. Wksp. Techn. Committee Commun. Qual. Reliab.*, 2012, pp. 1–6.

[46] M. Hajduczenia, M. Toy, E. Mallette, and C. Knittle, "DOCSIS provisioning of EPON (DPoE): architecture and services," *IEEE Commun. Mag.*, vol. 50, no. 9, pp. 58–65, Sep 2012.

[47] S. Akhtar, "DOCSIS ® provisioning of EPON/10EPON; DPOE ™ for business services scalability," in *Proc. Optical Fiber Communications Conference and Exhibition (OFC)*, Mar. 2011, pp. 1–4.

[48] E. Mallette and M. Hajduczenia, "Automating provisioning of demarcation devices in DOCSIS provisioning of EPON," *IEEE Communications Magazine*, vol. 50, no. 9, pp. 74–80, Sep. 2012.

[49] M. Emmendorfer and S. ZorluOzer, "A comparison of centralized vs. distributed access architectures for PON," in *INTX Spring Techn. Forum Proc.*, May 2016.

[50] P. Bhaumik, S. Thota, B. Mukherjee, K. Zhangli, J. Chen, H. Elbakoury, and L. Fang, "EPON protocol over coax (EPoC): overview and design issues from a MAC layer perspective?" *IEEE Commun. Mag.*, vol. 51, no. 10, pp. 144–153, October 2013.

[51] P. Bhaumik, A. S. Reaz, D. Murayama, K.-I. Suzuki, N. Yoshimoto, G. Kramer, and B. Mukherjee, "Iptv over epon: Synthetic traffic generation and performance evaluation," *Optical Switching and Networking*, vol. 18, pp. 180 – 190, 2015.

[52] A. Mercian, E. I. Gurrola, F. Aurzada, M. P. McGarry, and M. Reisslein, "Upstream polling protocols for flow control in PON/xDSL hybrid access networks," *IEEE Trans. on Commun.*, vol. 64, no. 7, pp. 2971–2984, Jul. 2016.

[53] E. I. Gurrola, M. P. McGarry, Y. Luo, and F. Effenberger, "Pon/xdsl hybrid access networks," *Optical Switching and Networking*, vol. 14, pp. 32 – 42, 2014, sI: PON Supported Networking. [Online]. Available: http://www.sciencedirect.com/science/article/pii/S1573427714000058

[54] Y. Luo, M. Sui, and F. Effenberger, "Energy-efficient next generation passive optical network supported access networking," *Optical Switching and Networking*, vol. 14, no. 1, pp. 43–52, Aug. 2014.

[55] A. Blenk, A. Basta, J. Zerwas, M. Reisslein, and W. Kellerer, "Control plane latency with SDN network hypervisors: The cost of virtualization," *IEEE Transactions on Network and Service Management*, vol. 13, no. 3, pp. 366–380, 2016.

[56] A. Blenk, A. Basta, M. Reisslein, and W. Kellerer, "Survey on network virtualization hypervisors for software defined networking," *IEEE Communications Surveys & Tutorials*, vol. 18, no. 1, pp. 655–685, 2016.

[57] R. Vilalta, A. M. López-de Lerma, R. Muñoz, R. Martínez, and R. Casellas, "Optical networks virtualization and slicing in the 5G era," in *Proc. OSA Optical Fiber Communication Conference*, 2018, pp. M2A–4.

[58] S. Zhang, L. Shi, C. S. Vadrevu, and B. Mukherjee, "Network virtualization over WDM and flexible-grid optical networks," *Optical Switching and Networking*, vol. 10, no. 4, pp. 291–300, 2013.

[59] B. Kurtz, "Exploring virtualization of the head end and flexibility in the node," in *Proc. Cable-Tec Expo*, Oct 2015, pp. 1–18.

[60] L. Zhang, X. Yang, and L. Xu, "Evaluation of virtualizing DOCSIS MAC by software in data center," in *Proc. INTX Spring Techn. Forum*, May 2016, pp. 1–6.

[61] A. Bernstein, "Availability for network function virtualization," in *INTX Spring Techn. Forum Proc.*, May 2016.

[62] A. Thyagaturu, "Software defined applications in cellular and optical networks," *arXiv preprint arXiv:1712.02951*, 2017.

[63] R. Amin, M. Reisslein, and N. Shah, "Hybrid sdn networks: A survey of existing approaches," *IEEE Communications Surveys & Tutorials*, vol. 20, no. 4, pp. 3259–3306, 2018.

[64] J. W. Guck, M. Reisslein, and W. Kellerer, "Function split between delay-constrained routing and resource allocation for centrally managed QoS in industrial networks," *IEEE Transactions on Industrial Informatics*, vol. 12, no. 6, pp. 2050–2061, 2016.

[65] A. S. Thyagaturu, Y. Dashti, and M. Reisslein, "SDN-based smart gateways (Sm-GWs) for multi-operator small cell network management," *IEEE Transactions on Network and Service Management*, vol. 13, no. 4, pp. 740–753, 2016.

[66] J. W. Guck, A. Van Bemten, M. Reisslein, and W. Kellerer, "Unicast QoS routing algorithms for SDN: A comprehensive survey and performance evaluation," *IEEE Communications Surveys & Tutorials*, vol. 20, no. 1, pp. 388–415, 2018.

[67] O. Hohlfeld, J. Kempf, M. Reisslein, S. Schmid, and N. Shah, "Guest editorial scalability issues and solutions for software defined networks," *IEEE Journal on Selected Areas in Communications*, vol. 36, no. 12, pp. 2595–2602, 2018.

[68] W. Kellerer, P. Kalmbach, A. Blenk, A. Basta, M. Reisslein, and S. Schmid, "Adaptable and data-driven softwarized networks: Review, opportunities, and challenges," *Proceedings of the IEEE*, vol. 107, 2019.

[69] L. Ferrari, N. Karakoc, A. Scaglione, M. Reisslein, and A. Thyagaturu, "Layered cooperative resource sharing at a wireless SDN backhaul," in *2018 IEEE International Conference on Communications Workshops (ICC Workshops)*. IEEE, 2018, pp. 1–6.

[70] P. Shantharama, A. S. Thyagaturu, N. Karakoc, L. Ferrari, M. Reisslein, and A. Scaglione, "Layback: SDN management of multi-access edge computing (MEC) for network access services and radio resource sharing," *IEEE Access*, vol. 6, pp. 57 545–57 561, 2018.

[71] K. Sundaresan, "SDNized cable access networks," in *INTX Spring Tech. Forum Proc.*, May 2015.

[72] E. Dai and W. Dai, "Towards SDN for optical access networks," in *INTX Spring Techn. Forum Proc.*, May 2016.

[73] S. Patel, J. Schnitzer, M. Chowdhury, and D. Early, "SDN ground truth:implementing a massive scale programmable DOCSIS network," in *INTX Spring Techn. Forum Proc.*, May 2016.

[74] V. Fuentes, J. Matias, A. Mendiola, M. Huarte, J. Unzilla, and E. Jacob, "Integrating complex legacy systems under OpenFlow control: The DOCSIS use case," in *Proc. IEEE Eur. Wksps on SDN*, 2014, pp. 37–42.

[75] A. Mendiola, V. Fuentes, J. Matias, J. Astorga, N. Toledo, E. Jacob, and M. Huarte, "An architecture for dynamic QoS management at layer 2 for DOCSIS access networks using OpenFlow," *Comput. Netw.*, vol. 94, no. C, pp. 112–128, Jan. 2016.

[76] N. Nandiraju, Y. Lee, and J. Salinger, "Delivering seamless subscriber aware services over heterogeneous access networks using a SDN and NFV framework," in *INTX Spring Techn. Forum Proc.*, May 2015.

[77] M. Amjad, F. Akhtar, M. H. Rehmani, M. Reisslein, and T. Umer, "Full-duplex communication in cognitive radio networks: A survey," *IEEE Communications Surveys & Tutorials*, vol. 19, no. 4, pp. 2158–2191, 2017.

[78] R. R. Tyagi, F. Aurzada, K.-D. Lee, S. G. Kim, and M. Reisslein, "Impact of retransmission limit on preamble contention in LTE-Advanced network," *IEEE Systems Journal*, vol. 9, no. 3, pp. 752–765, 2015.

[79] R. R. Tyagi, F. Aurzada, K.-D. Lee, and M. Reisslein, "Connection establishment in LTE-A networks: Justification of poisson process modeling," *IEEE Systems Journal*, vol. 11, no. 4, pp. 2383–2394, 2017.

[80] M. Reisslein and A. Thyagaturu, "Systems and methods for a smart gateway sdn-based backhaul architecture for small cells," Oct. 5 2017, uS Patent App. 15/476,611.

[81] ——, "Systems and methods for a layered sdn-based backhaul architecture for small cells," Dec. 6 2018, uS Patent App. 15/780,503.

[82] J. Acevedo, R. Scheffel, S. Wunderlich, M. Hasler, S. Pandi, J. Cabrera, F. Fitzek, G. Fettweis, and M. Reisslein, "Hardware acceleration for RLNC: A case study based on the xtensa processor with the Tensilica instruction-set extension," *Electronics*, vol. 7, no. 9, p. 180, 2018.

[83] F. Gabriel, S. Wunderlich, S. Pandi, F. H. Fitzek, and M. Reisslein, "Caterpillar rlnc with feedback (CRLNC-FB): Reducing delay in selective repeat ARQ through coding," *IEEE Access*, vol. 6, pp. 44 787–44 802, 2018.

[84] S. Kafaie, Y. Chen, O. A. Dobre, and M. H. Ahmed, "Joint inter-flow network coding and opportunistic routing in multi-hop wireless mesh networks: a comprehensive survey," *IEEE Communications Surveys & Tutorials*, vol. 20, no. 2, pp. 1014–1035, 2018.

[85] D. E. Lucani, M. V. Pedersen, D. Ruano, C. W. Sørensen, F. H. Fitzek, J. Heide, O. Geil, V. Nguyen, and M. Reisslein, "Fulcrum: Flexible network coding for heterogeneous devices," *IEEE Access*, vol. 6, pp. 77 890–77 910, 2018.

[86] A. Naeem, M. H. Rehmani, Y. Saleem, I. Rashid, and N. Crespi, "Network coding in cognitive radio networks: A comprehensive survey," *IEEE Communications Surveys & Tutorials*, vol. 19, no. 3, pp. 1945–1973, 2017.

[87] S. Pandi, F. Gabriel, J. A. Cabrera, S. Wunderlich, M. Reisslein, and F. H. Fitzek, "PACE: Redundancy engineering in RLNC for low-latency communication," *IEEE Access*, vol. 5, pp. 20 477–20 493, 2017.

[88] M. Taghouti, D. E. Lucani, J. A. Cabrera, M. Reisslein, M. V. Pedersen, and F. H. Fitzek, "Reduction of padding overhead for RLNC media distribution with variable size packets," *IEEE Transactions on Broadcasting*, 2019.

[89] S. Wunderlich, J. A. Cabrera, F. H. Fitzek, and M. Reisslein, "Network coding in heterogeneous multicore IoT nodes with DAG scheduling of parallel matrix block operations," *IEEE Internet of Things Journal*, vol. 4, no. 4, pp. 917–933, 2017.

[90] S. Wunderlich, F. Gabriel, S. Pandi, F. H. Fitzek, and M. Reisslein, "Caterpillar RLNC (CRLNC): A practical finite sliding window RLNC approach," *IEEE Access*, vol. 5, pp. 20 183–20 197, 2017.

[91] M. Zhan, Z. Pang, D. Dzung, and M. Xiao, "Channel coding for high performance wireless control in critical applications: Survey and analysis," *IEEE Access*, vol. 6, pp. 29 648–29 664, 2018.

[92] J. Gambini, S. Savazzi, P. Castiglione, U. Spagnolini, and G. Matz, "Wireless over cable in femtocell systems: A case study from indoor channel measurements," in *Proc. IEEE Wireless Commun. and Net. Conf. Wksps.*, April 2012, pp. 137–141.

[93] H. Mehmood and J. Cioffi, "User clustering for high-speed small cell backhaul over coaxial cable," in *Proc. IEEE Int. Conf. Commun. Wksp. (ICCW)*, June 2015, pp. 216–221.

[94] Z. Zhu, "Design of energy-saving algorithms for hybrid fiber coaxial networks based on the DOCSIS 3.0 standard," *IEEE/OSA Jour. of Optical Commun. and Net.*, vol. 4, no. 6, pp. 449–456, June 2012.

[95] P. Lu, Y. Yuan, Z. Yang, and Z. Zhu, "On the performance analysis of energy-efficient upstream scheduling for hybrid fiber-coaxial networks with channel bonding," *IEEE Commun. Letters*, vol. 17, no. 5, pp. 1020–1023, May 2013.

[96] K. Sundaresan, "Evolution of CMTS/CCAP architectures," in *INTX Spring Techn. Forum Proc.*, May 2015.

[97] A. A. Azzam, *High-speed Cable Modems: Including IEEE 802.14 Standards.* McGraw-Hill, Inc., 1997.

[98] C. Bisdikian, B. McNeil, R. Norman, and R. Zeisz, "MLAP: A MAC level access protocol for the HFC 802.14 network," *IEEE Communications Magazine*, vol. 34, no. 3, pp. 114–121, Mar. 1996.

[99] M. D. Corner, J. Liebeherr, N. Golmie, C. Bisdikian, and D. H. Su, "A priority scheme for the IEEE 802.14 MAC protocol for hybrid fiber-coax networks," *IEEE/ACM Transactions on Networking*, vol. 8, no. 2, pp. 200–211, Apr. 2000.

[100] A. A. Elfeitori and H. Alnuweiri, "A MAC protocol for supporting real-time VBR traffic over IEEE 802.14 based HFC access networks," in *Proc. IEEE Canadian Conf. on Electrical and Computer Engineering*, vol. 1, 1999, pp. 197–201.

[101] J. W. Eng and J. F. Mollenauer, "IEEE project 802.14: Standards for digital convergence," *IEEE Communications Magazine*, vol. 33, no. 5, pp. 20–23, May 1995.

[102] N. Golmie, Y. Saintillan, and D. H. Su, "A review of contention resolution algorithms for IEEE 802.14 networks," *IEEE Communications Surveys*, vol. 2, no. 1, pp. 2–12, First Qu. 1999.

[103] Y.-D. Lin, "On IEEE 802.14 medium access control protocol," *IEEE Communications Surveys*, vol. 1, no. 1, pp. 2–10, First Qu. 1998.

[104] Y.-D. Lin, C.-Y. Huang, and W.-M. Yin, "Allocation and scheduling algorithms for IEEE 802.14 and MCNS in hybrid fiber coaxial networks," *IEEE Trans. Broadcasting*, vol. 44, no. 4, pp. 427–435, Dec. 1998.

[105] S.-T. Sheu and M.-H. Chen, "A new network architecture with intelligent node (IN) to enhance IEEE 802.14 HFC networks," *IEEE Transactions on Broadcasting*, vol. 45, no. 3, pp. 308–317, Sep. 1999.

[106] A. Nasrallah, A. Thyagaturu, Z. Alharbi, C. Wang, X. Shao, M. Reisslein, and H. E. Bakoury, "Ultra-low latency (ull) networks: The IEEE tsn and ietf detnet standards and related 5g ull research," *IEEE Communications Surveys Tutorials*, p. 1, 2018.

[107] Z. Xiang, F. Gabriel, E. Urbano, G. Nguyen, M. Reisslein, and F. Fitzek, "Reducing latency in virtual machines enabling tactile Internet for human machine co-working," *IEEE J. on Sel. Areas Commun.*, 2019.

[108] A. Nasrallah, A. S. Thyagaturu, Z. Alharbi, C. Wang, X. Shao, M. Reisslein, , and H. ElBakoury, "Performance comparison of IEEE 802.1 TSN Time Aware Shaper (TAS) and Asynchronous Traffic Shaper (ATS)," *IEEE Access*, 2019.

[109] D. Fellows and D. Jones, "DOCSIS cable modem technology," *IEEE Communications Magazine*, vol. 39, no. 3, pp. 202–209, Mar. 2001.

[110] W. Al-Khatib, A. Rajeswari, and K. Gunavathi, "Bandwidth allocation algorithm for DOCSIS based HFC broadband networks," in *Proc. IEEE Int. Conf.*

on Signal Processing, Communications and Networking (ICSCN), 2007, pp. 452–458.

[111] S. Fulton, C. Godsay, and R. Bartoš, "DOCSIS as a foundation for residential and commercial community networking over hybrid fiber coax," in *Broadband Services: Business Models and Technologies for Community Networks*, 2005, pp. 201–214.

[112] S. Bhatia, R. Bartos, and C. Godsay, "Empirical evaluation of upstream throughput in a DOCSIS access network," in *Proc. IEEE Int. Conf. on Multimedia Services Access Networks (MSAN)*, 2005, pp. 106–110.

[113] R. Bartos, C. K. Godsay, and S. Fulton, "Experimental evaluation of DOCSIS 1.1 upstream performance," in *Proc. Parallel and Distributed Computing and Networks*, 2004, pp. 257–263.

[114] G. Chandrasekaran, M. Hawa, and D. Petr, "Preliminary performance evaluation of QoS in DOCSIS 1.1," *Information and Telecommunication Technology Center, University of Kansas, Tech. Rep. ITTC-FY2003-TR-22736-01*, 2003.

[115] J. Wang and J. Speidel, "Packet acquisition in upstream transmission of the DOCSIS standard," *IEEE Transactions on Broadcasting*, vol. 49, no. 1, pp. 26–31, Mar 2003.

[116] C. Bachhuber, E. Steinbach, M. Freundl, and M. Reisslein, "On the minimization of glass-to-glass and glass-to-algorithm delay in video communication," *IEEE Transactions on Multimedia*, vol. 20, no. 1, pp. 238–252, 2018.

[117] Y. Li, M. Reisslein, and C. Chakrabarti, "Energy-efficient video transmission over a wireless link," *IEEE Transactions on Vehicular Technology*, vol. 58, no. 3, pp. 1229–1244, 2009.

[118] A. Pulipaka, P. Seeling, M. Reisslein, and L. J. Karam, "Traffic and statistical multiplexing characterization of 3-D video representation formats," *IEEE Transactions on Broadcasting*, vol. 59, no. 2, pp. 382–389, 2013.

[119] M. Reisslein, K. W. Ross, and S. Rajagopal, "Guaranteeing statistical QoS to regulated traffic: The multiple node case," in *Proc. IEEE Conf. on Decision and Control*, vol. 1, 1998, pp. 531–538.

[120] ——, "Guaranteeing statistical QoS to regulated traffic: The single node case," in *Proc. IEEE INFOCOM*, vol. 3, 1999, pp. 1061–1072.

[121] M. Reisslein and K. W. Ross, "High-performance prefetching protocols for vbr prerecorded video," *IEEE network*, vol. 12, no. 6, pp. 46–55, 1998.

[122] P. Seeling and M. Reisslein, "Video traffic characteristics of modern encoding standards: H.264/AVC with SVC and MVC extensions and H.265/HEVC," *The Scientific World Journal*, vol. 2014, 2014.

[123] D. Bushmitch, S. Mukherjee, S. Narayanan, M. Ratty, and Q. Shi, "Supporting MPEG video transport on DOCSIS-compliant cable networks," *IEEE Journal on Selected Areas in Communications*, vol. 18, no. 9, pp. 1581–1596, Sep. 2000.

[124] W.-K. Kuo, "Efficient traffic scheduling for real time VBR MPEG video transmission over DOCSIS-based HFC networks," *IEEE/OSA J. Lightwave Technology*, vol. 27, no. 6, pp. 639–654, Mar. 2009.

[125] D. B. Lee, H. Joo, and H. Song, "An effective channel control algorithm for integrated IPTV services over DOCSIS CATV networks," *IEEE Transactions on Broadcasting*, vol. 53, no. 4, pp. 789–796, Dec 2007.

[126] S. E. Hong, O. H. Kwon, and S. K. Kim, "Performance analysis of single- and multi-channel contention resolution algorithm for the DOCSIS MAC protocol," in *Proc. IEEE ICC*, vol. 3, June 2006, pp. 1083–1088.

[127] J.-Y. Jung, D.-J. Choi, S. I. Lee, and J.-M. Ahn, "Analysis of access delay under high traffic conditions in CATV networks," in *Proc. IEEE Int. Conf. on Inform. and Commun. Techn. Convergence (ICTC)*, 2010, pp. 490–491.

[128] T. Pawasopon and S. Sittichivapak, "Analysis of random slot multiple access algorithms for DOCSIS network," in *Proc. Int. Conf. on Electrical Eng./Electr., Computer, Telecommun. and Inform. Techn.*, vol. 02, May 2009, pp. 896–899.

[129] ——, "Performance analysis of random slot multiple access algorithms for DOCSIS protocol," in *Proc. TENCON 2011 — IEEE Region 10 Conference*, Nov 2011, pp. 554–557.

[130] "Moving on Up: Remote PHY and what it means for the future of networking," Spring Technical Forum, 2016. [Online]. Available: https://www.intxshow.com/wp-content/uploads/2016/05/Session-13-MOVING-ON-UP.pdf

[131] J. Charzinski, "Activity polling and activity contention in media access control protocols," *IEEE Journal on Selected Areas in Communications*, vol. 18, no. 9, pp. 1562–1571, Sep. 2000.

[132] T. Li, D. Logothetis, and M. Veeraraghavan, "Analysis of a polling system for telephony traffic with application to wireless LANs," *IEEE Trans. Wireless Commun.*, vol. 5, no. 6, pp. 1284–1293, Jun. 2006.

[133] L. Musumeci, P. Giacomazzi, and L. Fratta, "Polling-and contention-based schemes for TDMA-TDD access to wireless ATM networks," *IEEE Journal on Selected Areas in Communications*, vol. 18, no. 9, pp. 1597–1607, Sep. 2000.

[134] P. Alvarez, A. Hill, N. Marchetti, D. Payne, and M. Ruffini, "Analysis of the maximum balanced load in long-reach PONs," in *Proc. IEEE Int. Conf. Opt. Netw. Design and Modeling (ONDM)*, 2016, pp. 1–6.

[135] F. Aurzada, M. Scheutzow, M. Herzog, M. Maier, and M. Reisslein, "Delay analysis of Ethernet passive optical networks with gated service," *OSA J. Optical Networking*, vol. 7, no. 1, pp. 25–41, Jan. 2008.

[136] X. Bai, A. Shami, and Y. Ye, "Delay analysis of Ethernet passive optical networks with quasi-leaved polling and gated service scheme," in *Proc. IEEE Int. Conf. on Access Networks & Workshops*, 2007, pp. 1–8.

[137] M. Bokhari and P. Saengudomlert, "Analysis of mean packet delay for upstream transmissions in passive optical networks with sleep mode," *Optical Sw. and Netw.*, vol. 10, no. 3, pp. 195–210, Jul. 2013.

[138] A. Dixit, B. Lannoo, D. Colle, M. Pickavet, and P. Demeester, "Delay models in Ethernet long-reach passive optical networks," in *Proc. IEEE Infocom*, 2015, pp. 1239–1247.

[139] B. Kundu, M. Hossen, S. Basu, and M. I. Arefeen, "An algorithm for reduction of packet delay and waiting time for unstable ONUs in PON," in *Proc. IEEE Int. Conf. on Informatics, Electronics and Vision (ICIEV)*, 2016, pp. 214–218.

[140] S. Miyata, K.-I. Baba, K. Yamaoka, and H. Kinoshita, "Exact mean packet delay analysis for long-reach passive optical networks," in *Proc. IEEE Globecom*, 2015, pp. 1–6.

[141] C. G. Park, D. H. Han, and K. W. Rim, "Packet delay analysis of symmetric gated polling system for DBA scheme in an EPON," *Telecommunication Systems*, vol. 30, no. 1, pp. 13–34, Nov. 2005.

[142] J. S. Vardakas and M. D. Logothetis, "Packet delay analysis for priority-based passive optical networks," in *Proc. IEEE Int. Conf. on Emerging Network Intelligence*, 2009, pp. 103–107.

[143] CableLabs, "Data-Over-Cable Service Interface Specifications, MAC and Upper Layer Protocols Interface Specification, v3.1-I09-160602," Jun 2016.

[144] ITU-T, "Digital multi-programme systems for television, sound and data services for cable distribution (ITU-T J.83)," 2007.

[145] W.-T. Lee, K.-C. Chung, K.-C. Chu, and J.-Y. Pan, "DOCSIS performance analysis under high traffic conditions in the HFC networks," *IEEE Trans. Broadcasting*, vol. 52, no. 1, pp. 21–30, Mar. 2006.

[146] T. Wauters, J. D. Bruyne, L. Martens, D. Colle, B. Dhoedt, P. Demeester, and K. Haelvoet, "HFC access network design for switched broadcast TV services," *IEEE Transactions on Broadcasting*, vol. 53, no. 2, pp. 588–594, June 2007.

[147] CableLabs, "Remote Out-of-Band Specification," 2016. [Online]. Available: https://www.cablelabs.com/wp-content/uploads/specdocs/CM-SP-R-OOB-I03-160512.pdf

[148] ——, "Data-over-cable service interface specifications, remote downstream external PHY interface specification," Jan 2016.

[149] ——, "Remote Upstream External PHY Interface Specification, Data-Over-Cable Service Interface Specifications," Jan 2016.

[150] J. L. M. Townsley and I. Goyret, "Layer two tunneling protocol–version 3 (L2TPv3)," IETF RFC 3931, Mar, Tech. Rep., 2005.

[151] H. Schulzrinne, A. Rao, and R. Lanphier, "RTSP: real time streaming protocol," *IETF RFC2326, April*, 1998.

[152] J. Sommer, S. Gunreben, F. Feller, M. Kohn, A. Mifdaoui, D. Saß, and J. Scharf, "Ethernet–a survey on its fields of application," *IEEE Commun.Sur. & Tut.*, vol. 12, no. 2, pp. 263–284, Second Qu. 2010.

[153] CableLabs, "Remote MAC-PHY Technical Report," Jan. 2016.

[154] A. Thyagaturu, A. Mercian, M. McGarry, M. Reisslein, and W. Kellerer, "Software defined optical networks (SDONs): A comprehensive survey," *IEEE Communications Surveys & Tutorials*, vol. 18, no. 4, pp. 2738–2786, Fourth Qu. 2016.

[155] B. Kantarci and H. T. Mouftah, "Bandwidth distribution solutions for performance enhancement in long-reach passive optical networks," *IEEE Commun. Surv. & Tut.*, vol. 14, no. 3, pp. 714–733, Third Qu. 2012.

[156] ——, "Two-stage report generation in long-reach EPON for enhanced delay performance," *Computer Communications*, vol. 36, no. 14, pp. 1570–1580, Aug. 2013.

[157] M. P. McGarry and M. Reisslein, "Investigation of the DBA algorithm design space for EPONs," *IEEE/OSA J. Lightwave Techn.*, vol. 30, no. 14, pp. 2271–2280, Jul. 2012.

[158] J. Zheng and H. T. Mouftah, "A survey of dynamic bandwidth allocation algorithms for Ethernet Passive Optical Networks," *Opt. Switching and Netw.*, vol. 6, no. 3, pp. 151–162, Jul. 2009.

[159] Y. Huang, P. A. Walsh, Y. Li, and S. Mao, "A distributed polling service-based MAC protocol testbed," *Int. Journal of Communication Systems*, vol. 27, no. 12, pp. 3901–3921, Dec. 2014.

[160] G. Kramer, B. Mukherjee, and G. Pesavento, "Interleaved polling with adaptive cycle time (IPACT): a dynamic bandwidth distribution scheme in an optical access network," *Photonic Network Communications*, vol. 4, no. 1, pp. 89–107, Jan. 2002.

[161] C. M. Assi, Y. Ye, S. Dixit, and M. A. Ali, "Dynamic bandwidth allocation for quality-of-service over Ethernet PONs," *IEEE J. Sel. Areas Commun.*, vol. 21, no. 9, pp. 1467–1477, Nov. 2003.

[162] X. Bai, A. Shami, and C. Assi, "On the fairness of dynamic bandwidth allocation schemes in Ethernet passive optical networks," *Computer Communications*, vol. 29, no. 11, pp. 2123–2135, Jul. 2006.

[163] M. P. McGarry, M. Reisslein, F. Aurzada, and M. Scheutzow, "Shortest propagation delay (SPD) first scheduling for EPONs with heterogeneous propagation delays," *IEEE Journal on Selected Areas in Communications*, vol. 28, no. 6, pp. 849–862, Aug. 2010.

[164] F. Shams, G. Bacci, and M. Luise, "A survey on resource allocation techniques in OFDM(A) networks," *Computer Networks*, vol. 65, pp. 129–150, Jun. 2014.

[165] L. Kleinrock, *Queueing Systems, Volume I: Theory.* Wiley Interscience, 1975.

[166] D. P. Heyman and M. J. Sobel, *Stochastic Models in Operations Research: Stochastic Optimization.* Courier Corporation, 2003, vol. 2.

[167] Cisco Inc., "Upstream Scheduler Mode Configuration for the Cisco uBR CMTS," 2006.

[168] "A side-by-side comparison of centralized vs distributed access architectures," Arris, 2014. [Online]. Available: https://www.arris.com/globalassets/resources/white-papers/arris_centralized_vs_distributed_access_networks_wp.pdf

[169] "Harnessing the power of HFC node facility," Huawei Technologies Co., May 2014.

[170] J. Lee, J. Y. Jung, and J. M. Ahn, "Simplified non-square quadrature amplitude modulation demapper for DOCSIS 3.1," *IEEE Transactions on Broadcasting*, vol. 63, no. 1, pp. 156–161, Mar. 2017.

[171] T. T. Nguyen, B. Berscheid, H. H. Nguyen, and J. E. Salt, "A novel iterative OFDMA channel estimation technique for DOCSIS 3.1 uplink channels," *IEEE Trans. Broadcasting, in print*, vol. PP, no. 99, pp. 1–15, 2017.

[172] G. Kramer, "Generator of self-similar network traffic, networks research lab dept. of computer science, university of california, davis, http://glenkramer.com/trf_research.shtml," 2000.

[173] CableLabs, "Data-Over-Cable Service Interface Specifications, MAC and Upper Layer Protocols Interface Specification, v3.0-I30-170111," Jan 2017.

[174] A. Mercian, E. Gurrola, F. Aurzada, M. P. McGarry, and M. Reisslein, "Upstream polling protocols for flow control in PON/xDSL hybrid access networks," *IEEE Trans. Commun.*, vol. 64, no. 7, pp. 2971–2984, Jul. 2016.

[175] S. Y. Choi, S. Lee, T.-J. Lee, M. Y. Chung, and H. Choo, "Double-phase polling algorithm based on partitioned ONU subgroups for high utilization in EPONs," *IEEE/OSA J. Opt. Commun. Netw.*, vol. 1, no. 5, pp. 484–497, Oct. 2009.

[176] A. Helmy, H. Fathallah, and H. Mouftah, "Interleaved polling versus multi-thread polling for bandwidth allocation in long-reach PONs," *IEEE/OSA Journal of Optical Communications and Networking*, vol. 4, no. 3, pp. 210–218, Mar. 2012.

[177] H. Song, B.-W. Kim, and B. Mukherjee, "Multi-thread polling: a dynamic bandwidth distribution scheme in long-reach PON," *IEEE J. Sel. Areas Commun.*, vol. 27, no. 2, pp. 134–142, Feb. 2009.

[178] J. Ahmed, J. Chen, L. Wosinska, B. Chen, and B. Mukherjee, "Efficient inter-thread scheduling scheme for long-reach passive optical networks," *IEEE Commun. Mag.*, vol. 51, no. 2, pp. S35–S43, Feb. 2013.

[179] A. Mercian, M. P. McGarry, and M. Reisslein, "Offline and online multi-thread polling in long-reach PONs: A critical evaluation," *IEEE/OSA J. Lightwave Techn.*, vol. 31, no. 12, pp. 2018–2028, Jun. 2013.

[180] P.-Y. Chen and M. Reisslein, "Fiwi network throughput-delay modeling with traffic intensity control and local bandwidth allocation," *Optical Switching and Networking*, vol. 28, pp. 8 – 22, 2018. [Online]. Available: http://www.sciencedirect.com/science/article/pii/S1573427717300401

[181] Y. Dashti, A. Mercian, and M. Reisslein, "Grouping by cycle length (gcl) for long-range fiwi networks," *Optical Switching and Networking*, vol. 21, pp. 43 – 57, 2016. [Online]. Available: http://www.sciencedirect.com/science/article/pii/S1573427716000023

[182] X. Wei, F. Aurzada, M. P. McGarry, and M. Reisslein, "DyCaPPON: Dynamic circuit and packet passive optical network," *Optical Switching and Networking*, vol. 13, pp. 135–147, 2014.

[183] F. Aurzada, M. Lévesque, M. Maier, and M. Reisslein, "FiWi access networks based on next-generation PON and gigabit-class WLAN technologies: A capacity and delay analysis," *IEEE/ACM Transactions on Networking*, vol. 22, no. 4, pp. 1176–1189, 2014.

[184] S. Bharati and P. Saengudomlert, "Analysis of mean packet delay for dynamic bandwidth allocation algorithms in EPONs," *IEEE/OSA Journal of Lightwave Technology*, vol. 28, no. 23, pp. 3454–3462, 2010.

[185] M. Hossen and M. Hanawa, "Dynamic bandwidth allocation algorithm with proper guard time management over multi-OLT PON-based hybrid FTTH and wireless sensor networks," *IEEE/OSA Journal of Optical Communications and Networking*, vol. 5, no. 7, pp. 802–812, 2013.

[186] Z. Alharbi, A. S. Thyagaturu, M. Reisslein, H. ElBakoury, and R. Zheng, "Performance comparison of r-PHY and r-macphy modular cable access network architectures," *IEEE Transactions on Broadcasting*, vol. 64, no. 1, pp. 128–145, Mar. 2018.

[187] A. S. Thyagaturu, Z. Alharbi, and M. Reisslein, "R-FFT: Function split at IFFT/FFT in unified LTE cran and cable access network," *IEEE Transactions on Broadcasting*, vol. 64, no. 3, pp. 648–665, Sep. 2018.